AFRL-SN-RS-TR-2002-238
Final Technical Report
September 2002

DEMONSTRATION OF A LOW COST, HIGH-SPEED FIBER OPTIC TRANSCEIVER

Focused Research, Incorporated

Sponsored by
Defense Advanced Research Projects Agency
DARPA Order No. B667

APPROVED FOR PUBLIC RELEASE; DISTRIBUTION UNLIMITED.

The views and conclusions contained in this document are those of the authors and should not be interpreted as necessarily representing the official policies, either expressed or implied, of the Defense Advanced Research Projects Agency or the U.S. Government.

AIR FORCE RESEARCH LABORATORY
SENSORS DIRECTORATE
ROME RESEARCH SITE
ROME, NEW YORK

This report has been reviewed by the Air Force Research Laboratory, Information Directorate, Public Affairs Office (IFOIPA) and is releasable to the National Technical Information Service (NTIS). At NTIS it will be releasable to the general public, including foreign nations.

AFRL-SN-RS-TR-2002-238 has been reviewed and is approved for publication

APPROVED:

        JAMES E. NICHTER
        Project Engineer

FOR THE DIRECTOR:

        RICHARD G. SHAUGHNESSY, Lt. Col., USAF, Chief
        Rome Operations Office
        Sensors Directorate

REPORT DOCUMENTATION PAGE

Public reporting burden for this collection of information is estimated to average 1 hour per response, including the time for reviewing instructions, searching existing data sources, gathering and maintaining the data needed, and completing and reviewing this collection of information. Send comments regarding this burden estimate or any other aspect of this collection of information, including suggestions for reducing this burden to Washington Headquarters Services, Directorate for Information Operations and Reports, 1215 Jefferson Davis Highway, Suite 1204, Arlington, VA 22202-4302, and to the Office of Management and Budget, Paperwork Reduction Project (0704-0188), Washington, DC 20503

1. AGENCY USE ONLY (Leave blank)	2. REPORT DATE SEPTEMBER 2002	3. REPORT TYPE AND DATES COVERED Final Jun 97 – Jun 00

4. TITLE AND SUBTITLE
DEMONSTRATION OF A LOW COST, HIGH-SPEED FIBER OPTIC TRANSCEIVER

5. FUNDING NUMBERS
C   - F30602-97-C-0144
PE - 63739E
PR - B667
TA - 00
WU - 04

6. AUTHOR(S)
Terri L. Dooley, Grant R. Emmel, Gert K. G. Hohenwarter,
Michael P. Nesnidal, Robert A. Marsland, Mark Rodell, and
Robert S. Williamson

7. PERFORMING ORGANIZATION NAME(S) AND ADDRESS(ES)
Focused Research, Incorporated
8551 Research Way, Suite 170
Middleton Wisconsin 53562

8. PERFORMING ORGANIZATION REPORT NUMBER

N/A

9. SPONSORING / MONITORING AGENCY NAME(S) AND ADDRESS(ES)
Defense Advanced Research Projects Agency   AFRL/SNDP
3701 North Fairfax Drive   25 Electronic Parkway
Arlington Virginia 22203-1714   Rome New York 13441-4515

10. SPONSORING / MONITORING AGENCY REPORT NUMBER

AFRL-SN-RS-TR-2002-238

11. SUPPLEMENTARY NOTES

AFRL Project Engineer: James E. Nichter/SNDP/(315) 330-7423/ James.Nichter@rl.af.mil

12a. DISTRIBUTION / AVAILABILITY STATEMENT
APPROVED FOR PUBLIC RELEASE; DISTRIBUTION UNLIMITED.

12b. DISTRIBUTION CODE

13. ABSTRACT *(Maximum 200 Words)*
A high-speed serial optical link suitable for a range of commercial and military short-haul applications, operating over a distance of up to 300 meters was developed. At the heart of the link lie a vertical-cavity surface-emitting laser (VCSEL) diode transmit and a gallium arsenide (GaAs) photo detector, driven and amplified by custom-designed GaAs integrated circuits. The transmit or receiver is individually hermetically sealed in a metal-ceramic surface-mounted package with a multimode fiber pigtail aligned to the laser or photodiode respectively. The transmitter and receiver are nearly identical externally and each is less than 0.2 cm in volume. The link is capable of > 10 gigabit per second operation, independent of signaling protocol and can transmit over distances of up to 300 meters on high-bandwidth multimode fiber.

14. SUBJECT TERMS
Transceiver, Digital Gigabit, VCSEL

15. NUMBER OF PAGES
161

16. PRICE CODE

17. SECURITY CLASSIFICATION OF REPORT	18. SECURITY CLASSIFICATION OF THIS PAGE	19. SECURITY CLASSIFICATION OF ABSTRACT	20. LIMITATION OF ABSTRACT
UNCLASSIFIED	UNCLASSIFIED	UNCLASSIFIED	UL

Table of Contents

List of Figures

List of Tables

i

Summary

We have developed a high-speed serial optical link suitable for a range of commercial and military short-haul applications, operating over a distance of up to 300 meters. At the heart of the link lie a vertical-cavity surface-emitting laser (VCSEL) diode transmitter and a gallium arsenide (GaAs) photodetector, driven and amplified by custom-designed GaAs integrated circuits. The transmitter or receiver is individually hermetically sealed in a metal-ceramic surface-mounted package with a multimode fiber pigtail aligned to the laser or photodiode respectively. The transmitter and receiver are nearly identical externally and each is less than 0.2 cm3 in volume. The link is capable of >10 gigabit per second operation, independent of signaling protocol, and can transmit over distances of up to 300 meters on high-bandwidth multimode fiber.

Our ability to fabricate these photodiodes and our partnership with several VCSEL manufacturers and GaAs foundries help to make this a relatively low-cost product. Furthermore, under this program we developed a low-cost automated fiber pigtailing and packaging facility, also an essential element to producing inexpensive photonic components.

Optoelectronic device development and characterization. We fabricated several hundred large area (~65μm diameter) GaAs photodiodes with bandwidth >9 GHz and with high responsivity. Although no these diodes do not represent a major development effort, improvements in the optical coatings and device layout resulted from this work. Early in the program we also evaluated the performance of diodes from other manufacturers. Our own diode design was settled upon as having the best combination of performance and cost.

VCSELs were evaluated from many manufacturers on a broad basis of performance characteristics, including bandwidth, series resistance, slope efficiency, and availability. We worked closely with several of these manufacturers to hone a specification that met our needs and is manufacturable. When this program began, very few sources existed for 850nm VCSELs at these speeds and all were developmental devices from the laboratory. As of the publication of this report, several manufacturers are offering VCSELs with sufficient performance for this application and are rapidly approaching maturity.

Transmitter and receiver chipset. This program encompassed from early experimental designs in silicon germanium to the final solution we settled on using a standard low-cost HBT GaAs process widely used in the wireless communications industry. Using this process we designed both a custom VCSEL driver IC as well as a low-noise TIA with integrated AGC functionality. These largely achieved our aggressive performance, power consumption, size, and cost goals.

Packaging. We developed a novel high-frequency surface-mount microwave package design and fiber optic pigtailing technique, as well as the specialized machinery and processes required for alignment and hermetic sealing. The package is very small, approximately 7mm on a side, and is surface-mountable and capable of high-frequency operation beyond 12 GHz, and is manufactured using standard metal-ceramic processes.

We also developed a novel fiber optic pigtailing method compatible with this package, designed to produce a truly hermetic package with low cost. This effort comprised design of the 8 package elements that affix and seal the fiber relative to the optical device and package, but also of the tooling and machinery required to perform the process. To this end, we developed a laserwelding system with tooling to hold the package components, a motion control system to align the fiber and move the weld heads, and the algorithms and control code required to make this a semiautomated process.

Link design. At the beginning of this effort, the link specifications were a set of target numbers loosely derived from gigabit Ethernet, Fiber Channel, and longwave SONET standards. Through our efforts, which were initiated by this program, the IEEE 802.3ae 10 Gb/s Ethernet standards committee and the Optical Internetworking Forum have each adopted similar specifications for this link, and Fiber Channel is soon to follow. This reflects an extremely high level of interest among a range of telecommunications companies, including suppliers of central office equipment, optical fiber, as well as transceiver vendors.

Production demonstration. We ultimately manufactured over 100 transmitter/receiver pairs that met nearly all of our required specifications. Accompanying this are the documents describing the flow of materials and controlling processes, such as detailed procedures for assembly and test, travelers, and manufacturing data.

Documentation / Program management. Throughout the course of this effort we have provided extensive documentation of our progress in the form of formal reports such as this one, presentation materials, and on-site meetings.

Introduction

There is a growing need for high-speed serial communications links that are lightweight, reliable, and cheap, for both commercial and military applications. Copper interconnections are heavy and expensive above speeds of several gigabits per second (Gb/s) even for distances below a hundred meters. Parallel optical connections with a dozen or more fibers have become available, providing speeds of 10 Gb/s and above, but these suffer from high interconnect cost and can be somewhat less reliable since many fibers and devices are required to produce a link. In addition, meeting eye-safety requirements can be difficult with 10 850-nm emitters operating at 1 Gbit/s. A much more appealing approach is a higher-speed, single-fiber approach. With the advent and approaching commercialization of reliable vertical-cavity surface-emitting lasers (VCSELs) with several gigahertz of bandwidth, single-fiber multi-mode serial interconnections become a feasible and inexpensive alternative.

We have developed an 850-nm, multi-mode, fiber-optic serial transmitter and receiver, operating at speeds up to 12.5 Gb/s, capable of transmitting over distances of over 300 meters. Our design is protocol-independent and can function either with DC-balanced code or in burst mode, making it broadly applicable to virtually any short-haul, high-speed, point-to-point communications application. We expect our highest payoff military application to be digital radar, and commercially, we predict much larger payoffs in local area networks (LANs), storage area networks (SANs), and telecommunication switch interconnections. The fact that shortwave serial over multimode fiber has been adopted both by the IEEE 802.3ae Ethernet standards committee and the Optical Internetworking Forum validates the capability and timeliness of this technology.

Several elements allow us to make this high-performance link low in cost as well. Using a single inexpensive VCSEL for the transmitter element, designed to operate at high modulation rates and over a wide range of environmental conditions, gives us reliability over competing parallel approaches and considerable cost savings over a traditional edge-emitting laser. The detector in the photoreceiver is similar to an established New Focus design that supports an already successful product family. Also important is a relatively inexpensive, reliable packaging approach; we are using a hermetically sealed, laser-welded package that can be fiber-aligned and sealed automatically with minimal operator involvement. Finally, we are developing a manufacturing process that allows for complete testing at early stages in the process, reducing the need for rework and low yield at the end of the assembly process.

This report summarizes our progress during the course of this three-year contract. In the following sections, we provide some background motivation and assumptions that have led us to take this approach. Next, we briefly summarize results of our program of component characterization, prototype link development, and packaging/fiber attachment. We conclude by summarizing many of the "lessons learned" in the course of this work and a forecast for the future of this technology. Finally, several appendices document in detail the design of the module itself, the GaAs integrated circuits, the welding robot, associated tooling and process documentation, the code used to drive the welder, and the previous

years' reports as well as a summary of the intellectual property developed.

Methods, Assumptions, and Procedures

Here we briefly discuss some of the technical rationale behind our approach.

When it is necessary to move large amounts of data very fast over a short (<100 meter) distance, there are at least five possible methods:
- parallel copper wires,
- parallel fibers driven from logic levels,
- parallel fibers driven by separate serial interfaces,
- parallel serial interfaces wavelength-multiplexed on one fiber, and
- a single serial interface on one fiber.

The single serial interface will be the optimal solution in many applications where reliability, robustness, size, and cost are the major considerations. A single fiber interface can incorporate controls on average laser power and receiver DC levels that would be too costly if repeated 12 or more times for a given link. Wavelength division multiplexing relies on the data being divisible into separate data streams. This is not the case for the digital radar application where the data is originating from a single A/D converter.

All things being equal, a single fiber is preferable to 12 and any fiber is preferable to a massive copper cable, which becomes too heavy and costly when sending data more than a few meters at > 1 gigabyte/second. The pressure on the serial link is to demonstrate cost and power requirements comparable to the other approaches. Table 1 summarizes this comparison, based on a 5 meter link with an aggregate bandwidth of 12 gigabits (transceiver and cable only). Clearly, the case for fiber solutions gets even better for lengths >5 meters, and is the only viable solution beyond 100 meters.

Power and cost estimates for parallel optical approach very widely because these units are only now going into production. For the purpose of comparison, 1 W was chosen as the power since this is the minimum power necessary to drive twelve 50-ohm lines at ECL levels from a 5V supply. The multiplexer/demultiplexer price is not included in Table 1. Since the data channel widths do not match the word length from the A/D, each technique compared in Table 5 will require a mux and demux although the 12 Gb/s parts will be the most expensive. For reference, a 10 Gb/s mux/demux chipset including the phase detector and timing circuitry is available from Vitesse in a BGA package; the pair of chips dissipates 3.1 W. Current pricing (2001) is $500 per pair in 1,000 quantities; they expect this device to eventually fall to a few hundred dollars in large quantities.

Table 1. Transceiver approach comparison

	Single Fiber 12 Gb/s	Parallel Optical Link, 12 Parallel, 1 Gb/s	Serial Copper Link	Parallel, Copper Link, 41 diff-parallel, 250 Mb/s
Power (W)	1 (2.5) [1]	1	1 (2.5) [1]	2
Cost Projection ($/Transceiver)	200	610 [2]	800	600 [3]
Diameter of cable(s) (mm)	0.125	3	7 [4]	100×10 [5]
Weight (5 m cable, kg) [6]	0.008	0.1	0.51	0.5
Reliability (MTTF hrs, VCSEL, 25°C)	$1.0 \cdot 10^7$ [7]	$0.75 \cdot 10^7$ [8]	N/A	N/A

[1] 2.5 W includes serializer/deserializer circuitry

[2] Based on $10 per Gb/s as target price of parallel optical link plus cable and connector cost

[3] Based on cost of 5 meters of W.L. Gore "RIBBON-AX" cable at $120/meter (no connectors)

[4] Based on UFE 276B high-isolation cable

[5] Based on bundle of 2, 2.25" wide "RIBBON-AX" cables

[6] Based on weight of cable only, no armor

[7] Based on 1E7 hour MTTF number from Honeywell preliminary data sheet

[8] Based on 12 VCSELs, log-normal distribution, $\sigma = 0.225$

Technical Approach

Presently, high-speed (~10 gigabit/second) fiber optic transmitters and receivers rely on singlemode long-wavelength laser diodes aligned to single-mode fibers. The alignment and packaging process is time-consuming, labor-intensive, and relatively low yield (<50%). Furthermore, it requires an expensive package that is prohibitively large for many applications.

We will build 12 gigabit per second transmitter and receiver modules that are inexpensive and substantially smaller in size (cubes less than 0.25 inches on a side) by taking advantage of multi-mode VCSEL laser chips, state-of-the-art foundry services, and, most importantly, a fast, low-cost, high yield fiber attachment technique. This fiber attachment technique will also be flexible and amenable to customization: it will allow us to accommodate different package styles or different fibers without dramatically increasing costs. Using newly available high-bandwidth multimode fiber will extend the distance over which this link can operate up to 300 meters.

Results and Discussion

Optoelectronic components

Photodiodes

We have demonstrated the ability to make high speed, high responsivity photodiodes sensitive at 850nm. These are relatively large area, approximately 65µm diameter, and therefore their *RC* frequency response is capacitance limited. We have measured the 3 dB bandwidth of these devices to be consistently greater than 9 GHz. One of these devices, bonded into a receiver module, is shown below in Figure 1.
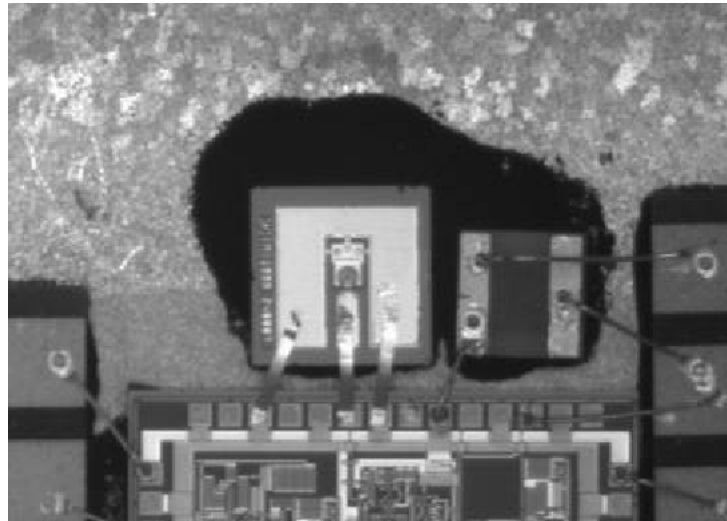

Figure 1. Photodiode bonded into receiver module with TIA/AGC integrated circuit.

The reliability of these photodiodes has also been demonstrated with high-temperature burn-in testing, and some preliminary results are shown in Figure 2 below for just 5 devices over 3600 hours. Note that all of the devices whose leakage current was within specification (below 10 nA) stayed within specification throughout the lifetime test. Note that one device began the test with too much leakage current, and this was maintained throughout the burn-in. Currently, a few hundred similar devices are undergoing temperature testing and show similar results demonstrating high-reliability and stable, low leakage current beyond 5000 hours.

We did learn that the silica nitride antireflection (AR) coating on these devices was highly non-optimal, accounting for about a 30% reflection and therefore a poor responsivity of about 0.4 A/W. With an improved coating design (which has been implemented in a recent run of devices), the responsivity is expected to exceed 0.6 A/W.

In the course of this work, we did examine photodiodes from several other manufacturers intended both as second sources and to support our prototyping efforts. The issues with these photodiodes ranged from high cost, limited availability, to designs that were not optimal for this application (e.g., too slow).

Photodiode Aging @ 200 C : PD Wafer: BNO64:QTR 1
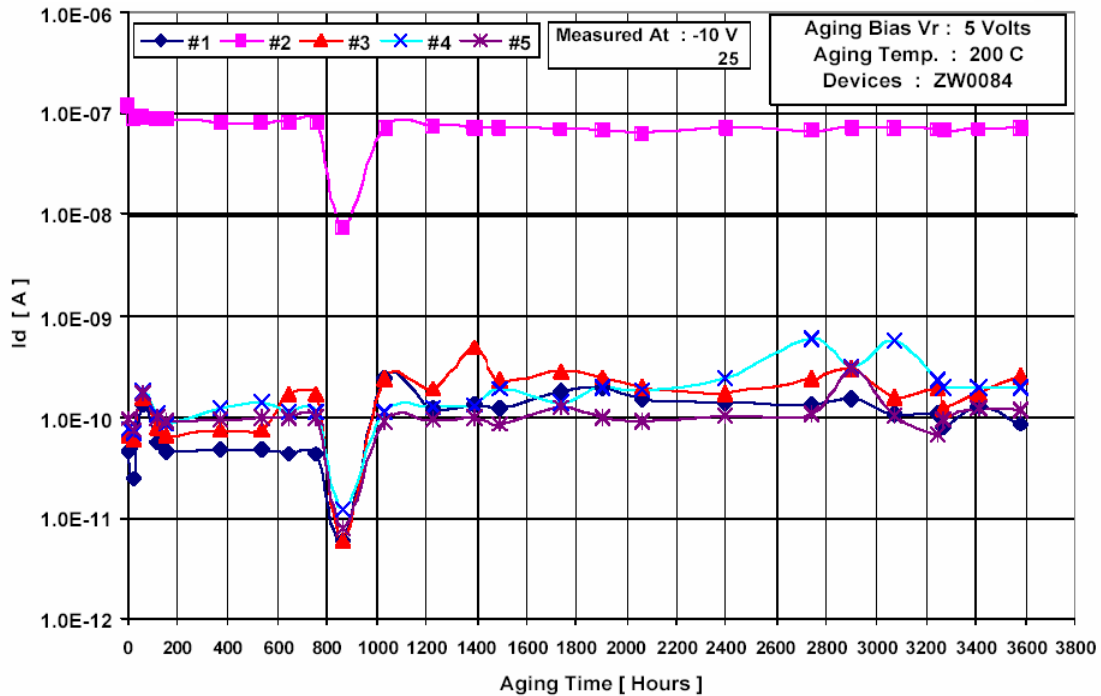
Figure 2. Photodiode aging data

VCSELs

Over the course of this work we examined VCSELs from several manufacturers, including MODE and Honeywell. We worked closely with MODE to develop a solid specification that meets our requirements and is also manufacturable (a copy of this is at the end of Appendix E, Year Two Summary). We eventually settled upon Honeywell as our supplier for these devices for nearly all of our module builds.

Below in Figure 3 we show the LIV performance of these VCSELs over temperature for a typical device. Note that the LI response is largely kink-free, but that there is considerable curvature; the slope changes by about 30% from the region below 5mA to the region above 9mA. This curvature is mostly addressed by components in the driver design which is discussed later.

Figure 4 shows DC and AC spectra showing the slight shift in the spectrum when modulation is applied. The most notable issue is that the spectrum does not broaden, nor does the number of dominant modes change either. This data is typical for all of the VCSELs we have used.

Figure 5 shows the spectrum shifting over temperature. The number of modes and power remain largely constant, but the wavelength centroid does indeed shift. This shift is well within our specification of 840-860nm.
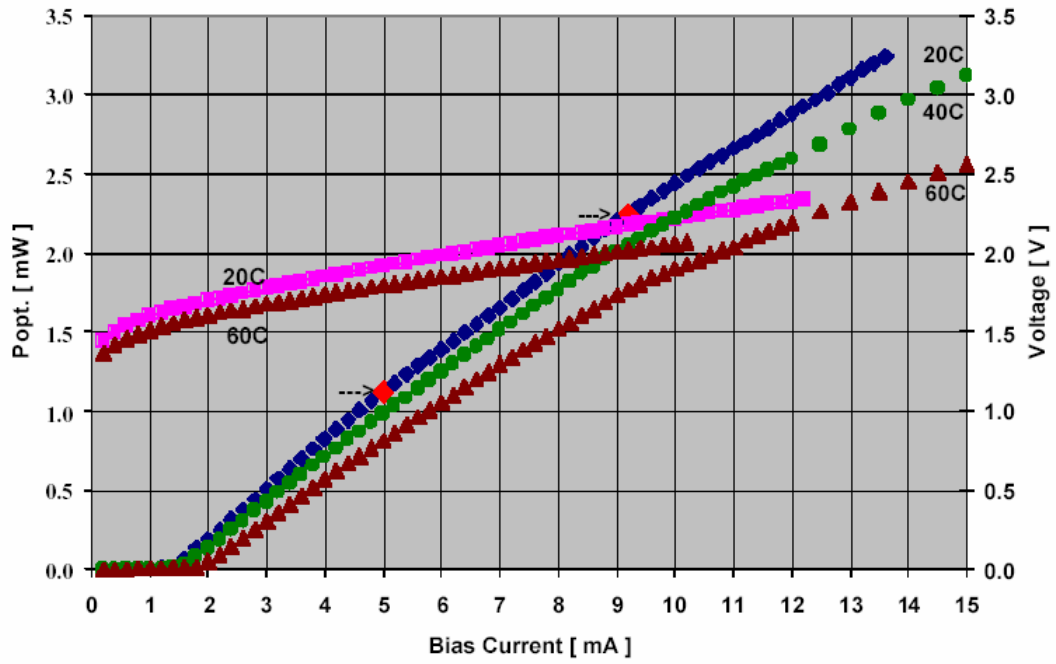
*Figure 3. LIV performance of the Honeywell VCSELs.*
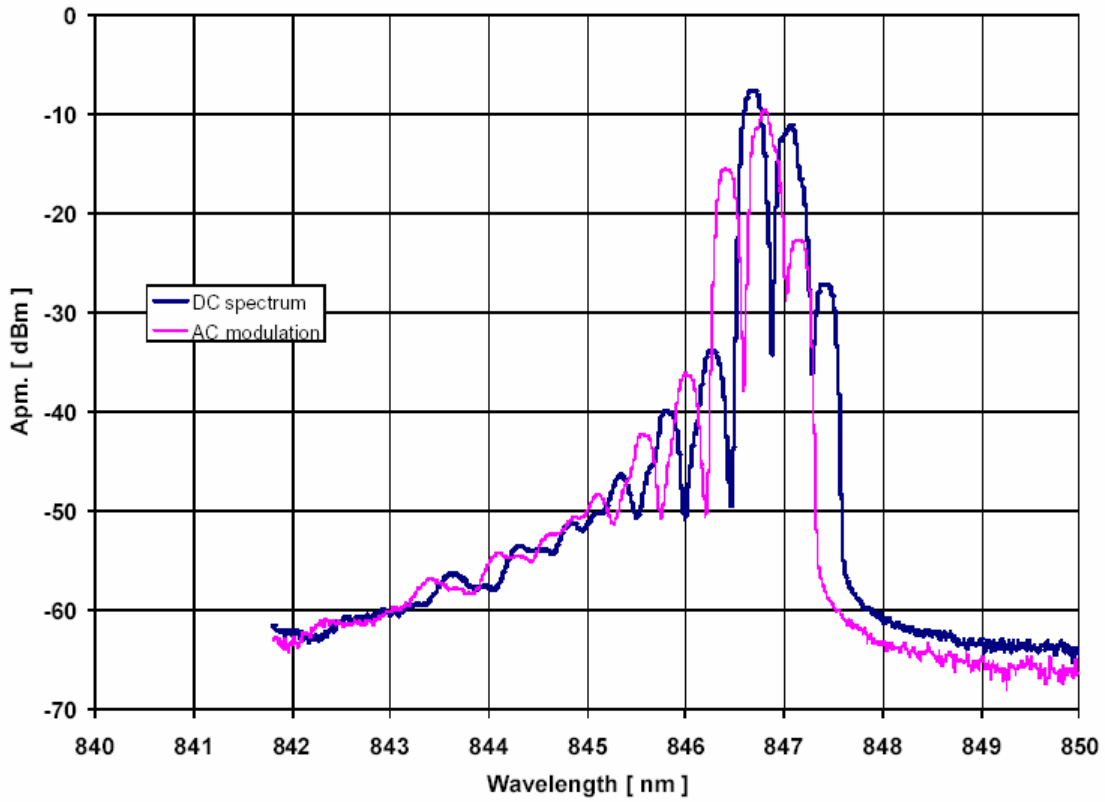

Figure 4. DC and AC VCSEL spectra.
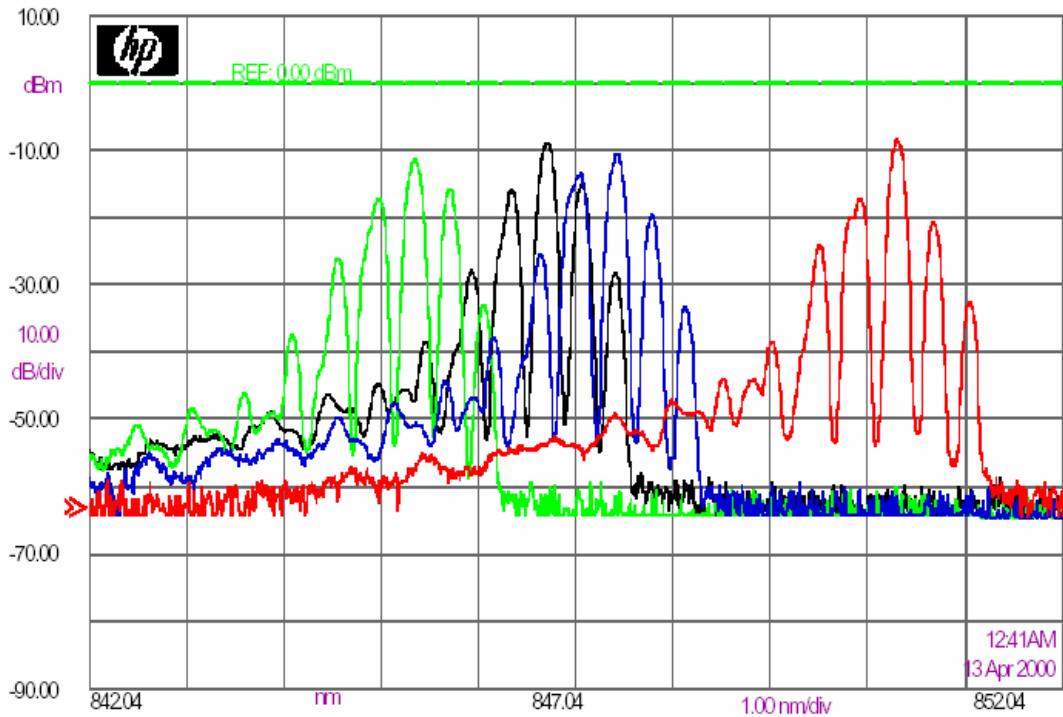
Figure 5. Optical spectrum versus temperature.

We also examined the key parameters of spectral width and wavelength distribution over several tens of devices. The wavelength distribution at room temperature ranges from 845 to 851 nm, which when combined with the temperature distribution still places us in the specification range. More importantly, the spectral width was consistently below 0.3nm FWHM for nearly every device. Note that the spectral width is a parameter which has a significant effect on the link model, dictating the maximum link length and power budget.

Transceiver chipset

Over the course of this contract, we evaluated several different chipsets, including external and internal designs. Here we comment briefly on each one of those designs and their performance highlights.

The contract was started using some prototype circuits done in silicon germanium on a shared mask with several other companies, done at no cost to us or to the contract. This gave us some confidence in some of our basic TIA and laser driver design ideas. The details of these chips' performance is detailed in Appendix E, Year Two summary.

The second generation of custom-designed parts were executed in GaAs using a standard heterojunction bipolar transistor (HBT) process from a foundry called EiC based in California. Their capabilities were well-suited to this application. The details of the chipset design, both circuitry and layout, are located in Appendix B and a broad discussion of the overall design approach is discussed in Appendix E, Year Two summary.

8

The key features of the receiver TIA/AGC integrated circuit are

- Automatic Gain Control
- DC level restore
- DC coupled signal path
- Differential inputs and outputs

- Insensitivity to PD capacitance < 0.5pF
- Minimum external components
- Portable to other bipolar technologies
- 200 mA, 5.2V operation w/ GaAs HBT process

The key features of the transmitter laser driver circuitry are

- Differential CML input
- DC coupled
- Plus and minus supply

- 40 mA supply current
- Present design runs at 5.2 V

We will comment on the performance of this chipset in more detail in the "Link evaluation" and Conclusions section below, since the operation is intimately linked to the associated optoelectronic components and packaging method.

Packaging

We have developed a complete optoelectonic component packaging system for this datalink, with the primary effort focused on designing a high-speed, low-cost hermetic package and a fiber pigtailing system. The packaging area has several facets: design of a differential microwave package and interface, design of the pigtailing method and components, construction and demonstration of apparatus and tooling to perform the pigtailing operation.

Package design

The package, as shown in Figure 6 below, consists of a metal-ceramic surface-mount microwave package (290) with a special lid (210) and ferrule-fiber assembly (144). All metal pieces are kovar and are plated with nickel and gold, the ceramic dielectric is a standard low-loss microwave material.

The electrical interface of the package is a differential design, and was fully simulated before construction. In Appendix E, in the sections entitled "Year two summary" and "Package analysis and optimization" we detail some of the studies of the package interface performance, as well as evaluate further improvements. These detailed models of the package interface are supported by laboratory TDR data and the ultimate link performance operating in the package, both in test fixtures and on soldered evaluation boards. Further details of the package and piece parts are included in Appendix A, Transmitter (and Receiver) mechanical drawings.

A photo of the final packaged parts, showing a transmitter/receiver pair soldered to an evaluation board, is shown in Figure 7 below. The package body is approximately 3x6x8mm; the pigtail ferrule and boot extend approximately 15mm beyond the lid of the package (the boot is not shown in this view). The package is soldered to the evaluation board (or any standard PC board) using standard methods.
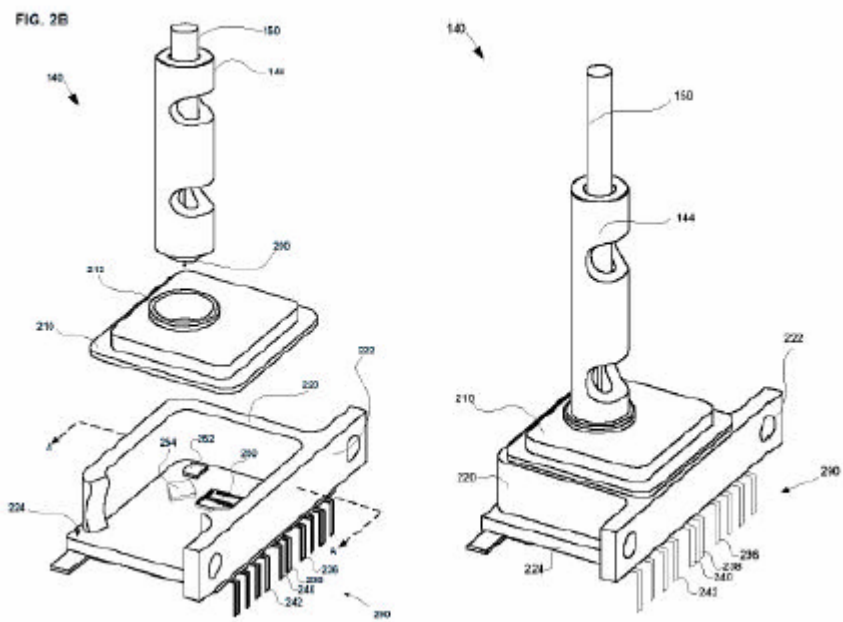
Figure 6. Outline drawing of the package assembly.
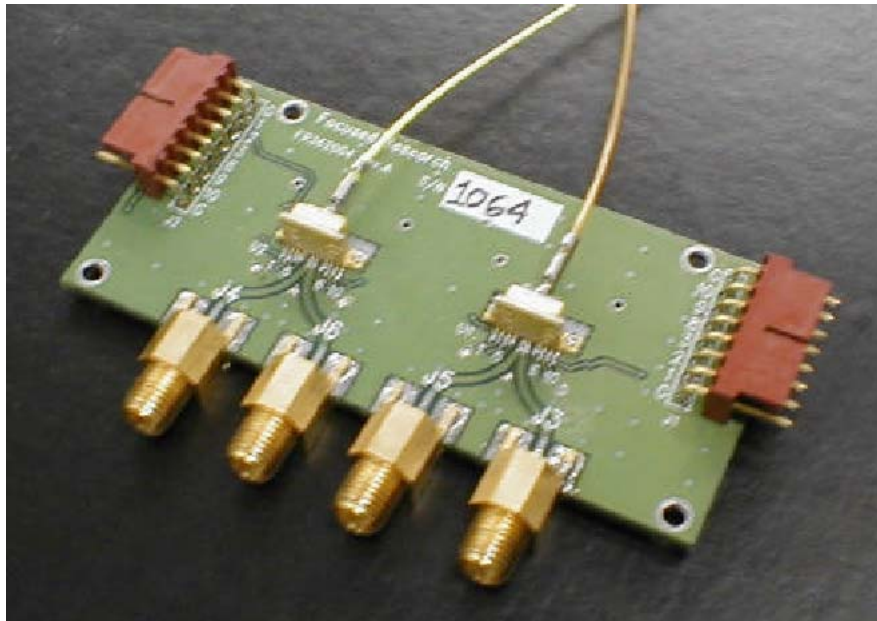
Figure 7. Evaluation board assembly.

Pigtailing method

Figure 6 above shows the three primary subassemblies of the pigtail: the ferrule, the lid, and the package with the optical and electrical components bonded inside. These three pieces are laserwelded together using a Nd:YAG laser welder.

The ferrule and fiber are mated as shown in figure 8 below, and consists of a gold-plated kovar ferrule, a gold-plated fiber tip, and solder and epoxy. The optical fiber is metalized with gold plating and soldered using traditional solder to the ferrule body, then strain-relieved with epoxy. An outer protective plastic jacket is also added and epoxied into place in the ferrule. The distal end of the fiber is connectorized with a standard FC/PC fiber.
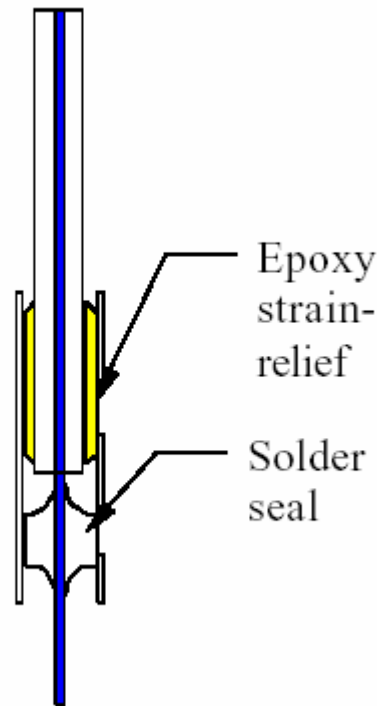

Figure 8. Detail of fiber-ferrule subassembly, showing hermetic solder seal to metalized fiber and epoxy strain relief to fiber buffer.

The lid, part 210 in Figure 6 above, is also gold-plated kovar. The lid has several features machined in it to aid in the laser welding process. The outer lip has been thinned to allow a hybrid butt-lap weld joint, which is ideal for reduced weld shift laser welding. In similar fashion a boss (feature 212 in Figure 6) has been added to the lid: this boss melts during the weld process and becomes a fillet between the lid and ferrule, adding strength to this joint.

The assembly process is shown schematically in Figure 9. Using a three-axis jig, the ferrule is roughly aligned with the device visually through a microscope or camera; the height at which contact or near-contact between the fiber tip and device is noted. The

ferrule is retracted, the lid is placed on the package, and loosely clamped by a small retractable arm. The ferrule is brought back down near the device and the lid is spot-welded in place, the ferrule-holding chuck is released and retracted, and a seam weld is performed to produce a solid lid-ferrule subassembly. The ferrule chuck is lowered and clamped for a final time and a fine alignment is made in the x-y plane to center the fiber. The lid-ferrule assembly is then tack-welded to the package body with four simultaneous spot welds. The ferrule chuck is finally retracted, and several additional tack welds are added. Finally, the package is then continuously seam-welded around its perimeter.

Note that the alignment process used for both the receiver and transmitter is fully active in that we apply a pulsed waveform and optimize the alignment of the fiber to the detector or laser. This helps to ensure that the final electrical performance is what is expected. With additional development, the alignment of the detector to the fiber could likely be replaced with a DC alignment procedure. However from our observations, it is likely that an AC alignment procedure (albeit a potentially simplified one) would be necessary to ensure good transmitter performance.

Appendix D details the entirety of the welding process, including a detailed summary of the "lessons learned" using this welding process, manufacturing data, detailed specifications of the package weld geometry and weld process parameters, process flow diagrams, and detailed operation and alignment procedures.
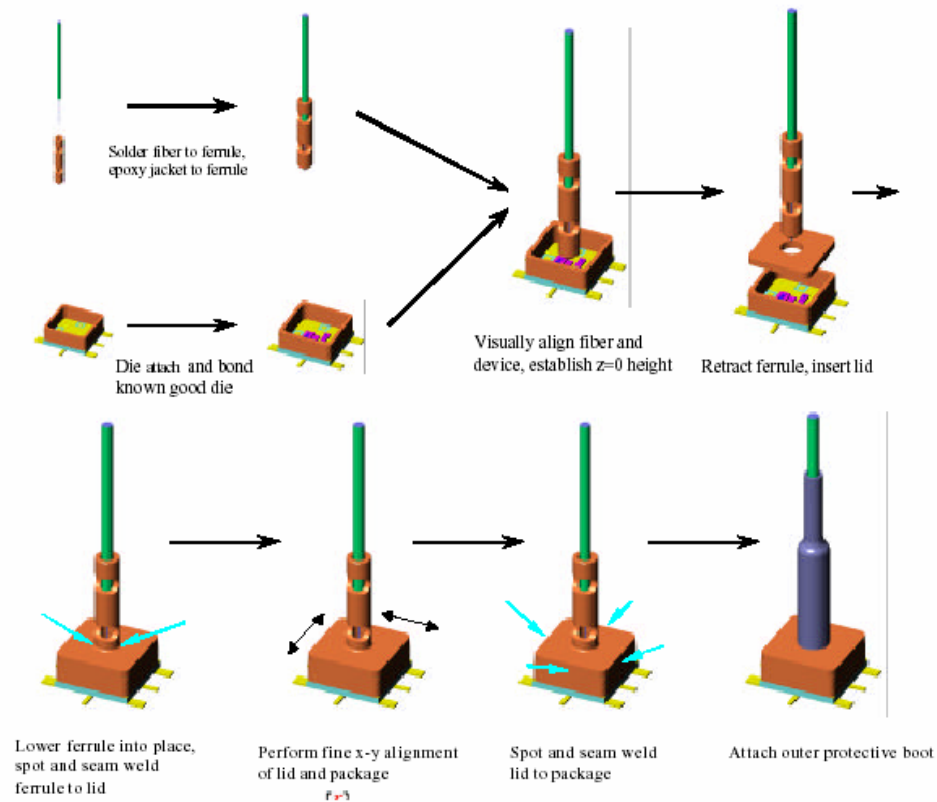

Figure 9. Assembly process sequence.

Apparatus and tooling

In the course of this program, we have built all of the tooling and machinery required to implement and develop this pigtailing process. A photograph of the complete system is shown in Figure 10 below, including not only the pigtailing robot with associated motion control stages and drivers, but also the instrumentation used to actively align the fiber and evaluate the performance of the coupling.

The system we developed uses a twelve-axis motion control system: four of these axes are for fine motion control of the fiber-ferrule with respect to the package and opto device 20 (XYZT) and the remaining eight provide two axes of motion for each of four weld heads. All twelve axes are controlled centrally by a single board DSP computer mounted in a standard industrial PC. The motion control system and stages were purchased from Aerotech, and we integrated into them a working robot as well as wrote the control software. The industrial PC also controls the laser welder. The result is a semi-automated system in which all welding processes are automated, and the operator interacts to load and unload parts, as well as to perform the fine alignment adjustments.
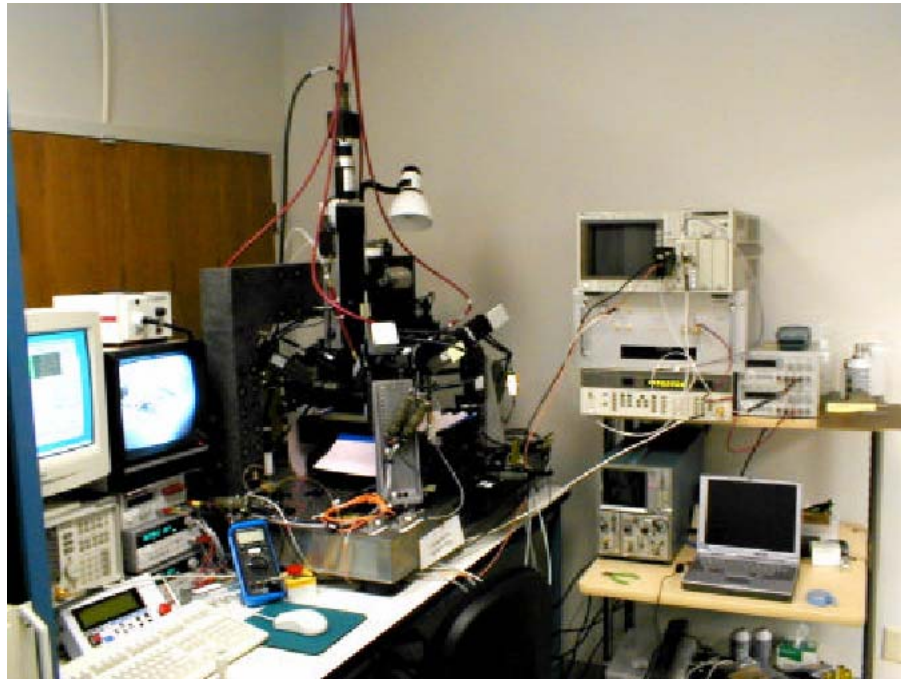

Figure 10. Photograph of the package pigtailing workstation.

In Appendix C we show detailed assembly and part drawings for the laser welder robot and integral microwave package nest, as well as the tooling used to assemble the fiber-ferrules. Appendix E, Year one summary, also highlights the subassemblies of the laser welder robot.

Link evaluation

Through the course of this and follow-on work, we evaluated the overall performance

of about 100 module pairs. For most of these modules, we compared the performance was against our final specification, which is listed in detail at the beginning of Appendix A. This specification represents an evolution of our original specification towards an industry-standard specification, through our work with the IEEE 802.3 10 Gig Ethernet standards committee and with the Optical Internetworking Forum.

The transmitter performance reflects the capabilities of the VCSEL themselves, the transmitter chipset, and the quality of the alignment. The VCSELs tested alone have shown adequate performance characteristics except in that they show long fall times (>40 ps) and a drop in output power at elevated temperature. Furthermore, these measurements are necessarily a limited sample set since our supplier provided all of our VCSELs from a single developmental wafer.

When integrated with a driver chip, we noted that the extinction ratio of the VCSELs was limited to about 6 dB, the risetime was good (35-40ps), the fall time was poor (~50ps), and the total jitter was in the 35-40ps range. These translated into a high proportion of eye mask failures. However, the eye mask that we were using represented the Gigabit Ethernet eye mask, scaled to 10Gb/s, which is overly aggressive. Later measurements using a newly proposed, relaxed eye mask (shown in Appendix A) showed a much higher fraction of the devices complying with the mask.

The GaAs chipset we used to build nearly all of the transmitters suffered from a flaw that rendered the optical feedback circuit inoperable. If operating, this circuit uses a large-area photodiode to sample some of the light from the output of the VCSEL that is not coupled into the fiber tip to control the output of the VCSEL, thus compensating for changes in temperature and aging of the VCSEL. The repaired chipset did not arrive in time to fully evaluate it, but careful modeling of the optical/electrical train showed that it should be capable of maintaining the overall output power within approximately 1dB, while maintaining the waveform extinction ratio, and across various manufacturing variations. Without this feature operating, the output of our transmitters varied from –1 to –4 dBm, mostly due to manufacturing variations and variations in the LIV curves of the VCSEL.

The receiver modules meet all of the required specifications except for overall sensitivity and fall times. The poor fall time was obscured by the transmitter's poor fall times and the risetime of the transmitter has to be deconvolved. Unlike long-wave (1.55µm) applications, no reference transmitters with known high performance currently exist at 850nm.

The low sensitivity in these devices reflects both the improper AR coating on the diode (account for about a 30% degradation in responsivity) and the limited speed performance of the EiC HBT process. Experiments with an outside vendor's TIA (which uses a different GaAs process) and our photodiode demonstrated sensitivity of about –12 dBm (required spec is – 13dBm), but this chipset did not have sufficient overall gain to warrant it's use in this module. With a proper AR coating for the photodiode and an improved foundry, the receiver circuit design should be able to meet the sensitivity specifications.

Together, both receiver and transmitter combined as a system, we measured a

sensitivity of approximately –12.5 dBm at 10Gb/s with a 2_{15}-1 PRBS and 10_{-12} BER. We feel that with a proper photodiode AR coating, access to a high-performance foundry to fabricate the Tx and Rx (which would improve both noise and bandwidth), this link should be able to achieve –13dBm sensitivity and meet all of the other required specifications.

Conclusions

We have successfully developed a physically compact, low-power consumption shortwave serial datalink capable of sending data at 10 Gb/s over multimode optical fiber. Our datalink meets nearly all of the required performance specifications we originally set out to meet. During this development, we learned several lessons regarding our approach and technology.

At the outset of this program in 1997, shortwave (850nm) VCSELs capable of operating at 10 Gb/s were just becoming available as laboratory samples. We tested many of these devices and developed a mature set of specifications for these devices. Currently, several manufacturers are making devices capable of meeting these specifications; at least three will sell the devices directly, and several others manufacture them for their own transceiver modules. Early this year, at least three manufacturers have announced the availability of long-wave (1300 nm) VCSELs capable of being modulated at 10 Gb/s.

The early devices we tested suffered from defects typical of early developmental devices, including poor metal adhesion (which hampered building prototypes because they were exceedingly difficult to bond to), insufficient bandwidth, and varying differential resistance from lot to lot. We eventually located a supplier (there are now at least two) who could meet our specifications and produced usable devices; these were used to build several hundred prototypes. These devices met nearly all of our specifications, falling short by having marginal fall times and barely sufficient rise times.

Although no extensive development of photodiodes was done in this program, we did fabricate photodiodes that were optimized for this application (with large area, sufficient speed, and sensitivity at short wavelengths). A poor AR coating design hampered the ultimate link sensitivity. After most of the prototypes were built and tested, we were able to fab another round of diodes with an optimized coating.

Early in the program, the first laser driver and receiver chipset was fabricated in IBM's SiGe process, which at the time (1997) has just become available on a very limited basis. These first devices demonstrated the soundness of the overall circuit designs, especially the high-gain AGC plus TIA combination, which with 10 GHz of electrical bandwidth and 14 dB of dynamic range, is the first such circuit of its type to be fabricated. These chips also enabled us to construct our critical first prototype and demonstrate the soundness of our differentially driven input and output.

Our next generation of transceiver chipset was fabricated using a GaAs HBT process, primarily because of the low cost and ready availability. This chipset was used to construct most of our prototypes. The transmitter driver had a differential input and is capable both of modulating the VCSEL current at high speed as well as regulating the DC drive current

through automatic power control (APC). The APC circuit is a unique design with high gain, and uses light collected from an external photodiode to regulate the current provided to the VCSEL.

The receiver chip contained both a transimpedance amplifier (TIA) and automatic gain control (AGC). The TIA was designed to function well even when loaded with a capacitive photodiode input, and the AGC has a broad range of gain to provide sufficient dynamic range and sensitivity. The vendor's HBT process provided transistors with just enough gain-bandwidth product to build a high-gain receiver such as this and was capable of meeting our power dissipation requirements. It expected that future manifestations of this design would be fabricated in SiGe, which would improve the frequency and noise performance as well as further lower the power consumption; the laser driver could also be designed to utilize a single power source. Near the end of the contract period, several commercial vendors of laser drivers and TIA started to become available as well.

The package we developed was based on a standard metal-ceramic microwave package. We modified this design to accommodate a differential electrical interface that is capable of operating on its edge. To this we added an optical fiber pigtail interface, which is fully hermetically sealed. The resulting package is indeed tiny, 3x6x8 mm, and can be soldered as a surface-mount component to a PC board.

To support the fabrication of these devices, a semi-automated robotic welder and associated tooling were constructed which allows a fiber pigtail to be aligned with the optical element and to be permanently fixed in place using a laser welding process. This tooling allows the performance of the VCSEL or photodiode to be continuously monitored at full speed while the fiber is being aligned and welded. The robot and tooling has been shown to be robust enough to build several hundred modules, and we have shown a cycle time of less than 30 minutes. We also demonstrated that the tolerances of our design are sufficient to achieve good yield.

The packaging portion of this project turned out to be one of the most challenging. One goal of this effort was to eliminate one layer of packaging by performing the alignment and sealing of the package in the same step without additional component parts. The fiber, lid, and package are brought into alignment, spot welded into place to hold their alignment, and then seam-welded afterwards using the laser. This final seam weld after the parts are in alignment is challenging not only because it must preserve the alignment of the pieces, but also must achieve hermeticity. We eventually achieved holding the alignment during seam welding, but in order to get a reliable hermetic joint, the gold must be removed from the joining surfaces.

The other challenging aspect of the package was cost. Even in high volume (10,000 units), the cost of the metal piece parts, especially the package, metalized fiber for soldering, fiber lensed-end treatment, and machined lid with selective plating, made it difficult to meet our original cost target of $200.

Putting all of these elements together, we successfully built and demonstrated several hundred operational datalinks. During the testing of these parts, most of the performance space was explored and evaluated, including temperature, manufacturing variation, and using a variety of component pieces. Ultimately we were unable to reach our final

sensitivity goal of −13 dBm at 10 Gb/s, but came very close with −12.5 dBm and identified two key areas for improvement: proper AR coating of photodiode (easy) and choosing an IC foundry with slightly higher performance (costly but doable) or using a commercially available chip.

During the course of this effort, several industry organizations have come to embrace the shortwave VCSEL-based solution, aided in part by this contract and our efforts in those organizations. The IEEE Ethernet standard 802.3 adopted this transceiver approach as one intended to meet the 300m distance objective with low cost. The Optical Internetworking Forum has also adopted a similar specification for VSR (very short reach, 300m) device interconnections at 10 Gb/s in SONET/SDH applications. The Fiber Channel standard, which is widely used in storage area networks, is also seriously considering this specification.

This standards activity has also led, in part, to two other important industry milestones. The eye safety limit (which was influenced by, but not directly driven by these efforts) was relaxed by the CDRH and FDA, giving welcome relief to the shortwave requirements especially, allowing the sensitivity requirement to rise to −13 dBm from approximately −16 dBm. The high bandwidth multimode fiber required for operation of this link up to 300 meter distances has been standardized (within the EIA/TIA). At least three manufacturers are shipping fiber that is expected to meet this specification.

This has been a challenging and interesting effort overall, and definitely worth the time and resources dedicated to it both from DARPA and Focused Research. Not only have we built, demonstrated, and delivered working prototypes of the datalink, that meet the performance guidelines of the original OMNET program, but these efforts have enabled us to strongly influence industry standards to adopt this technology. The cost target has proven difficult, and could probably be met with a non-hermetic or modified packaging design. Several manufacturers are now building components and systems to meet these standards.

Appendices

Product literature

10-Gb/s VCSEL-based transceiver

These 10-Gb/s transmitters and receivers are ideal for cost-effective, multimode, fiberoptic links between network equipment within a central office. These transceivers feature extremely small form factors and low power consumption with telecom quality, reliability, and performance. The transmitter includes a directly modulated 850-nm VCSEL (vertical-cavity surface-emitting laser) with laser driver circuitry and automatic power control; the receiver includes a transimpedance amplifier with automatic gain control (AGC) and DC restoration. The units use a differential CML electrical interface.

Selected Applications

- **VSR (very short reach) links (≤ 300m)**
- **OC-192 central office interconnect**
- **back-plane/proprietary link**
- **10 G Ethernet**

19
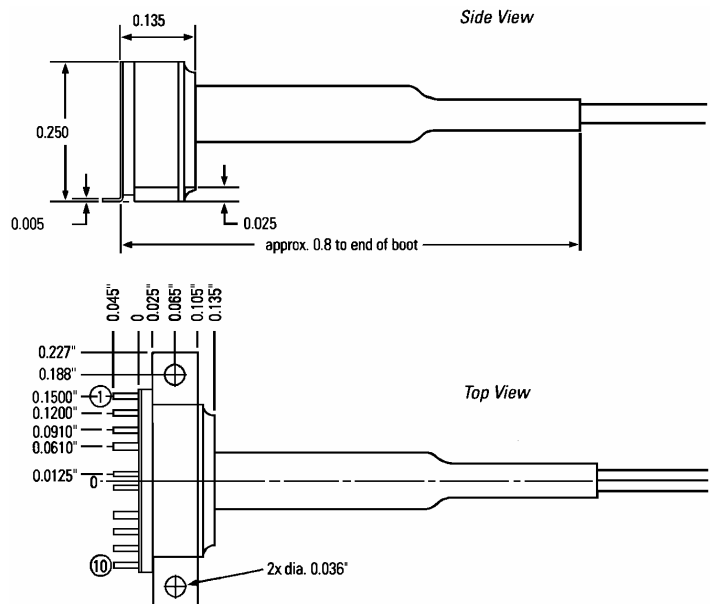
10-Gb/s VCSEL-based transceiver

Absolute Maximum Ratings

Parameter	Units	Minimum	Maximum
Storage Temperature (case temperature)	°C	–40	100
Operating Temperature (case temperature)	°C	0	80
Supply Voltage	V	–7.0	0.5
Data-Input Voltage	V	V_{ee}	0.5
Transmitter Differential Input Voltage	V		0.9
Transmitter Output Current	mA		10
Operating Relative Humidity	%	5	95

Transmitter Optical Characteristics

Parameter	Units	Minimum	Nominal	Maximum
Wavelength	nm	820	850	860
Spectral Width	nm	0.2		0.5
Coupled Output Power	dBm	–5		–2
Optical Rise/Fall	ns			0.045
Deterministic Jitter	%(p-p)			20
Relative Intensity Noise (RIN)	mA			–125
Extinction Ratio	db	4	5	6
Fiber Core/Cladding	µm		50/125	
Fiber Range	m			300*

Depends on fiber type. This spec is based on 2000MHz-km 50/125 µm multimode fiber.

Transmitter Electrical Characteristics

Parameter	Units	Minimum	Nominal	Maximum
Line Rate	Gb/s			10.6
Data-In Sensitivity **	mV	200	500	
V_{cc} Power Control Bias	V	4.75	5	5.5
V_{cc} Supply Current	mA		10	20
Circuit Bias(V_{ee})	V	–4.7	–5.2	–5.7
Vee Supply Current	mA		30	40

***These are peak-to-peak single-ended values. Transmitter input and receiver output are differential.*

Receiver Optical Characteristics

Parameter	Units	Minimum	Nominal	Maximum
Wavelength	nm	770	850	860
Input Power (10–13 BER)	dBm	–11		
Optical-Return	dB	12		
Fiber Core/Cladding	µm		62.5/125	

Receiver Electrical Characteristics

Parameter	Units	Minimum	Nominal	Maximum
Data Rate	Gb/s			10.6
Bit-Error Rate (BER)				1×10^{-13}
Data-Out Rise/Fall	ns	−5		−2
Data-Out Load	Ω		50	
Data-Out Voltage Swing***	mV	100	125	300
Circuit Bias (V_{ee})	V	−4.7	−5.2	−5.7
V_{ee} Supply Current	mA		200	

*These are peak-to-peak single-ended values. Transmitter input and receiver output are differential.

Transmitter Schematic
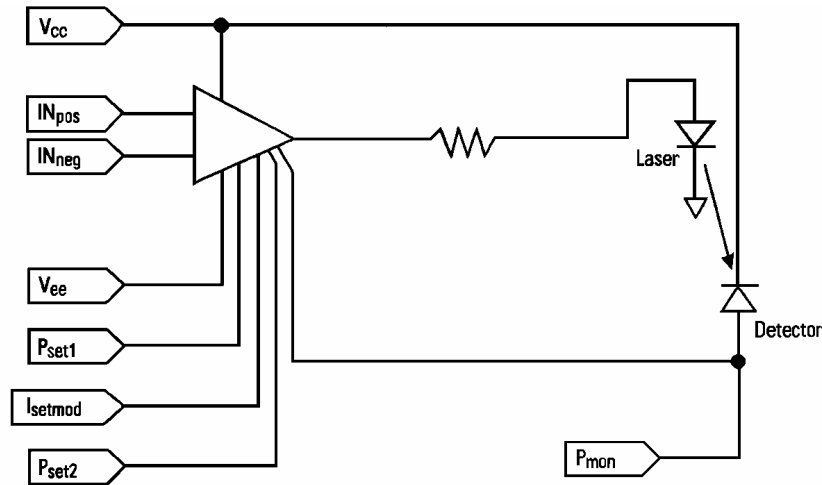
Transmitter Pin-Out

Pin Name	Pin Number	Function
P_{mon}	1	*Power monitor* is connected to the monitor photodiode and provides a signal from 0 to –3.5 V, indicating laser output power vs. set point. A capacitor connected to this point sets the automatic power control loop bandwidth.
I_{setmod}	2	*Laser modulation current* is an input for a programming resistor to ground for setting the laser modulation current. Approximate programming resistor value is 5 k for 10-mA modulation.
V_{ee}	3	*Negative power* supply that powers the high-speed circuitry
GND	4,7	*Signal ground.* Both ground pins are connected to the circuit ground and to the case ground.
IN_{neg}	5	*Negative* differential high-speed signal input
IN_{pos}	6	*Positive* differential high-speed signal input
P_{set2}	8	*Laser power set reference* is an output for providing a stable voltage for the Pset1 programming current.
P_{set1}	9	*Laser power set* is an input for a programming resistor that is connected between this pin and Pset2 to set the average laser power. Approximate programming resistor value is 50 k. This pin can also be switched to V_{ee} to disable the transmitter.
V_{cc}	10	*Positive power supply* powers the DC-laser control circuitry. The positive supply allows the use of commonly available cathode-grounded VCSELs.

Receiver Schematic
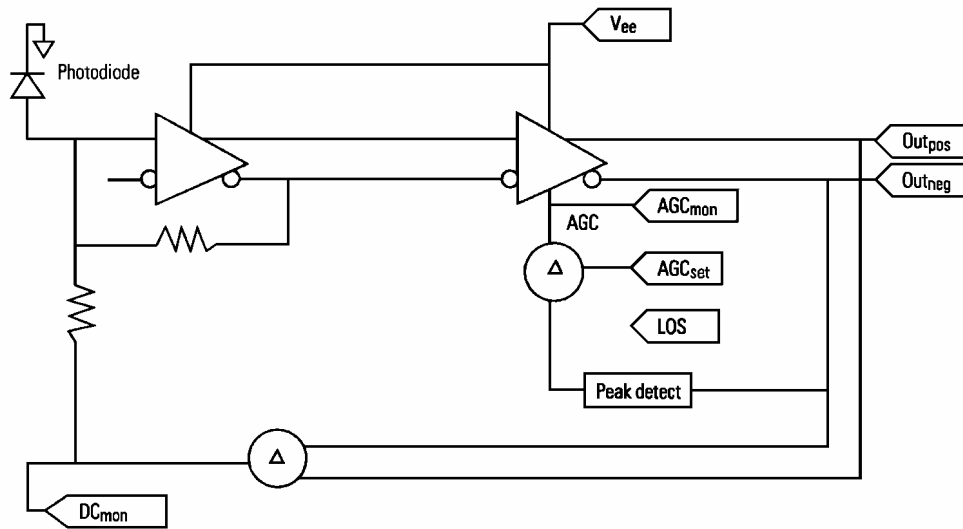
Receiver Pin-Out

Pin Name	Pin Number	Function
DC$_{mon}$	1	*DC-restore monitor* is connected to the signal that adjusts the input stage bias to cancel out the output DC photocurrent. A capacitor to ground from this pin will set the DC-restore time constant (see notes below).
AGC$_{mon}$	2	*AGC monitor* is connected to the signal that controls the AGC gain. A capacitor to Vee from this pin will set the AGC time constant (see notes below).
V$_{ee}$	3	*Negative power* supply for the stages
GND	4,7	*Signal ground.* Both ground pins are connected to the circuit ground and to the case ground.
OUT$_{neg}$	5	*Negative* differential high-speed signal output
OUT$_{pos}$	6	*Positive* differential high-speed signal output
LOS	8	*Loss of output signal*
AGC$_{set}$	9	*AGC setpoint* is an input pin for setting the output-signal swing

Proper use of this receiver will require attention to the following details:

• The differential outputs are designed to drive a differential 50-Ω load. That is, each of the two high-speed output pins expects to see 50 Ω to ground. For the AC signal, this could mean two isolated "single-ended" 50-Ω lines, or a single "balanced line" with 50-Ω impedance from each terminal to a virtual ground. For DC biasing, the proper load is also 50 Ω to ground from each pin.

• The AGC**set** pin is provided to allow selection of the output-signal swing. The specifications are achieved with a 0.5-mA current sink connected to this pin. A nominal value of 5.7 kΩ to –5.2 V will achieve the same result but will make the output-signal swing stability dependent on the stability of the –5.2-V power supply. This pin should be bypassed to ground with at least a 0.001-µF surface-mount ceramic capacitor.

• The DCmon and AGCmon pins are provided to allow monitoring of the DC-restore and AGC loops respectively. Additional capacitance may be added to these pins to control the low-frequency pole of the two control circuits. The DC-restore pole is computed according to $f=1/(2\pi(C+80pF)\times760)$. The AGC pole is computed according to $f=1/(2\pi(C+80pF)\times280)$.

• The power dissipation of this part is approximately 1 W. The body should be bolted to the PC-board in a region that provides good heat transfer and good RF grounding for EMI reduction.

Transmitter assembly drawings

REV	REV DESCRIPTION	DRAWN	APP'D	D

SCALE 1:1
FERRULE BOOT PULLED BACK

DETAIL A
SCALE 5 : 1
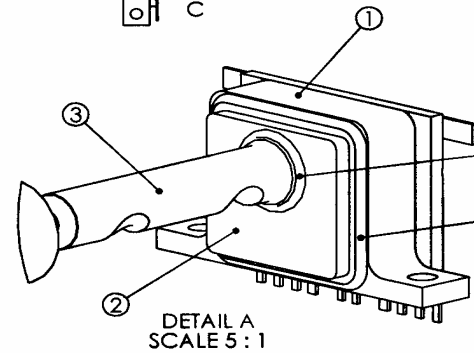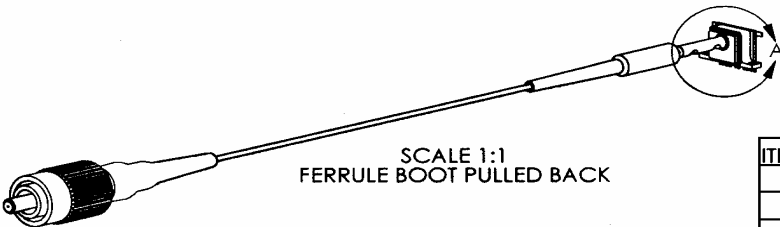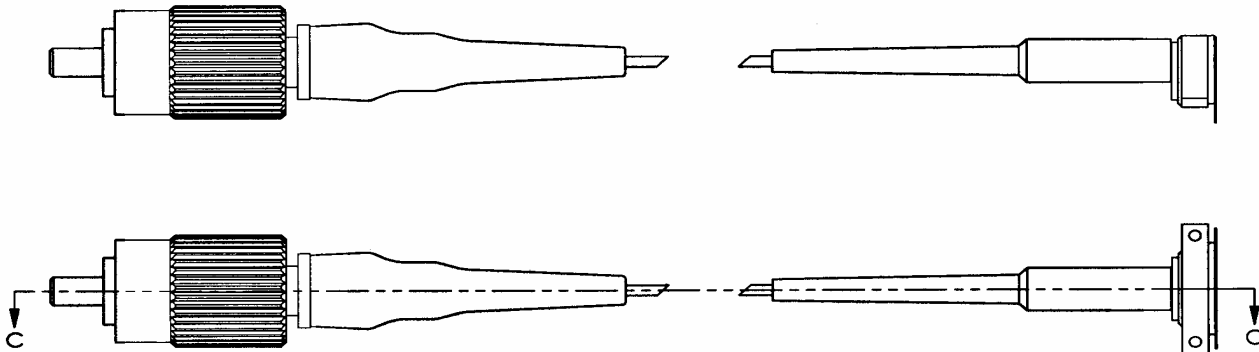
ITEM NO.	QTY.	DESCRIPTION	PART N
1	1	Tx Bonded Subassembly	ZW013
2	1	Differential Package Lid	ZW011
3	1	Tx Connectorized Ferruled Fiber	ZW011
4	1	laser weld (ferrule)	
5	1	laser weld (lid)	

MATERIAL AS NOTED	FINISH		SCALE 2:1	DESC Welded Module Tx (ZW0104)	

[r] FOCUSED RESEARCH, INC
MADISON, WISCONSIN

©2000 FOCUSED RESEARCH INC.

TOLERANCES:	UNLESS OTHERWISE SPECIFIED:		
.XX ± .005	DIMENSIONS ARE IN INCHES.		
.XXX ± .001	TOLERANCES PER ANSI Y14.5M 1982		
.XXXX ± .0005	AND NFI SPEC 01-004.		
ANGLES ± 1°	THIRD ANGLE PROJECTION		

DRAWN JJC	CHK'D RCN	DATE 9/18/00	PRO
FILE NAME Welded Tx Module [FR365025]			
DWG NO. FR365025		REV. A	SH

Receiver assembly drawings

SCALE 1:1
FERRULE BOOT PULLED BACK

DETAIL A
SCALE 5 : 1

ITEM NO.	QTY.	DESCRIPTION	PART NO.
1	1	Rx Bonded Subassembly	ZW0135
2	1	Differential Package Lid	ZW0114
3	1	Rx Connectorized Ferruled Fiber	ZW0142
4	1	laser weld (ferrule)	
5	1	laser weld (lid)	

MATERIAL AS NOTED

FINISH

SCALE 2:1

DESC Welded Module   Rx (ZW0103)

TOLERANCES:
.XX ± .005
.XXX ± .001
.XXXX ± .0005
ANGLES ± 1°

UNLESS OTHERWISE SPECIFIED:
DIMENSIONS ARE IN INCHES.
TOLERANCES PER ANSI Y14.5M 1982
AND NFI SPEC 01-004.

THIRD ANGLE
PROJECTION

(r) FOCUSED RESEARCH, INC
MADISON, WISCONSIN
©2000 FOCUSED RESEARCH INC.

DRAWN JJC   CHK'D RCN   DATE 9/14/00   PROJ.ENGR JJC

FILE NAME
Welded Rx Module [FR365024]

DWG NO. FR365024   REV. B   SHEET 1 OF 2

Application Note for H6121-02B:
10 Gb/s Transceiver Evaluation Board
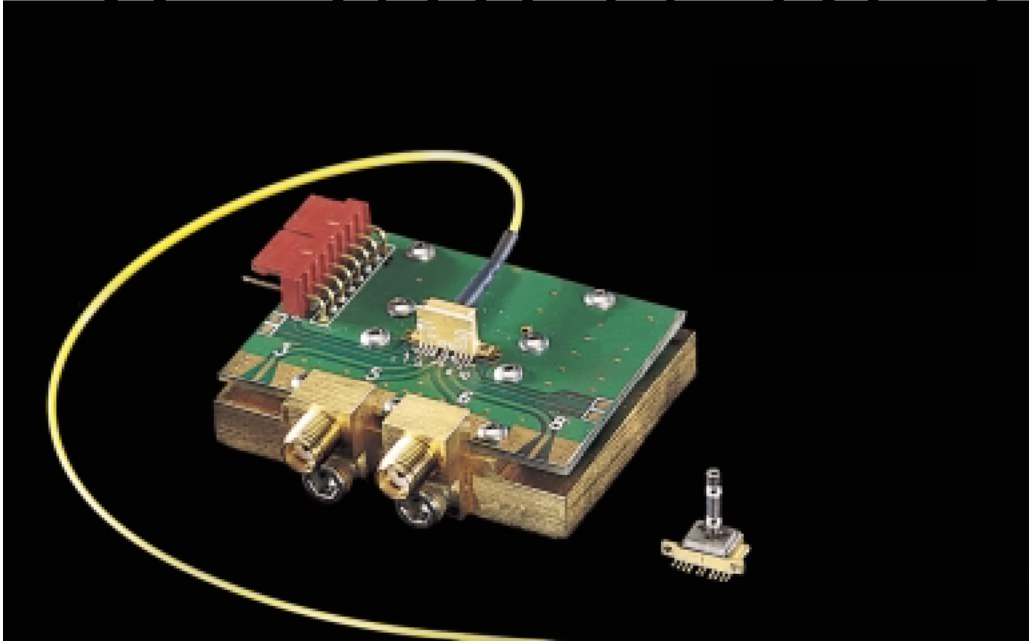
Overview

The H6121-02B is an evaluation board containing a complete New Focus 10 Gb/s transceiver, consisting of transmitter module H6101-02 and receiver module H6111-02. The board is an easy-to-use platform for evaluating these parts, providing easy access to the high-speed differential inputs and outputs and to the DC power connections.

This document provides information for using the New Focus H6121-02B, 10 Gb/s Transceiver Evaluation Board. Described here is the evaluation board layout, connections, and required power considerations. This document also illustrates the general procedure for performing bit error rate (BER) testing and includes sample eye diagrams taken using this transceiver. Additional information about the transceiver components is contained in the separate datasheet .10-Gb/s VCSEL-based transceivers.. These transceivers are still under development. Final performance specifications are not being met on all parameters and may vary from sample to sample.

Evaluation board description

This section provides a description of the evaluation board connections. The overall mechanical board layout is shown in Figure 1 with positions of the mounting holes given as coordinates from the lower left corner of the PCB. Two standard 8-pin headers (right angle, 0.1 inch centers) are provided to apply power, and four SMA board-edge connectors provide high-speed access to the differential inputs and outputs.
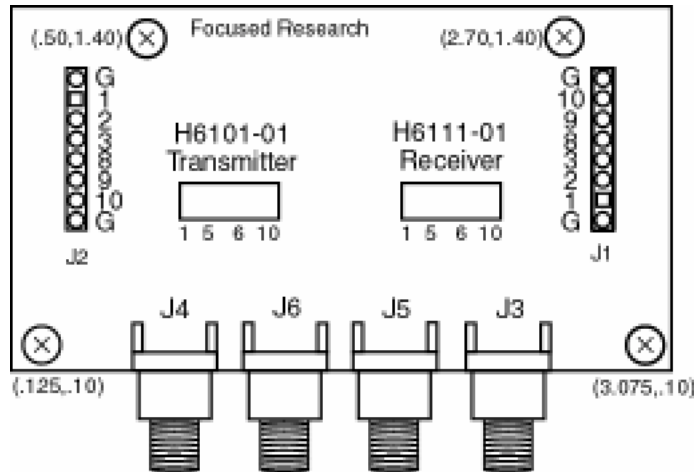
Figure 1: Evaluation board layout (top view)

Table 1: Transmitter DC connector J2 pinout

Pin Number	Pin Name	Function
1,2,8,9	Not connected	Reserved for future use.
3	VEE	*Negative power* supply, -5.2 V nominal. Operates high-speed circuitry
10	VCC	*Positive powe*r supply, +6.0 V nominal. The positive supply biases the cathode-grounded VCSEL.
G	GND	*Signal ground*. Both G pins are connected to ground

Table 2: Receiver DC connector J1 pinout

Pin Number	Pin Name	Function
1,2,8,9	Not connected	Reserved for future use.
3,10	VEE	*Negative power* supply, -5.2 V nominal
G	GND	*Signal ground*. Both G pins are connected to ground

Table 3: High-frequency SMA connections

Connection	Signal Name	Function
J4	INneg (Tx)	Differential CML input
J6	INpos	Differential CML input
J5	OUTneg (Rx)	Differential output, dc-terminate with 50-ohms to ground
J3	OUTpos	Differential output, dc-terminate with 50-ohms to ground

Operation and board configuration

The SMA connections, J3-J6, should be first connected to the respective test equipment through high-quality coaxial cable. Note that the receiver's differential output (J5 & J3) requires a DC 50-ohm connection for proper operation. The transmitter's inputs can be DC- or AC-coupled to the 50-ohm differential serial data source.

Power for Vcc and Vee can be applied simultaneously to both receiver and transmitter if desired, but the power buses for the receiver and transmitter are kept separate. Typically, Vee (Rx) is 190mA, Vee (Tx) is 30mA, and Vcc (Tx) is 20mA. Due to the AGC amplifier operation, the RX Vee current draw can be anywhere between 160 and 210mA depending on input signal level.

All DC pins of both the receiver and transmitter package are decoupled near the package module with 0.1uF capacitors.

On the transmitter, a 27kΩ resistor is attached between module pin 8 to pin 9 to set the average laser power output. A 5kΩ resistor has also been included from module pin 2 to GND to set the laser modulation current.

On the receiver, a 10kΩ. resistor is placed from module pin 2 to ground. A 5kΩ resistor from module pin 9 to Vee sets the nominal output level voltage swing to 180mV$_{p-p}$.

Bit Error Rate Testing

This section describes the basic test setup for performing BER testing using the evaluation board. The basic configuration is shown in Figure 2. The specific equipment that was used for our measurements is provided in Table 4. Sample eye diagrams at 10 Gb/s using a $2x10^7$-1 pattern are shown for four relevant power levels in Figure 3. All eye diagrams were taken using 300m of 850-nm optimized high-bandwidth multimode 50/125 μm fiber.
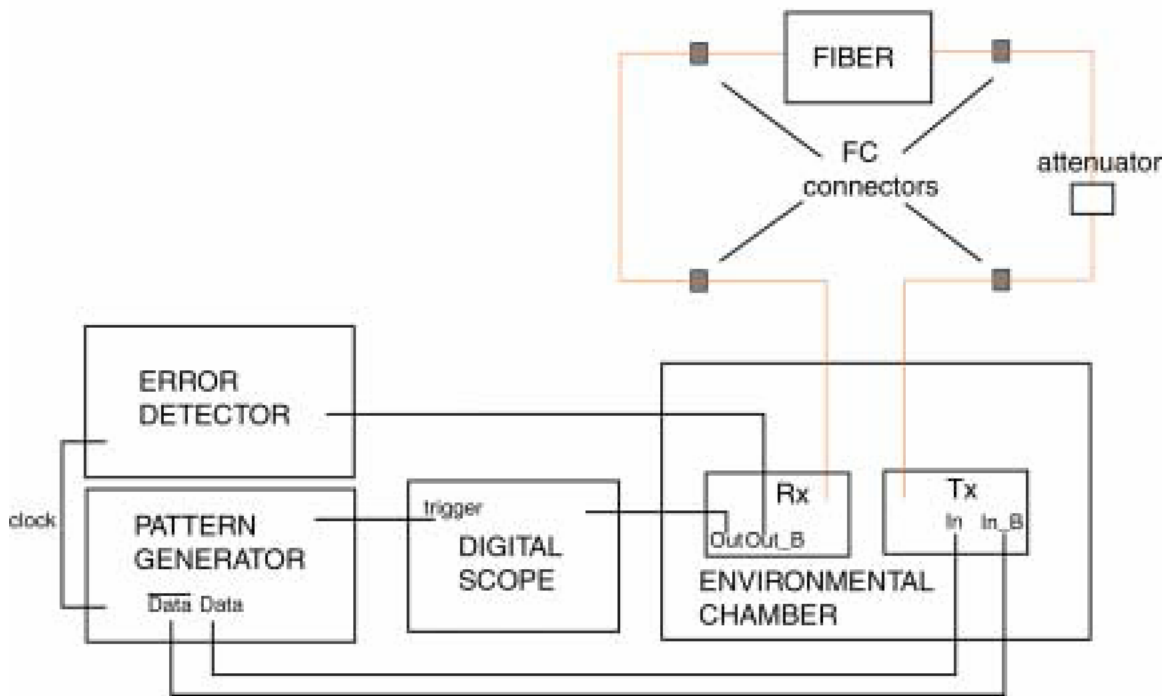
Figure 2: BER Test Setup

Table 4: Equipment used for generating sample BER test data

Part	Model	Description
Error Detector	Anritsu MP1764A	Compares the signal from the pattern generator to the output of the receiver to determine the number of errors that have occurred.
Pattern Generator	Anritsu MP1763B	Generates the pattern for the transmitter.
Digital Scope	HP 54750A	Allows the operator to monitor the testing.
Environmental Chamber	ESPEC ECT-2	Provides a constant, controllable environment for testing the part performance.
Fiber	Fiber 50/125 ∝m MM, Lucent LazrSPEED	Allows the bit error rate to be tested over full distance range. The length used for this data was 300m.
Attenuator	JDS MV40	Allows the power at the receiver to be varied.
Power Supply	HP E3630A	Provides power to the receiver and transmitter (not shown in diagram).
Amplifier	PSPL 5828	Depending on the sensitivity of the error detector, an amplifier on the error detector input may be required.

0 dBm: Receiver overload power condition.   **-5 dBm:** Minimum transmitter power
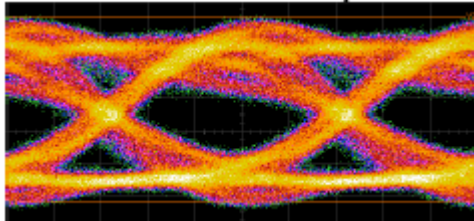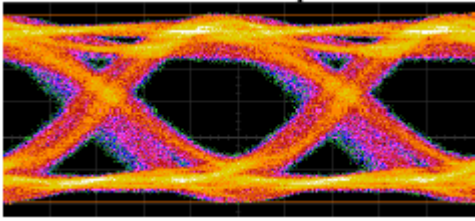
-2 dBm: Maximum transmitter power.   **–8 dBm:** Measured at RX.
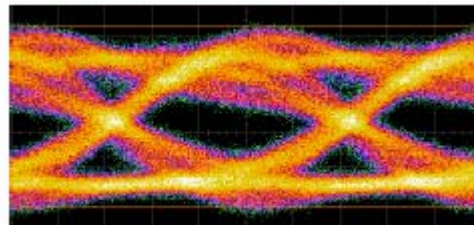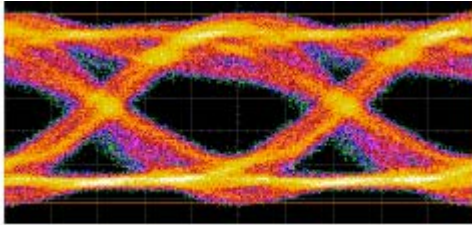
Figure 3: Sample eye-diagrams measured with 300-m fiber and test set-up described above. Error free operation was observed down to –8dBm where this sample is limited due to RX eye-closure.

Sales and ordering information:

Part Description	Part Number
Evaluation Board with Transmitter and Receiver, 50/125	H6121-01B
Stand-alone Transmitter, 50/125 ∝m fiber	H6101-01
Stand-alone Receiver, 50/125 ∝m fiber	H6111-01
Evaluation Board with Transmitter and Receiver, 62.5/125	H6121-02B
Stand-alone Transmitter, 62.5/125 μm fiber	H6101-02
Stand-alone Receiver, 62.5/125 ∝m fiber	H6111-02

For additional information, please call:

Herman Chui
New Focus, Inc.
2630 Walsh Avenue
Santa Clara, CA
95051-0905 USA
Phone: 408-980-8088 x367
Fax: 408-919-2776
Email: hchui@newfocus.com
Web: http://www.newfocus.com

Appendix B - Tooling documentation

Welder Robot Tooling

Welder drawing index

Drawing Name.	Drawing No.
Welder motion control block diagram	
Welder assembly drawing	FR360011A
Granite structure	
Base	FR360003G
Gantry Riser	FR001034C
Gantry Bridge	FR001035B
Stages	
Cable Relief Slot for theta-stage	FR001040B
Ferrule Holder assembly	FR001091B
Stirrup Rod	FR001063A
Actuator Rod	FR001064A
Counterweight Bar	FR001065A
Collet Mount Block	FR001066B
Collet Load Block	FR001067B
Ferrule Collet (ver. 2)	FR001068-2A
Stirrup Plate	FR001062A
Collet Clamp Sleeve	FR001069A
Ferrule Holder Baseplate	FR001072A
Ferrule Chuck Counterweight	FR180005B
Vertical Focus Stage assembly	FR360012A
Assembly Instructions	FR360006A
Granite Pillars for Laser Heads	FR360004D
Mounting Wedge for Focusing Stages	FR360002H
STD Miyachi Weld Head Bracket	FR001041B
Video Microscope assembly	
Video Microscope Clamp Plate	FR001047A
Package Nest Holder assembly	FR360014A
Diff Package Mount Plate	FR001049F
Ferrule Rest	FR001090B
Cover Hold-Down Swing Arm	FR001087D
Lid Hold-Down Load Arm	FR001088C
Cover Hold-Down Spring	FR001086A
Modified Thumbscrew	FR180004A
Accessories	
FO Connector Bracket	FR183026A
Gas Flow Regulator Bracket (ver. 2)	FR180021A
SMA Flex-Cable Bracket	FR180006A
Welder Control Rack	
Opto 22 Chassis Plate	FR184001A
Opto 22 Back Plate	FR184002A

Welder robot drawings

Welder motion control block diagram

REV	REV DESCRIPTION	DRAWN	APP'D	DA

MATERIAL		FINISH		SCALE 1:8	DESC Welder II (for layout)			

TOLERANCES:
.XX ± .005
.XXX ± .001
.XXXX ± .0005
ANGLES ± 1°

UNLESS OTHERWISE SPECIFIED:
DIMENSIONS ARE IN INCHES.
TOLERANCES PER ANSI Y14.5M.1982
AND NFI SPEC 01-004.

THIRD ANGLE
PROJECTION

FOCUSED RESEARCH, INC
MADISON, WISCONSIN

©2000 FOCUSED RESEARCH INC.

DRAWN DH   CHK'D   DATE 9/12/2000   PROJ ENG DH

FILE NAME
Overall Welder II Layout [FR360011]

DWG NO. FR360011   REV. A   SHEET 1

SCALE	SIZE	DWG NO.	REV.	SHEET
1:5	A	FR360011	A	
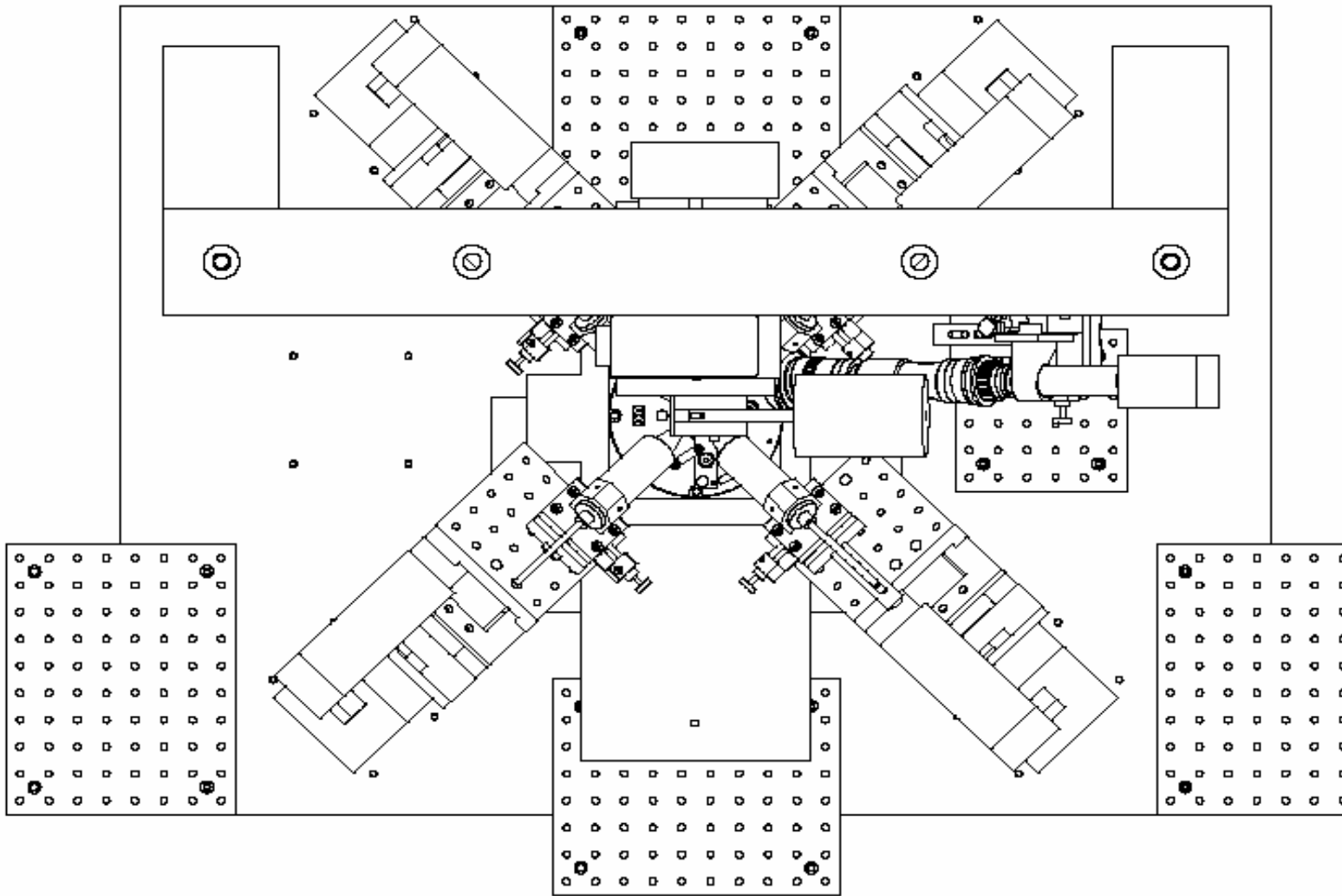
SCALE 1:8	SIZE A	DWG NO. FR360011	REV. A	SHEET 3

ATS0300

FR360004D

FR360002H

ATS0300

Ferrule assembly tooling

Ferrule clamp
(spring-loaded)

Ferrule

Fiber clamp

Centering tool

Fiber

V-groove ferrule-
holding block

Rack and pinion
sliding carriage
(with adjustable stop)

Adjustable stop
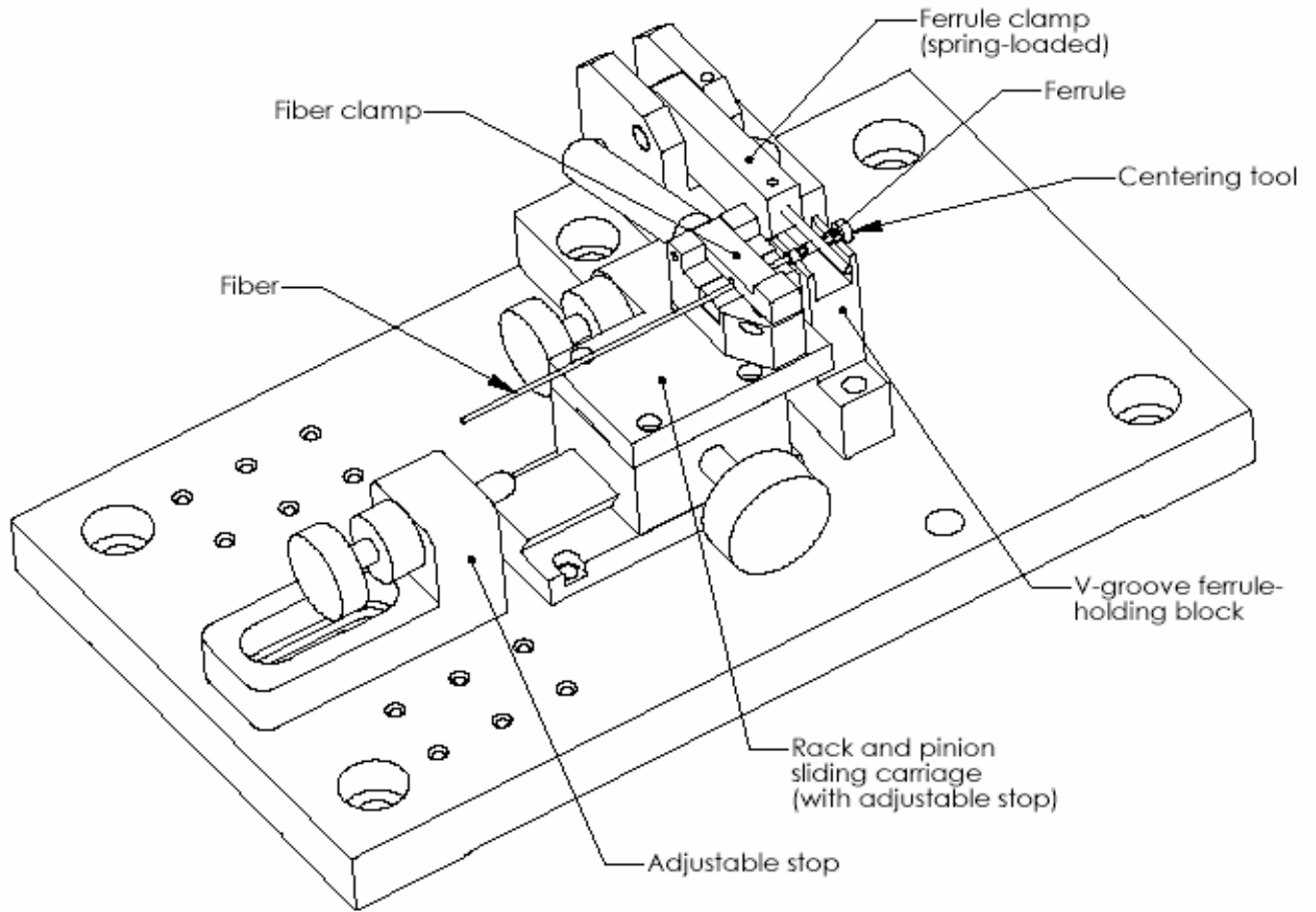
SCALE 1:1	SIZE A	DWG NO. FR002006	REV. B	SHEET OF 2

Other assembly tooling

.1890 +.0000 / -.0005
.1800 +.0000 / -.0005
2× BREAD EDGE ALL AROUND
SCRIBE OR MILL APPROX. .001 IN. DEEP
.0945

.040 TYP
.020 TYP
.020 TYP
.040 TYP

.001

DETAIL B
SCALE 15 : 1

.0376   .0330
.0330   4× R.002
ALL AROUND
16

DETAIL A
SCALE 15 : 1

.500
Ø.160 ▼.113
⌵ Ø.26 X 90°
.250
.038
0
4 DIMPLES FOR ID,
APPROX. Ø.005 ▼.005

.120
.0760±.0005
.041
.007
0

.20   .2090 +.0000 / -.0005

.1045

4× R.046±.010   4× R.050±.010

Appendix C – Welder Process documentation

Lessons learned from welding 10 Gbit/s Datalink modules
Dominik Hoffmann   March 2001

Weld schedules
Our laser-welding consultant, Simon Engel, made two suggestions. First, we should apply
the same pulse power to our seams as we do to the spot and tack welds. Second, this power
should be applied only for the beginning of a shaped pulse and then drop off to 80% of the
peak value.

The spike in the beginning, as short as possible (0.1 ms with our lasers), vaporizes the gold
plating—gold is a type I material and thus requires higher energy densities to weld and
exposes the material beneath. The remainder of the pulse melts and flows the nickel
plating and underlying Kovar, both of which are type II materials. The lowered power in
the main portion of the pulse prevents the vaporization of bulk material and thus reduces
sputter and sparking.

Sputter and sparking is an indicator of potentially imperfect weld beads with inclusions of
bubbles. Such bubbles can lead to cracks and therefore leaks.

Very important, also, is the placement of the focal point of the weld beams relative to the
weld spots. The beams are focused a substantial distance below the surface of the weld (cf.
weld schedule documents). This can contribute to the forming of voids, because the
energy density reaches its peak inside of the weld seam and generates vaporization at
pulse energies necessary to melt the bulk of the material. The ideal placement would be
0.1 mm above the seam with the pulse energies adjusted appropriately.

Shield gas delivery
Prior to any improvements shield gas was delivered through commercial blow-off nozzles.
These are designed to drag ambient air into the emerging jet to increase the overall flow.
The mixture of gas delivered to the weld spot thus included air, which has to be kept away
from the weld to avoid oxidation of the welded materials. The presence of
metal oxides contributes to weld embrittlement.

Furthermore, the flow rate had been in the 3–4 cfm (85–155 *l*/min) range. A flow rate
suitable to laser welding is in the 30–75 cfm (15–35 *l*/min) range, according to Simon
Engel.

The new nozzles consist of ¼" I.D. copper tubing terminating about 1" above the package
nest and about ½" away from the chuck axis. They are angled downward at 45° to the
normal. The intent is to both cover the ferrule-to-lid weld, which occurs with the chuck
holding on to the ferrule, and the spot, tack and seam welds occurring at the lid-package
interface.

Welding grade argon is acceptable. Higher-grade argon (grade 5) did not show any weld
improvements.

Package preparation

All datalink package parts are specified to have 75 µin of nickel plating (according to the standard QQ-N-290) and a maximum of 50 µin of gold (type III, according to standard MIL-G-45204). In the laser-welding classification, gold is a type I material, whereas Kovar is a type II material. The difference is that with gold the laser power density to liquefy it is about 100 times that of Kovar. It can thus lead to weld embrittlement and subsequently to cracking.

In order to test the weld integrity we initially welded lids without holes for ferrules to package seal rings. The edges of these "dummy" lids have the same features and dimensions as those with holes.

These packages were immersed in a bubble leak checker for gross leak testing after having been welded. In that setup leaks manifest themselves as streams of small bubbles that emanate from them. The presence of gross leaks coincides perfectly with microcracks observable under a microscope at 25× magnification. There are two things contributing to the disappearance of the cracks. First, the proper delivery of shield gas to the package during welding, which avoids the introduction of ferrous oxides into the weld, was very important. Second, we have had success with removing the gold plating on the top of the package seal ring and the underside of the package lid.

Testimony from laser welding experts is ambiguous. Some claim that all gold has to be removed from the contact surfaces involved in the weld. Others deny that the gold is the problem, but that nickel plays a role. Most of our tests with dummy lids produced hermetic packages only when the plating was removed from the contact surface. We had two batches of dummy lids. The majority had a gold plating thickness of 85 µin, which is well outside of the spec. Of those that were plated by a different vendor to 48 µin of gold three out of five welded into a package that passed gross leak. This would indicate that an even further reduction of the gold plating thickness could be very beneficial.

Since the gold on the lid underside is necessary for the automatic gain control of the transmitter, because it better directs stray light from the VCSEL to the photo diode in the package, the gold would have to be removed only from a strip around the edges. This would add cost to the product, which is already under price pressure.

Further insight might be gained from performing weld tests on batches of lids with varying plating thickness. In addition there should be batches of lids with nickel plating only, in order to separate the nickel's influence on the quality of the weld.

Package sections

We gathered several insights from sections performed on our welded packages. The first set of packages sent in had dummy lids welded to them.
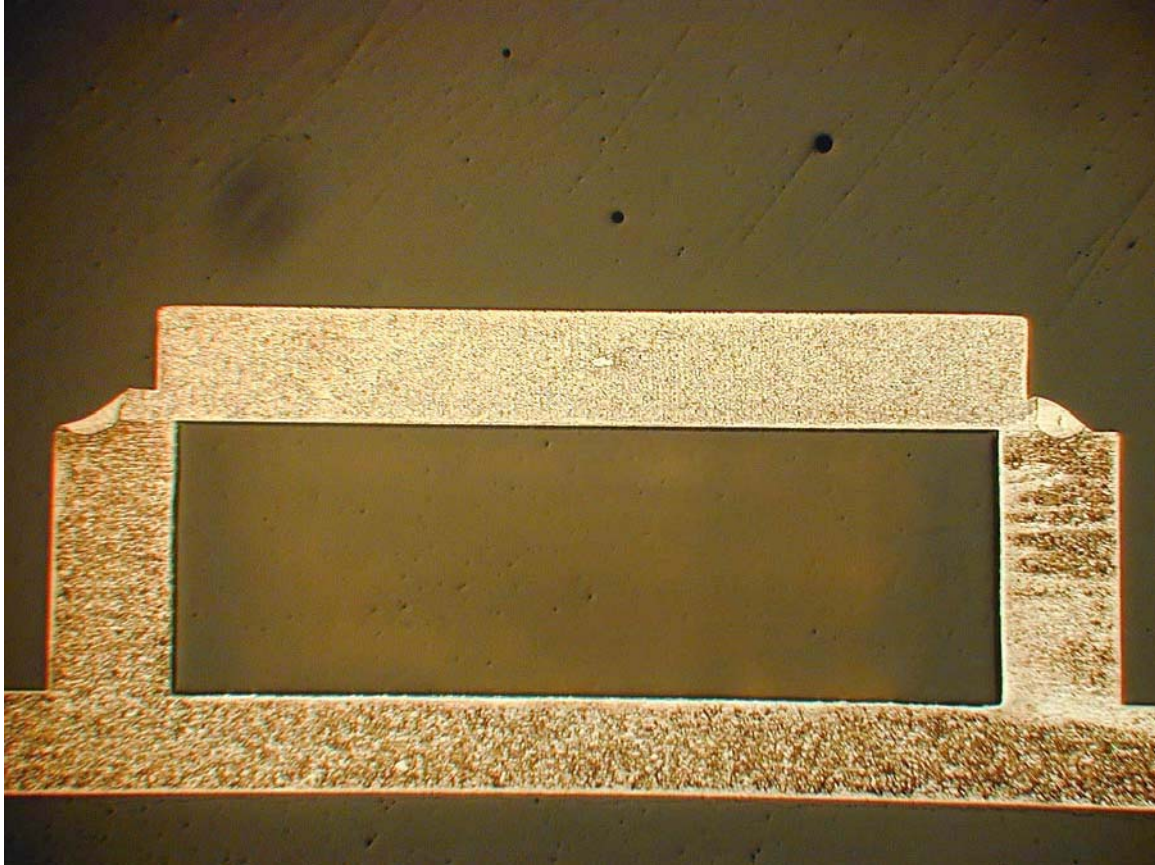
This section shows welds asymmetrically applied on opposite edges. The consequence is differential expansion and shrinkage, which can lead to cracking. Such cracks are visible below in the magnified details of the above picture.
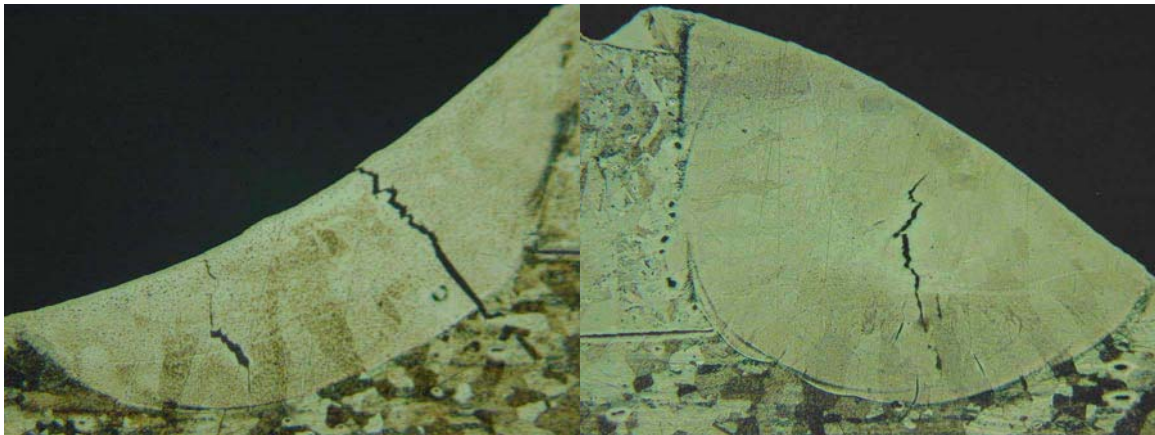

Furthermore, sections performed on modules with a ferrule in the lid showed evidence of contamination of the weld with foreign substances.
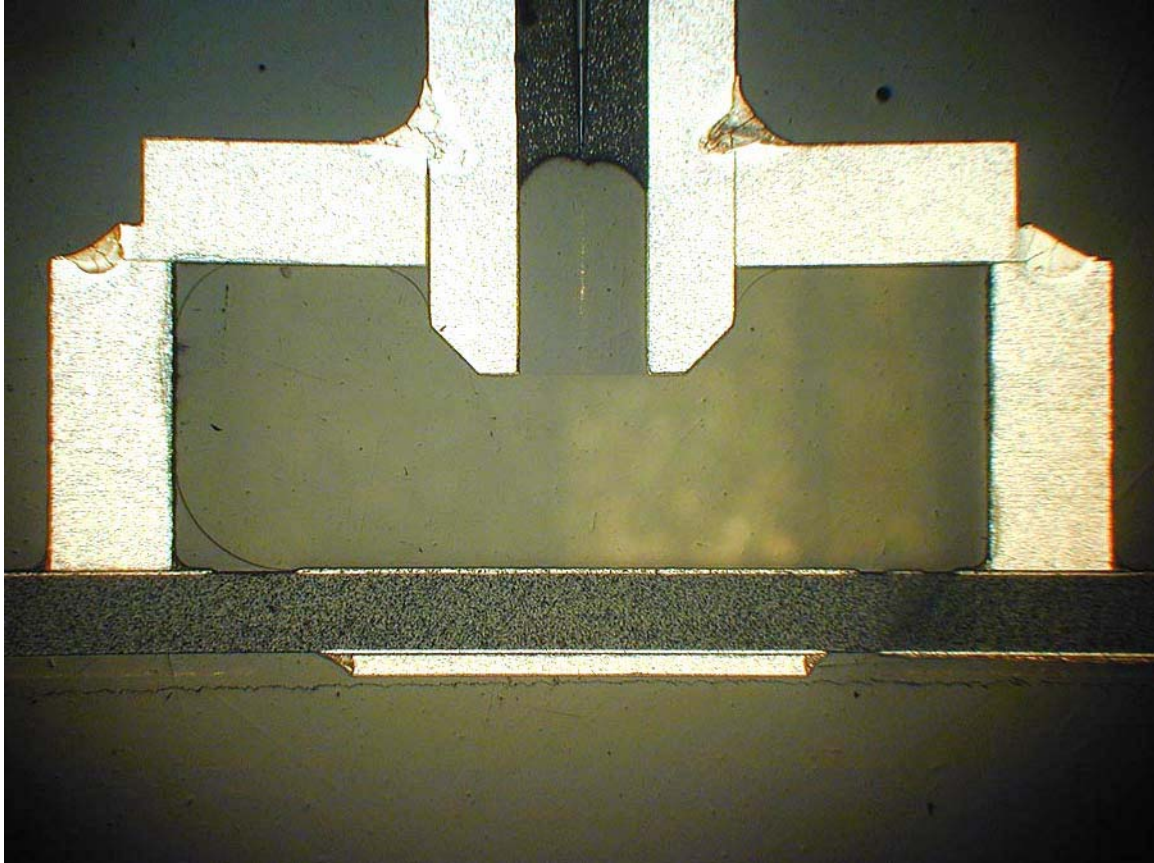
In the picture above that shows the cross section through a ferruled package, it is evident that the lid is deformed. This poses its own set of problems and presumably results from a non-concentric insertion of the ferrule into the lid. Other lids with welded ferrules that were not welded to a package do not show this effect. Thus the conclusion is that the lid is not always deformed.

Blow-ups of the ferrule-lid weld reveal a distinctive heat-affected zone, in which the Kovar grain disappeared. However, the cracks do not extend into the zone, which would not have been reflown during welding. Thus it was never exposed to those foreign substances.
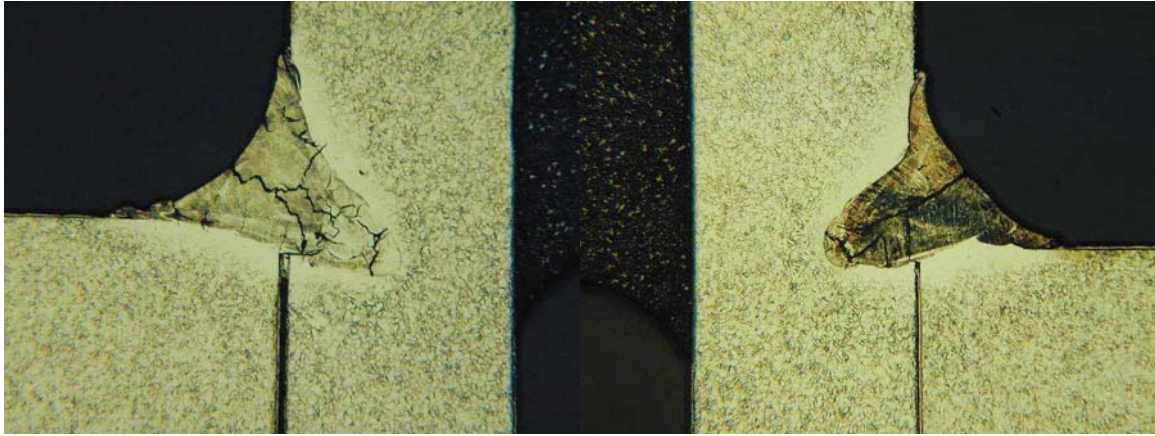
This is further borne out by the direct comparison of packages with and without plating present in the weld seam. The first package has a gold-plated seal ring, but no gold on the underside of the lid. Its welds clearly show cracks. The second had the plating removed from both the lid underside and the top of the seal ring. The second is hermetic and without cracks. Note that on the left there is a visible plating layer, while on the right there is not. Both were welded with the same weld schedule. The one on the right had slightly different shield gas coverage, which should not be able to account for the different weld penetration. Perhaps a slightly different lid placement can, however.
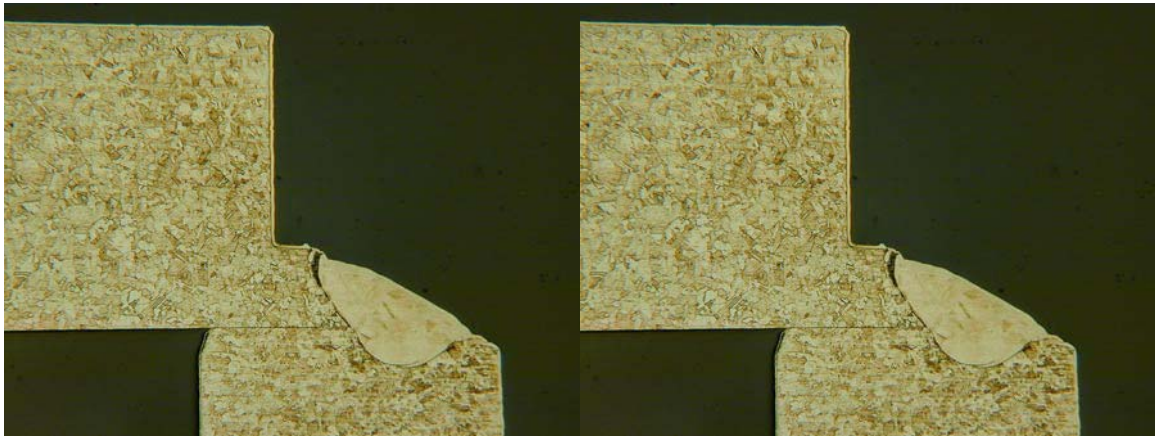
Procedure improvements

Maintaining alignment of the fiber to the VCSEL source in the transmitter module during the application of successive welds is difficult. ZW0104-Spec calls for cumulative losses of coupling to be less than 0.5 dB. To reach this goal several things are implemented:

1) The powers in the individual beams should be balanced to within 5%. Power imbalances results in asymmetric welding of seams opposite to each other and causes the lid to shift through the differential expansion and shrinkage of the weld bead.

2) Very similarly, the beams should be well aligned to the package features. A periodic check of the alignment by running through the various alignment procedures can ensure this. Like in 1), asymmetric application of weld pulses causes the lid to shift.

3) It is very important that, after the ferrule has been welded to the lid, the fiber is realigned, in order to compensate for any distortion caused in the ferrule-lid weld. If this is not done, subsequent welds will likely shift the alignment further from optimum. Since the insertion of the ferrule into the lid can already introduce strains into the system (tooling, ferrule, lid), it was helpful to introduce another alignment step. This step occurs after the ferrule is inserted into the lid and before the ferrule-lid is applied.

4) The clearance between ferrule O.D. and lid I.D. should be at least 0.0005". If the fit is too tight, ferrule and lid are not truly concentric after the ferrule is inserted into the lid. This typically becomes manifest in that the alignment steps described in 3) are ridden with a lot of stiction. Such stiction can render continuing with the process impossible, because the coupling cannot be returned to its pre-weld value.. The presence of stiction implies strain in the tooling, which can partially relieve itself in the application of subsequent welds, thereby pushing the fiber out of alignment.

Package integrity testing

The Telcordia standard GR-468 specifies that telecommunications modules have to pass the MIL-STD-883E criteria for hermeticity and internal water content.

We have the ability to test welded modules for hermeticity down to leak rates of 10^{-3} atm cm^3/s. To do that we immerse the modules in a tank of perfluorocarbon liquid heated to 125° C. The liquid heats the package and thereby pressurizes the inside of the package, driving parts of the internal atmosphere through any existing leaks. The escaping gas shows as streams of small bubbles through the window on the perfluorocarbon tank. A module is considered to have passed this gross leak test, if over the extent of 30 s no bubbles were visible at 1.5× magnification. (Cf. attached procedure.)

With an internal volume of less than 50 μ. the package needs to have a leak rate of less than 5×10^{-8} atm cm3/s (acc. to MIL-STD-883E Method 1014.10 Test Condition A$_1$) to be considered hermetic. To measure this low a leak rate, we have sent sealed packages to an outside vendor who performs the fine leak test on them.

Fine leak testing is done by detecting the helium leak rate from the package with a helium leak detector. Before the package is put into the helium leak detector it is subjected to a 75 psia helium atmosphere for 2 h. This would allow some helium to leak into the package. In the leak detector, this enclosed helium will leak out again and will be thus detectable.

Packages that pass fine leak can be evaluated for internal water vapor content. MIL-STD-883E Method 1018.2 specifies that the internal water vapor content may not exceed 0.5% of the included atmosphere.

We send packages to an external vendor to measure the internal water vapor content. The standard specifies residual gas analysis as one of the methods for making that measurement. Our vendor punctures the package—it is thus a destructive test—under vacuum and leads the escaping internal gas to a mass spectrometer. There the presence of water is detected. The internal water vapor content can be determined from that measurement.

Our packages pass the internal water vapor content test if they have been heated to 125° C for at least 2 h under ambient atmosphere. A more appropriate preparation would be heated a bakeout under a low-pressure dry nitrogen atmosphere.

Conclusions

The big issues in achieving hermetic packages with weld shifts resulting in sufficiently small coupling losses are:

- Shield gas coverage
- Plating integrity and thickness
- Tooling stiffness
- Laser head energy density balance

We have achieved the following:

- The shield gas delivery has been improved
- Weld laser head balance was improved
- We can hermetically weld the lid-package seams if no plating is involved
- The ferrule-lid weld shows no cracks, which indicates a hermetic weld, but the presence of the ferrule results in cracked lid-package seams
- If the tooling is in good shape, low coupling-loss parts can be welded

What remains to be done:

- Further experiments have to determine the appropriate plating thicknesses and vendors
- More experiments investigating the ferrule-lid weld have to be conducted
- Tooling that is more rugged and allows for more stress-free fixturing of ferrule and lid has to be developed

Appendix D - Reports and Presentations

Year One Summary

Optical Link for Radar Digital Processor

Andrew Davidson, Terri L. Dooley, Grant R. Emmel, Robert A. Marsland, and Robert S. Williamson III

Focused Research, Inc.
555 Science Drive
Madison, Wisconsin 53711

July 1998

Abstract

We present our progress toward manufacturing a low-cost, high-speed (10 Gigabits/second), multi-mode fiber optical link based on an 850-nanometer vertical-cavity surface-emitting laser (VCSEL) transmitter and an amplified high-speed gallium arsenide photodiode receiver. Our approach is to combine VCSELs and transmitter/receiver chips built to our specifications by outside foundries, our own photodiodes (based on a proven product) fabricated on-site, and a fiber attachment technique based on a laser-welding approach. Several first-generation prototypes of the complete transceiver, partially using commercially available die and an epoxy based fiber attachment technique, have been built and tested, and show promising performance. Based on these results we have revised our overall link specifications, the second-generation VCSEL specification, and adjusted our approach to make our product compatible with the needs of commercial customers. We have also assembled and begun to test the tooling, motion-control hardware, and laser welder used to perform semi-automated fiber alignment and hermetic package sealing.

Contents

Figures and Tables

Summary

We are developing a high-speed serial optical link suitable for several commercial and military short-haul applications, most notably digital phased-array radar. At the heart of the link lies a vertical-cavity surface-emitting laser (VCSEL) diode transmitter and a gallium arsenide photodetector, coupled by multi-mode optical fiber. The devices are hermetically packaged with basic control circuitry (diode driver and amplifier) and pigtailed in a metal-ceramic surface mount package less than 0.2 cm$_3$ in volume. The link is capable of >8.5 gigabit per second operation, is protocol independent, and can transmit over distances of nearly 100 meters. Our ability to fabricate photodiodes on-site and our partnership with Micro-Optical Devices (MODE), a VCSEL manufacturer, will help make this a low-cost product. Furthermore, under this program we are developing a low-cost automated fiber pigtailing and packaging facility, an essential element to producing inexpensive photonic components.

This first year we have met several of our planned milestones and learned more about potential commercial insertions of our design. We have demonstrated that MODE is able to make oxide-confined VCSELs that are suitable for our application, and have revised the design to create the second-generation devices, based on our characterization efforts. Several modified photodiodes, similar to proven New Focus designs, have been created and we completed a first fabrication attempt.

Some progress has been made on receiver and transmitter chip design, although there have been delays in getting material from Rockwell and IBM. So far, this has not hampered our progress, and we have located other commercially available chips if this becomes necessary. The link specification and design has been completed and considered in light of the only currently established aerospace standard (ARINC 636). Plans have also been developed to make our package compatible with potential commercial buyers, who express a strong desire for integrated mux/demux capability.

Several packaged prototypes have been sent to various groups, and the response has been positive overall. The complete prototype link operates above 8.5 Gb/s with good eye opening and BER of 10$_{-12}$, but does not yet meet sensitivity specifications. However, these prototypes use early VCSELs, a non-optimized third-party photodiode, and a VCSEL with no driver circuitry. With the introduction of our newly revised components on all fronts, we expect major improvement in sensitivity and overall performance.

The development of prototypes using an epoxy-based attachment procedure has helped us begin to understand many of the issues of pigtailing. The epoxy-based approach is fairly mature and has been transferred for use in another FRI high-speed photoreceiver product. However, this approach is neither scalable nor hermetic, and thus we proceeded with a laser-welded approach.

A combination fiber and lid assembly has been designed and fabricated, and all of the tooling needed to produce this assembly has been acquired. This tooling is flexible enough to allow for changes in the package lead-frame and even overall size with only minor revisions. A laser welding system and motion control system have been acquired and the first steps taken towards system integration. We have welded a lid and package on-site using the system.

Introduction

There is a growing need for high-speed serial communications links that are lightweight, reliable, and cheap, for both commercial and military applications. Even for distances below a hundred meters, copper interconnections are heavy and expensive above speeds of several gigabits per second (Gb/s). Parallel optical connections with a dozen or more fibers have just become available, providing speeds of 10 Gb/s and above, but these suffer from high interconnect cost and can be somewhat less reliable since many fibers and devices are required to produce a link. A much more appealing approach is a higher-speed, single-fiber approach. With the advent and approaching commercialization of reliable vertical-cavity surface-emitting lasers (VCSELs) with several gigahertz of bandwidth, single-fiber multi-mode serial interconnections become a feasible and inexpensive alternative.

We are developing an 850 nm multi-mode fiber-optic serial transmitter and receiver, operating at 8.5-12 Gb/s, capable of transmitting over distances of nearly 100 meters. Our design is protocol-independent and can function either with DC-balanced code or in burst mode, making it broadly applicable to virtually any short-haul, high-speed, point-to-point communications application. We expect our highest payoff military application will be digital radar, and commercially, we expect storage area networks (high-speed disk drive arrays) and supercomputer backplane interconnections to be major players.

Several elements allow us to make this high-performance link low in cost as well. Using a single inexpensive VCSEL for the transmitter element, designed to operate at high modulation rates and a wide environmental conditions, gives us reliability over competing parallel approaches and considerable cost savings over a traditional edge-emitting laser. The photoreceiver is similar to an established New Focus design that supports an already successful product family. Also important is a relatively inexpensive, reliable packaging approach; we are using a hermetically sealed, laser-welded package that can be fiber-aligned and sealed automatically with minimal operator involvement. Finally, we are developing a manufacturing process that uses tested devices (known good die), reducing the need for rework and low yield at the end of the assembly process.

This report summarizes our first year of progress in this three-year program. In the following sections, we provide some background motivation and assumptions that have led us to take this approach. Next, we describe the results of our program of component characterization, prototype link development, and packaging/fiber attachment. Finally, we conclude and discuss our plans for the coming year.

Methods, Assumptions, and Procedures

Here we briefly discuss some of the technical rationale behind our approach.

When it is necessary to move large amounts of data very fast over a short (<100 meter) distance, there are at least five possible methods:

• parallel copper wires,
• parallel fibers driven from logic levels,
• parallel fibers driven by separate serial interfaces,
• parallel serial interfaces wavelength-multiplexed on one fiber, and
• a single serial interface on one fiber.

The single serial interface will be the optimal solution in many applications where reliability, robustness, size, and cost are the major considerations. A single fiber interface can incorporate controls on average laser power and receiver DC levels that would be too costly if repeated 12 or more times for a given link. Wavelength division multiplexing relies on the data being divisible into separate data streams. This is not the case for the digital radar application where the data is originating from a single A/D converter.

All things being equal, a single fiber is preferable to 12 and any fiber is preferable to a massive copper cable, which becomes too heavy and costly when sending data more than a few meters at >1 GByte/second. The pressure on the serial link is to demonstrate cost and power requirements comparable to the other approaches. Table 1 summarizes this comparison, based on a 5 meter link with an aggregate bandwidth of 12 gigabits (transceiver and cable only).

Power and cost estimates for parallel optical approach very widely. For the purpose of comparison, 1 W was chosen as the power since this is the minimum power necessary to drive twelve 50-ohm lines at ECL levels from a 5V supply. The multiplexer/demultiplexer price is not included in Table 1. Since the data channel widths do not match the word length from the A/D, each technique compared in Table 5 will require a mux and demux although the 12 Gb/s parts will be the most expensive. For reference, a 10 Gb/s mux/demux including the phase detector and timing circuitry is available from Vitesse for $2500 in a prototype package and dissipates 5 W. They expect this device to fall below $100/ea in quantity as yields improve.

Table 1. Transceiver approach comparison

	Single Fiber 12 Gb/s	Parallel Optical Link, 12 Parallel, 1 Gb/s	Serial Copper Link	Parallel, Copper Link, 41 diff-parallel, 250 Mb/s
Power (W)	1 (2.5) [1]	1	1 (2.5) [1]	2
Cost Projection ($/Transceiver)	200	610 [2]	800	600 [3]
Diameter of cable(s) (mm)	0.125	3	7 [4]	100×10 [5]
Weight (5 m cable, kg) [6]	0.008	0.1	0.51	0.5
Reliability (MTTF hrs, VCSEL, 25°C)	$1.0 \cdot 10^7$ [7]	$0.75 \cdot 10^7$ [8]	N/A	N/A

(1) 2.5 W includes serializer/deserializer circuitry
(2) Based on $10 per Gb/s as target price of parallel optical link plus cable and connector cost
(3) Based on cost of 5 meters of W.L. Gore "RIBBON-AX" cable at $120/meter (no connectors)
(4) Based on UFE 276B high-isolation cable
(5) Based on bundle of 2, 2.25" wide "RIBBON-AX" cables
(6) Based on weight of cable only, no armor
(7) Based on 1E7 hour MTTF number from Honeywell preliminary data sheet
(8) Based on 12 VCSELs, log-normal distribution, $\hat{\sigma}$ = 0.225

Technical Approach

Presently, high-speed (>2.5 gigabit/second) fiber optic transmitters and receivers rely on single-mode long-wavelength laser diodes aligned to single–mode fibers. The alignment and packaging process is time-consuming, labor-intensive, and relatively low yield (<50%). Furthermore, it requires an expensive package that is prohibitively large for many applications.

We will build 12 gigabit per second transmitter and receiver modules that are inexpensive and substantially smaller in size (cubes less than 0.25 inches on a side) by taking advantage of multi-mode VCSEL laser chips, state-of-the-art foundry services, and, most importantly, a fast, low-cost, high yield fiber attachment technique. This fiber attachment technique will also be flexible and amenable to customization: it will allow us to accommodate different package styles or different fibers without dramatically increasing costs.

Constructive Plan

The fiber attachment technique will involve the following steps:
- bonding the fiber to the lid, using a tool to align along the *z*-axis, and strain-relieving the fiber
- aligning the lid-fiber subassembly to the transmitter or receiver package, and
- welding the lid in place.

Results and Discussion

Our progress this year has three main aspects, in the acquisition and characterization of the devices for the link; producing prototype receivers and transmitters and testing the link performance; and creating the packaging and fiber attachment process.

Component acquisition and characterization

VCSELs

We have received several rounds of devices from MODE this past year, beginning with one batch of some early ion-implant devices, followed by several minor revisions of oxide-confined VCSELs. These minor revisions have mainly reflected various process improvements at MODE, especially attempts to improve the polyamide process, which affects the adhesion of the top-side metallization. Poor metallization has caused problems wire-bonding to the bond pads, and we have modified our bonding procedure to overcome this in the short-term, but MODE is working to fix this problem. Electrically, the devices have been relatively consistent from batch to batch, and the measurements we present here demonstrate the suitability of the MODE design and have resulted in a revised design specification which we expect MODE to ship early in the next contract year.

Below in Figure 1 we show a TDR of a 12μm VCSEL from this early batch directly bonded into our Kyocera package, showing an internal impedance of about 60Ω. The impedance of these lasers scales approximately as the active area of the VCSEL, and we measure an impedance of roughly 75Ω for a 10μm device, and 90Ω for an 8Ωm device. These impedances should present no problem once the transmitter/driver chips become available; in the near term a resistor in parallel with the laser, used to bias the laser, is chosen to bring this impedance to a nominal 50Ω.
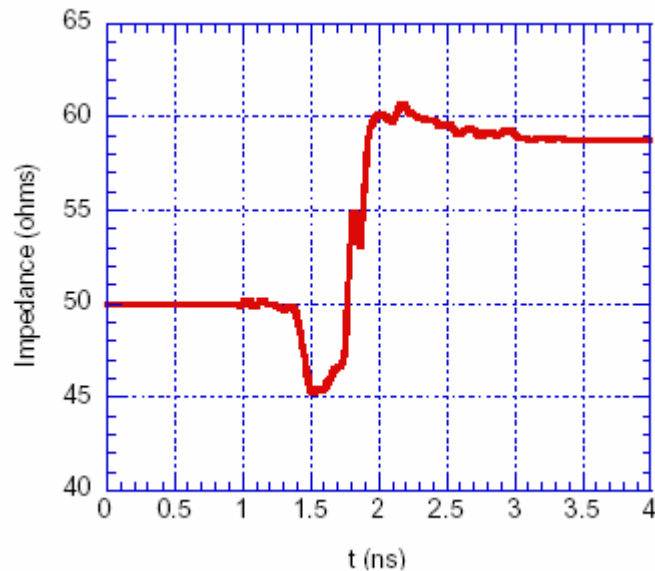
Figure 1. TDR of a 12μm diameter oxide-confined VCSEL mounted in our Kyocera package, operating with 5mA of drive current. The VCSEL is driven through a high-speed bias tee.

Using a simple bias circuit and an external DC block, we drove the VCSEL with enough current to produce an output of 0.8 mW and applied a sinusoidal RF source of −10dBm. The output of the VCSEL was sent through a length of 50/125 μm graded-index fiber and detected by a New Focus model 1534 photodetector backed by a model 1422 amplifier and measured using the FFT analysis function of an HP 54750 20 GHz digitizing scope.

Below, in Figure 2, we show the response of three different diameter VCSELs, all from the same die. A number of interesting things can be gleaned from this data. First, it appears that the response of the 12μm diameter VCSEL is slightly slower than the 8μm or 10μm, and it seems that the 10μm device gives slightly better overall responsivity.
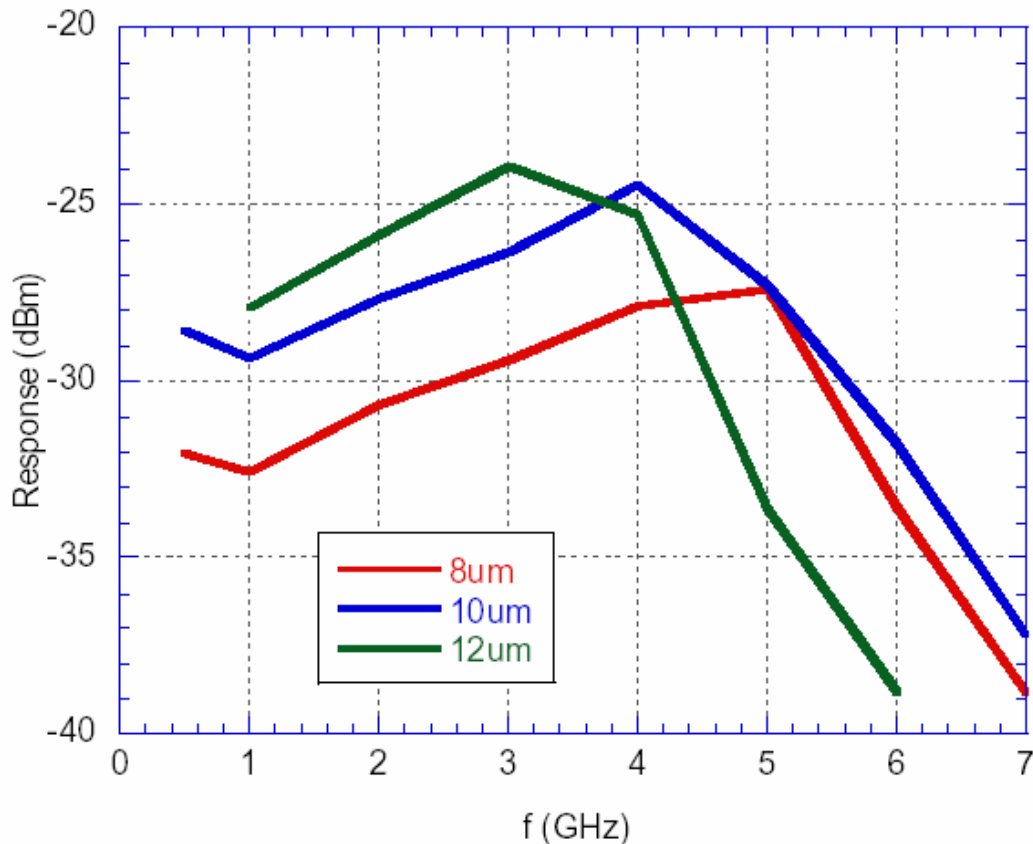
Figure 2. Modulation bandwidth of 8, 10, and 12 ∝m diameter oxide-confined VCSELs in Kyocera package.

Second, there is evidence of a small amount of gain peaking near 4 GHz, but this should have little effect on a digital transmitter. For the 10μm laser, the −3dB point is at about 6 GHz, which meets our goal.

We have also performed on-die RIN measurements of the MODE VCSELs that are quite encouraging. In Figure 3, we see a spectrum of the RIN up to 2.9 GHz. Judging from the shape of the spectrum, we expect the RIN to meet specifications up to at least 6 GHz. We expect to perform more measurements to measure device-to-device uniformity now that we have received the mature final batch of devices.
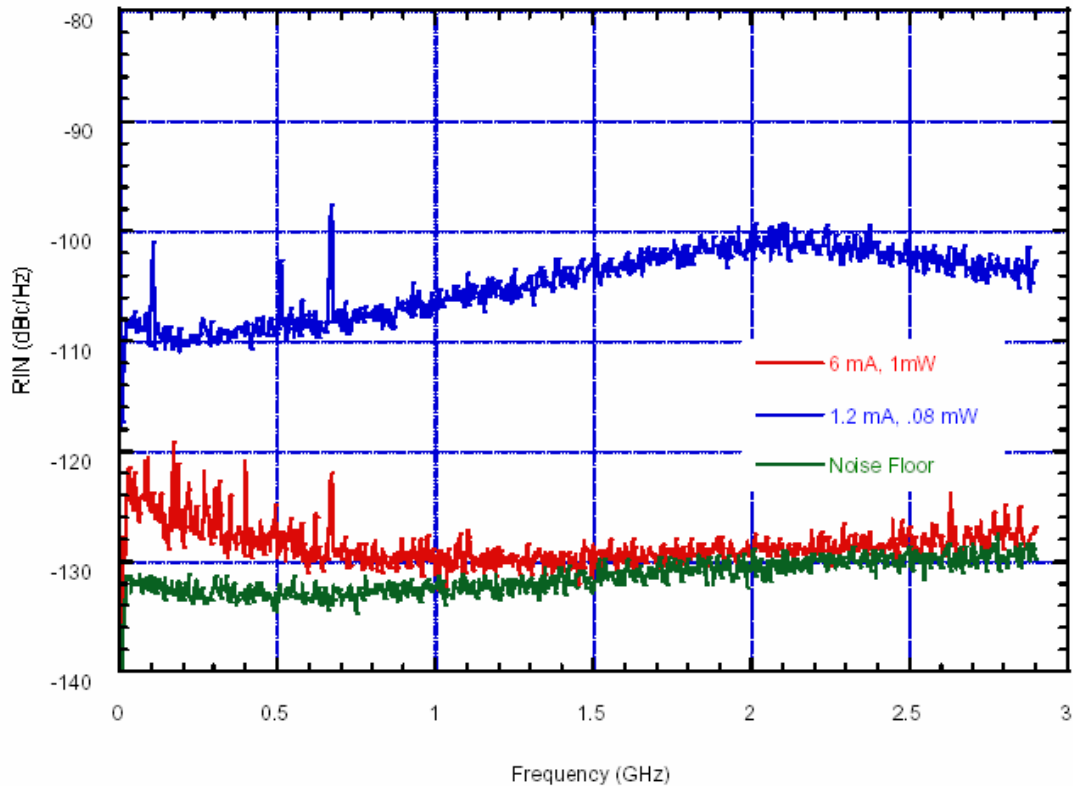
Figure 3. Relative-intensity noise measurements of a MODE 10 μm VCSEL, probed on-die using a New Focus model 1534 photodetector. At the expected eye-safe level of –5 dBm, the RIN should still be well below our target specification of –122 dBc/Hz. Furthermore, other measurements of the spectral shape beyond 6 GHz indicate the spectrum is relatively flat. The spikes below 1 GHz are artifacts, picked up from local radio traffic; the second generation of VCSELs, with top-side metallization, will allow more robust RF probing.

Photodiodes: tests, design, and fabrication

To speed development of early prototypes, we temporarily used some commercially available photodiodes (GAP 60) for our receivers. These have served us well for this first year, but they suffer from poor optical sensitivity and a very small bond pad, making rapid, reliable microassembly difficult. We describe both early measurements of these photodiodes as well as describe the modified New Focus design and initial fab run.

The primary photodiode test apparatus at Focused Research consists of 180 fs pulse-width mode-locked laser and a 20 GHz HP sampling scope. When the receiver is operated at low intensity and is thus linear, the impulse response provides the complete small-signal transfer function of the system. The impulse can be integrated to provide the step-response or Fourier transformed to provide the frequency response. The impulse response curves are shown in Figure 4.
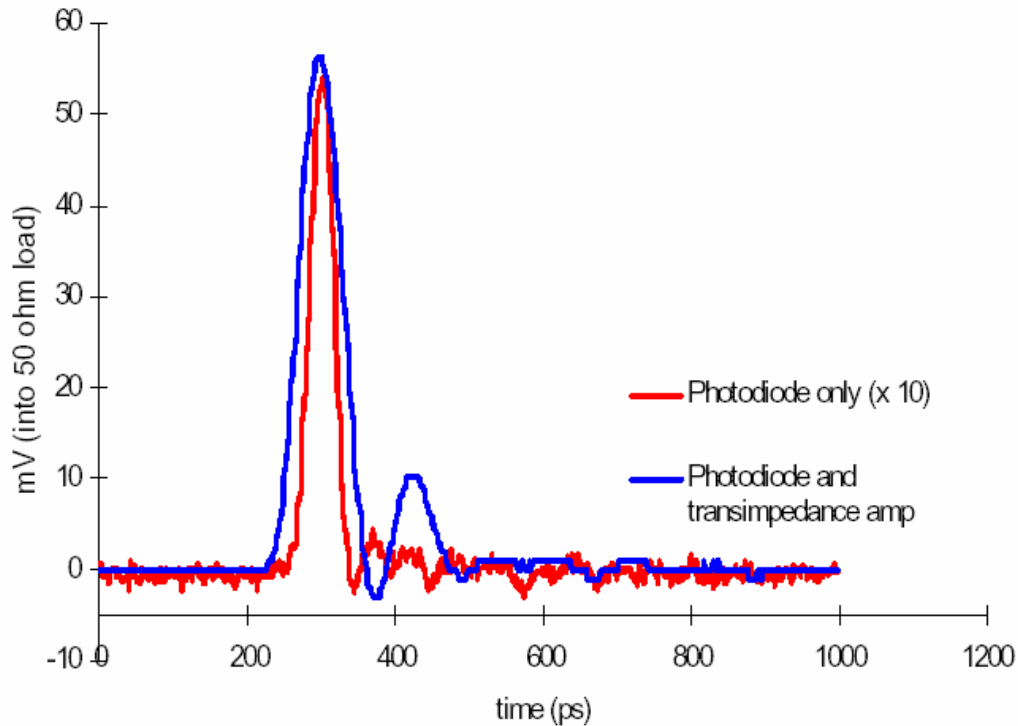
Figure 4. Impulse response of the packaged InGaAs detector(red) and the detector packaged with the receiver transimpedance amplifier (blue). The FWHM of the detector alone is 38ps, and of the detector/amplifier combination is 66ps.

Although we are not conducting any significant new development of detectors under this program, we have found that all existing commercially available detectors are unacceptable for this application. Current New Focus designs come close, requiring only minor modification. However, in an effort to further improve upon the design, we are including three additional types of photodiodes on the mask set. All of the detectors are Schottky photodiodes fabricated on GaAs using proton isolation and silicon nitride passivation, with an active area thickness of 1.5μm. Active area sizes will accommodate fiber diameters of 50, 62.5, and 100 microns.

Of the 11 diodes which have been designed for this mask set, 3 (one for each diameter) are based directly on existing New Focus designs and should thus pose no risk. These diodes have semi-transparent thin gold Schottky contacts, integrated biasing circuitry, and plated bond pads. The nitride layer serves to reduce reflections from the thin gold contact.

In the second design, the thin gold contact is replaced with a thicker interdigitated Ti/Pt/Au contact, with 1.5μm wide fingers and 3μm gaps. These dimensions are chosen to produce higher transmission into the semiconductor than for the case of thin gold contacts.

A third design employs a dual-purpose opaque metal guard around the active area. The guard is fabricated from the plated top metal and covers the area immediately around the active area. Furthermore, in our air-bridge process, this is used to cantilever the edge of the guard over the active area. This prevents light from falling on regions outside the active

area, eliminating the slow current component of carriers created in low-field regions. The guard also electrically shields the ohmic contact, diminishing the field at its edge and possibly improving device reliability.

The fourth design foregoes bias circuitry and the need for isolation, and thus results in a die that consumes half as much real estate and requires 4 instead of 7 masks. The principal concession in this device design is a small bond pad.

We processed half of a three-inch wafer for our initial run. The devices have a 1.5 micron thick intrinsic absorbing layer, a thin 100 nm top p+ layer, and a silicon nitride anti-reflection coating/passivation layer. Figure 5 shows the forward I-V characteristics for a $100 \cdot 100 \ \mu m^2$ PIN diode test structure. The p^+ ohmic contact has not been annealed on this test structure, hence the contact resistance has not been minimized. The slope of the "on" portion of the curve indicates a 39 ohm resistance.
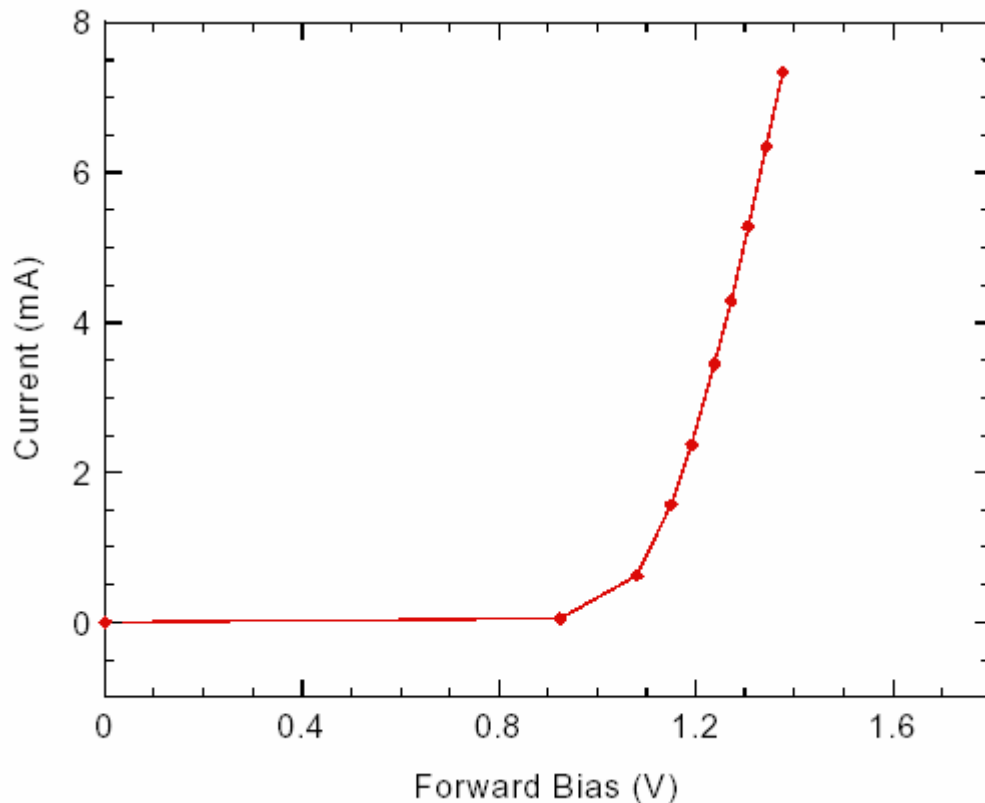
Figure 5. Forward I-V Curve of 100 $\propto$m GaAs PIN photodiode, prior to annealing and final processing.

After final annealing, it was determined that this first run produced devices with high ohmic contact resistance. High speed device tests confirmed that the resistance is too high for our receivers. We suspect that the etch to the n^+ layer was incomplete, but have not confirmed this. We will repeat the fab run at the beginning of the next contract year.

Link characterization and design

Using the first batch of oxide-confined VCSELs from MODE we built working an unamplified transmitter and an amplified receiver module using an epoxy-based lid attach

method, described in full previously tested at our facility using a pulsed laser and high-speed scope, then tested in further depth by the Mayo Foundation. A second, somewhat more mature pair of devices was later send to Lucent, who provided us with additional test data. Their results appear quite promising, and the response from other groups we have sent prototypes to has been very positive.

Mayo Foundation Tests

Mayo has performed bit-error rate measurements on our receiver and on a complete link using both our receiver and transmitter. The receiver used for these tests used a 60 μm diameter VIXEL GaAs photodiode, whose sensitivity is a big improvement over the GAP60 previously tested, but still have the GAP's tiny 25μm diameter bond pads. Furthermore these prototype photodiodes are not commercially available in any quantity. The amplifier section is a prototype Rockwell RSC111 transimpedance amplifier. This has similar performance to the TIA section of our expected final receiver design. The major drawback of the RSC111 is its sensitivity to input capacitance: less than 100 fF is required for 10 Gb/s operation. Using the large area photodiodes we require for multi-mode operation, the maximum observed data rate of the RSC111 is 8.5 Gb/s.

In Figure 6 below we show eye diagrams at 9 Gb/s. At left is the eye diagram of the test source, a Honeywell 850 nm VCSEL, measured using a New Focus model 1434 25 GHz photoreceiver and HP70843A BERT. At middle is the response of the packaged FRI photoreceiver, and at right is the FRI transmitter in a Kyocera package as measured using a NF model 1434.
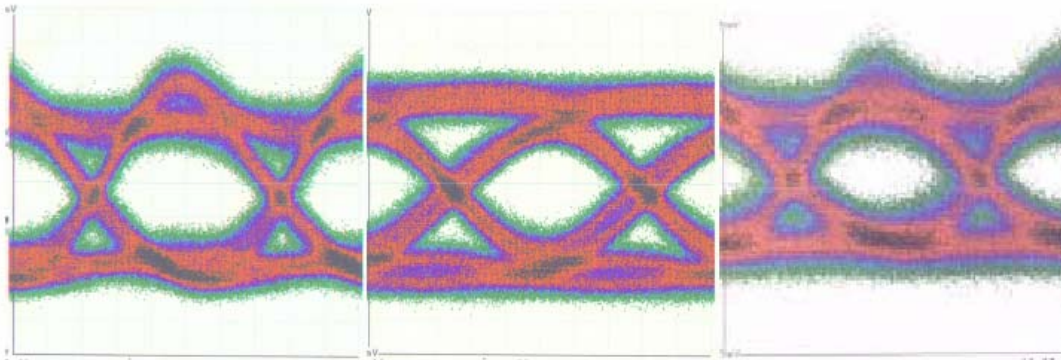
Figure 6. Eye diagrams from Mayo BER tests. The horizontal scale for all three figures is 20 ps/div; the vertical scale, from left to right, is 25mV/div, 20mV/div, and 10mV/div.

To determine overall link optical power budget, the receiver was tested at 8.5 Gb/s, chosen to maintain a good eye opening, and the incident power adjusted to determine at what sensitivity one can still achieve a 10^{-12} BER Using a Honeywell VCSEL, this level is −11.1 dBm and with the MODE VCSEL, this level is −8.3 dBm. Thus our receiver is only a factor of three away from our target sensitivity of −16 dBm and that the complete link is only a factor of six away. Note that these are not only first generation devices, but the first fabrication run of devices as well. We expect improvement once we begin using our own photodetectors and mature MODE VCSELs, as well as begin to integrate the IBM receiver chips.
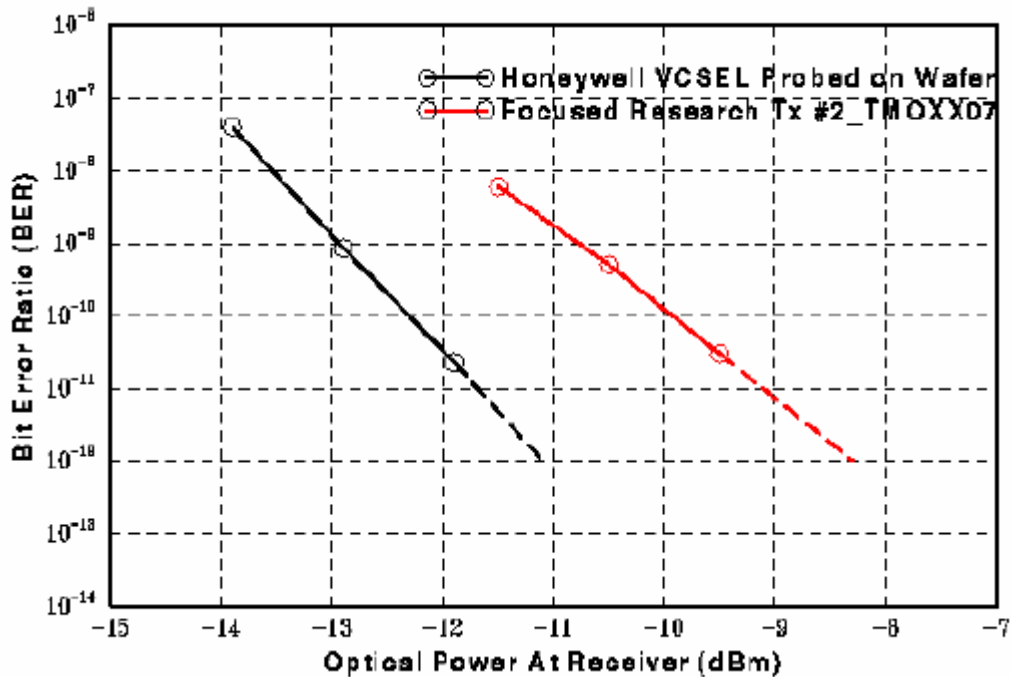
Figure 7. Bit-error rate measurements of our receiver using a Vixel photodiode and a Rockwell RSC111 TIA,measured both with a packaged MODE VCSEL and an on-wafer-probed Honeywell VCSEL.

Mayo also measured the BER at lower speeds with a –16 dBm signal, measuring a BER of 3×10^{-11} at 5 Gb/s and a rate below the BERT's measurement capability of 10^{-12} at 4 Gb/s.

Lucent Tests

A team at Lucent Technologies, consisting of M. Nuss, G. Giaretta, A. Krishnamoorthy, and T. Woodward, requested that we send them prototypes of our link. Using our epoxied lid approach we sent them a pigtailed amplified receiver and free-space VCSEL transmitter, assembled into a user-friendlier test fixture with SMA input/outputs. The results they obtained confirmed and further clarified the previous Mayo results.

In Figure 8 below, we show their measurements of the VCSEL spectrum near and above threshold. Note that it shows nearly single-mode operation near threshold, and becomes fully multi-mode above. This corroborates well with the observation of significantly higher RIN near threshold, due to fewer modes coupling into the fiber and the anticorrelation of noise in adjacent modes. Small-signal modulation bandwidth was determined to be 7.5GHz (-3dBm RF, 2mA bias) and RIN of –120dB/Hz at 10GHz.
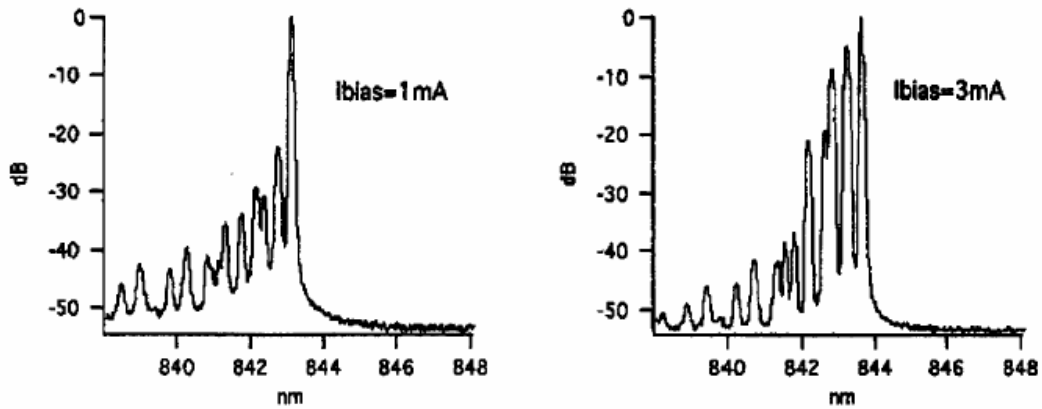
Figure 8. Optical spectrum of FRI VCSEL transmitter module near (I_{bias} = 1mA) and well above (I_{bias} = 3mA) threshold (I_{th} = 0.75mA), as measured by Martin Nuss and Giorgio Giaretta's group at Lucent Technologies. Note also the shift in the spectrum toward longer wavelengths above threshold; this is a typical VCSEL characteristic.

They tested the link using simple OOK (on-off keying) modulation at 9 Gb/s. In Figure 9 below, we show their data for BER as a function of received power. These are encouraging results, especially for such an early prototype. We expect to meet our goal of 10^{-12} BER at 10 Gb/s with −16 dBm power using an improved amplifier, our photodiode design, and better fiber coupling. Eye diagrams show a clearly open eye at 9 Gb/s and 12.5 Gb/s, but BER was very high (10^{-4}) at 12.5 Gb/s.
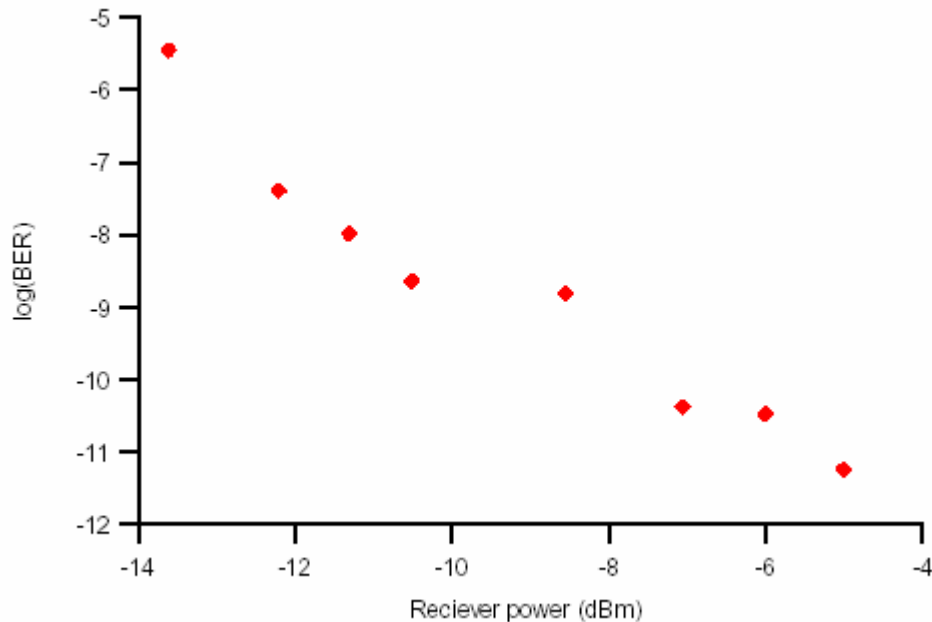
Figure 9. Bit-error rate (BER) as a function of receiver power for a complete FRI link, as tested by the LucentTechnologies group.

Receiver chip design

Finally, during this period we were able to design and simulate some prototype receiver chip designs for inclusion in the Mayo Foundation SiGe fabrication run with IBM. The circuit designs were provided to Mayo where they performed the mask design in conjunction with other ongoing work including transmitter chip design. This initial SiGe run was not planned, it just happened that the Mayo Foundation had room on the mask set,

63

and FRI managed to get some designs ready in time for the deadline. It is hoped that these quick designs will provide good design insight for the next iteration and for choosing the right technology: SiGe or GaAs.

This period we have not yet received the SiGe transceiver chips from IBM, but this has not yet hampered our efforts. Next quarter we expect to produce the next generation of prototypes, and we have located a commercial (albeit expensive) source for receiver chips (Anadigics), but we expect to receive the SiGe die by that time.

Fiber attach and packaging

Packaging scheme

Our approach for a hermetic, laser-welded package, is simple and straightforward, but contains several elements that should make it readily manufacturable and robust. The fiber and ferrule are created first as a separate assembly, streamlining manufacturing. This subassembly is shown in Figure 10. The gold metalized fiber is soldered to the tube through the lower hole forming a hermetic seal. Epoxy is applied through the upper hole to attach the fiber buffer to the ferrule to act as a strain relief. This operation is performed in a jig that keeps the fiber centered in the ferrule while the soldering operation is performed. By soldering first, then epoxying the buffer, and treating this as a separate assembly, we avoid the troubles of building-in strain or twist in the fiber that can plague other approaches. Furthermore, this also confines low-tolerance operations to a single step.
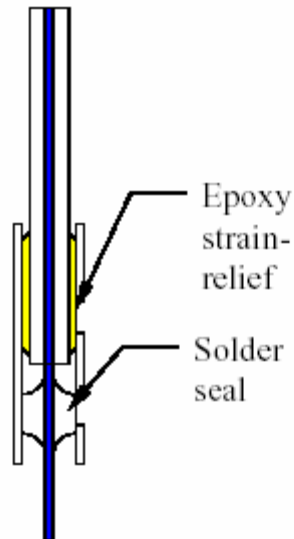
Figure 10. Detail of fiber-ferrule subassembly, showing hermetic solder seal to metalized fiber and epoxy strain relief to fiber buffer.

A cross-section of the entire package is shown below in Figure 11, consisting of a co-fired kovar/ceramic package, a relatively thick kovar lid (to prevent pressure-induced buckling), and the fiber/ferrule subassembly just described. The joints between the package and lid, and between the tube and lid, are laser welded with a continuous bead. The lid-tube joint is welded first to fix the fiber z-axis height, and the lid-ferrule combination is moved over the package to make a final high-resolution x-y alignment, then spot and seam welded.
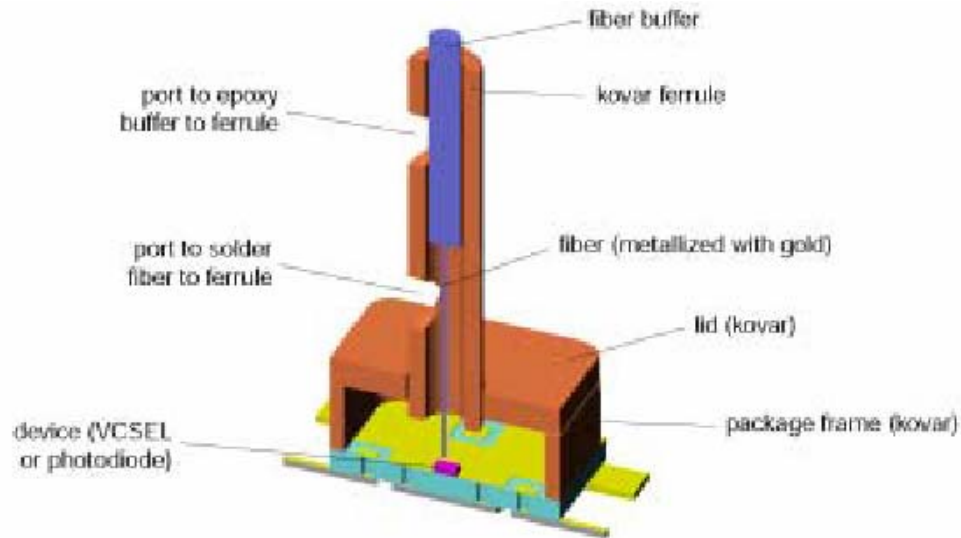
Figure 11. Cross-sectional view showing structure of the welded fiber attach method.

Prototype production and package evaluation

This task has been attacked on many fronts. In terms of facilities and personnel, we have hired a micro-assembler who was quickly trained to use our die attach and deep-access wire bonder; she has produced two rounds of prototypes, including those sent to Mayo for BER testing. Our facility is in the process of becoming a class 10,000 clean room.

A prototype lid assembly and attachment method was designed to facilitate production of prototypes for early link evaluation, before the final welder fiber attach apparatus is built. The attachment fixture is shown in Figure 12. We designed, fabricated, and evaluated a microwave and optical test fixture capable of testing our Kyocera package and components.
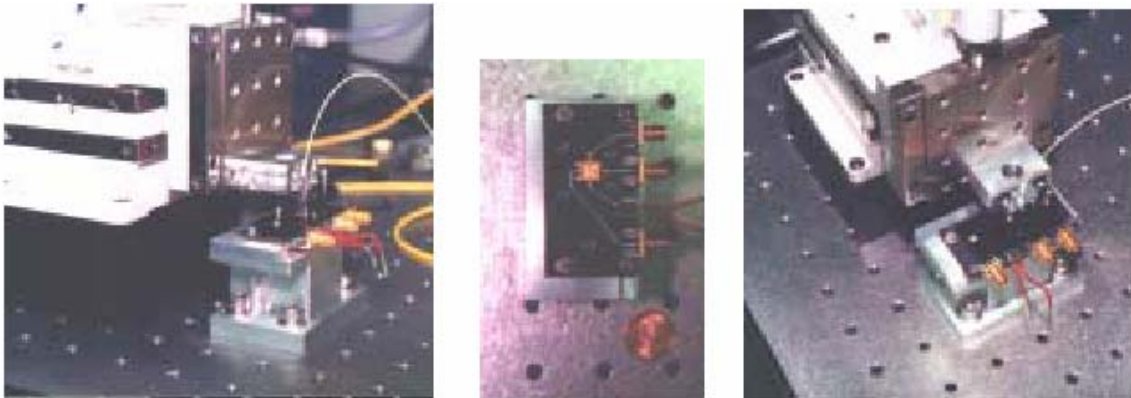
Figure 12. Several different views of the prototype lid-attachment apparatus. The package is clamped in place and makes electrical contact to the pc-board without damage to the package leads. The SMA connectors provide >10 GHz bandwidth connection to the package for use in engineering tests or active fiber alignment.

These transmitters were pigtailed using 0° cleaved 125/50μm fibers and an epoxied lid. The lid consists of two pieces: a fiber connector bulkhead machined to 0.38" outer diameter and a standard FC-type optical fiber ferrule. The ferrule slides in the connector bulkhead to provide z-axis motion without inducing x- or y-axis deviations.

We introduce the fiber ferrule by itself, and visually determine the z-axis height and x-y rough alignment, marking the z-location with a high-precision (±1μm) indicator. Furthermore, the coupling efficiency (indicated by strength of a photodiode signal) is noted. When packaging a photodiode, a pulsed laser and oscilloscope are used, and the pulse height is optimized, when packaging a laser, it is modulated at high frequency (2-8GHz) and the signal from an external photodiode is optimized. The ferrule is then retracted along the z-axis, epoxy is applied to its surface and to the top perimeter of the package, then the bulkhead is inserted and the ferrule is lowered into place. The electrical feedback is used to optimize the coupling, and we perform a final x-y alignment. The epoxy is then allowed to cure.

As a process, this procedure is nearly identical to that proposed for the welded lid, and provides us with some idea of at least the mechanical difficulties involved. Below in Figure 13 we show a cross-section of the epoxied lid approach.
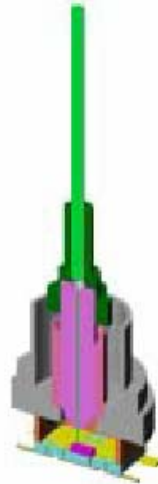
Figure 13. Cross-sectional view of the epoxied lid technique for prototypes.

Coupling efficiency is monitored during the cure cycle and showed only 5-10% variation as the epoxy cured. In addition, for the transmitter, the response with 6GHz modulation was monitored, and for the receiver, the pulse impulse response is monitored. This simple approach has proved quite useful for producing small quantities of prototypes, but the gluing procedure is somewhat time-consuming, as we have chosen our epoxy to have very low cure shrinkage (0.03%) and a relatively small thermal expansion coefficient. We began with a preliminary evaluation of the mechanical alignment tolerances for the VCSEL devices and 50 μm core fibers. The results shown in Figure 14 indicate that the *z*-axis tolerance of more than 0.004" may be sufficiently great to allow simple passive alignment in this direction. The transverse alignment is more stringent but still rather flexible at 0.0005". We plan to use a simple active alignment technique for the *x*- and *y*-directions.
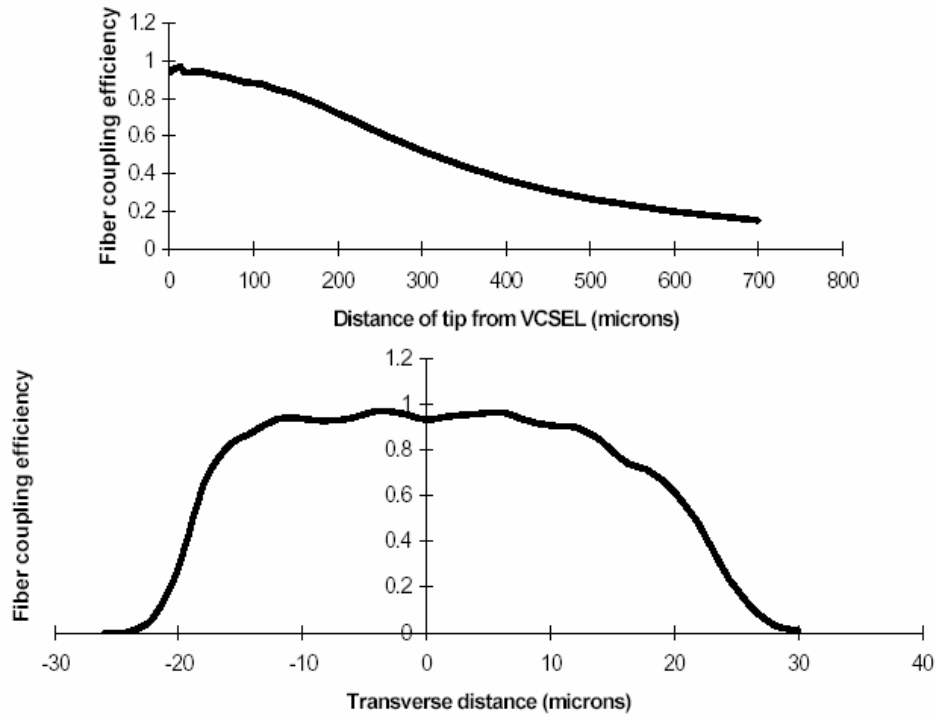
Figure 14. Longitudinal (top) and transverse (bottom) alignment sensitivity for the 12-μm VCSEL and 50-μm core multi-mode fiber.

The test fixture was used to evaluate the Kyocera package electrical integrity to >10GHz using time-domain reflectometry (TDR). Figure 15 shows the test results. The traces show a first reflection due to the SMA-connector to microstrip on FR-4 board, then a second reflection at about 925 ps that is due to the package and its contents. Note that with our test stimulus step rise time of 35 ps, all reflections were less than 10% and thus present no material obstacles to the package's use at 10GHz.
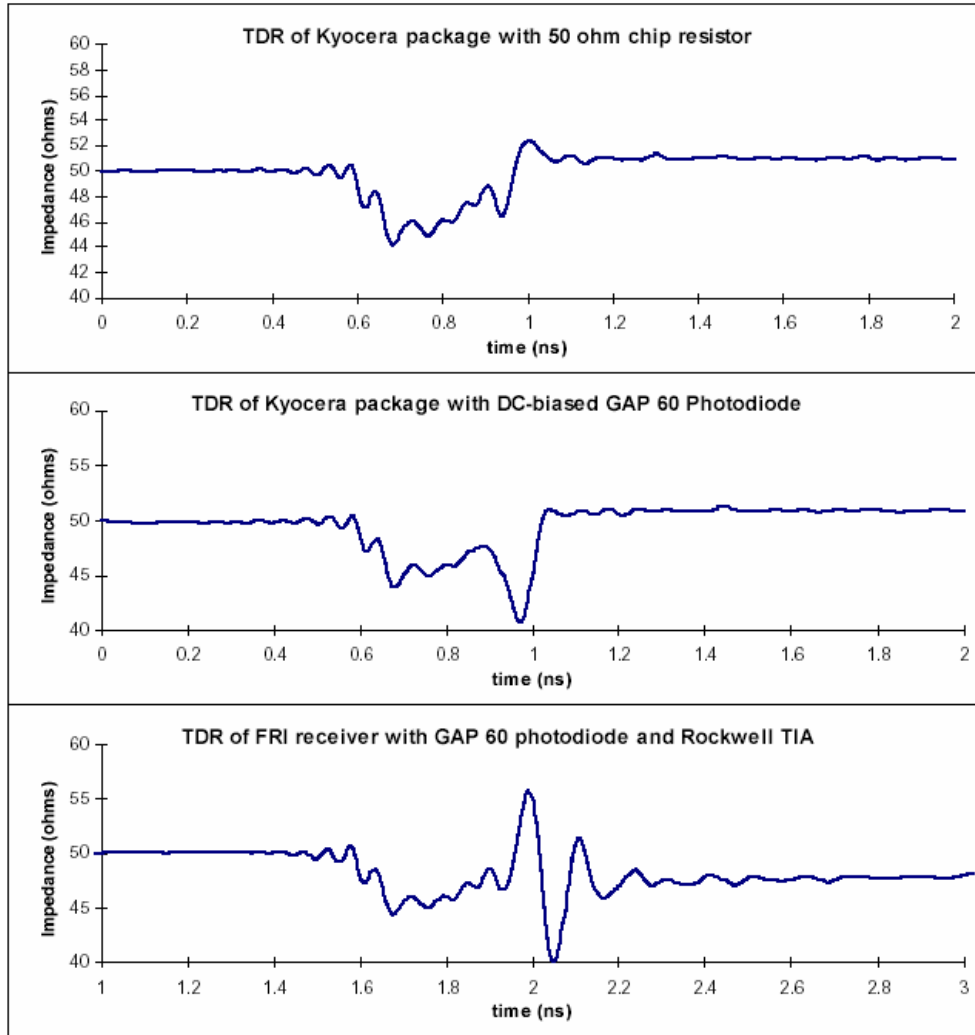
Figure 15. TDR traces for the selected Kyocera package on the evaluation board with various elements in the package. At top, the terminated package shows excess capacitance of 400 fF and no measurable inductance. In the middle, we observe that the photodiode adds another 400 fF. At the bottom, we see that the output of the Rockwell TIA introduces a small inductive component as well. This is under investigation.

Manufacturing Process

Here we describe our proposed manufacturing procedure, shown schematically in Figure 16. Using a three-axis jig, the ferrule is roughly aligned with the device visually through a microscope or camera; the height at which contact or near-contact between the fiber tip and device is noted. The ferrule is retracted, the lid is placed on the package, and loosely clamped by a small retractable arm. The ferrule is brought back down near the device and the lid is spotwelded in place, the ferrule-holding chuck is released and retracted, and a seam weld is performed to produce a lid-ferrule subassembly. The ferrule chuck is lowered and clamped for a final time and a fine alignment is made in the x-y plane to center the fiber. At this point, some force can be placed on the package vertically by the ferrule chuck to reduce weld shifts. The lid is tack-welded in place with four simultaneous spot welds, the ferrule chuck is finally retracted, and the package is then continuously seam-welded around its perimeter.

68
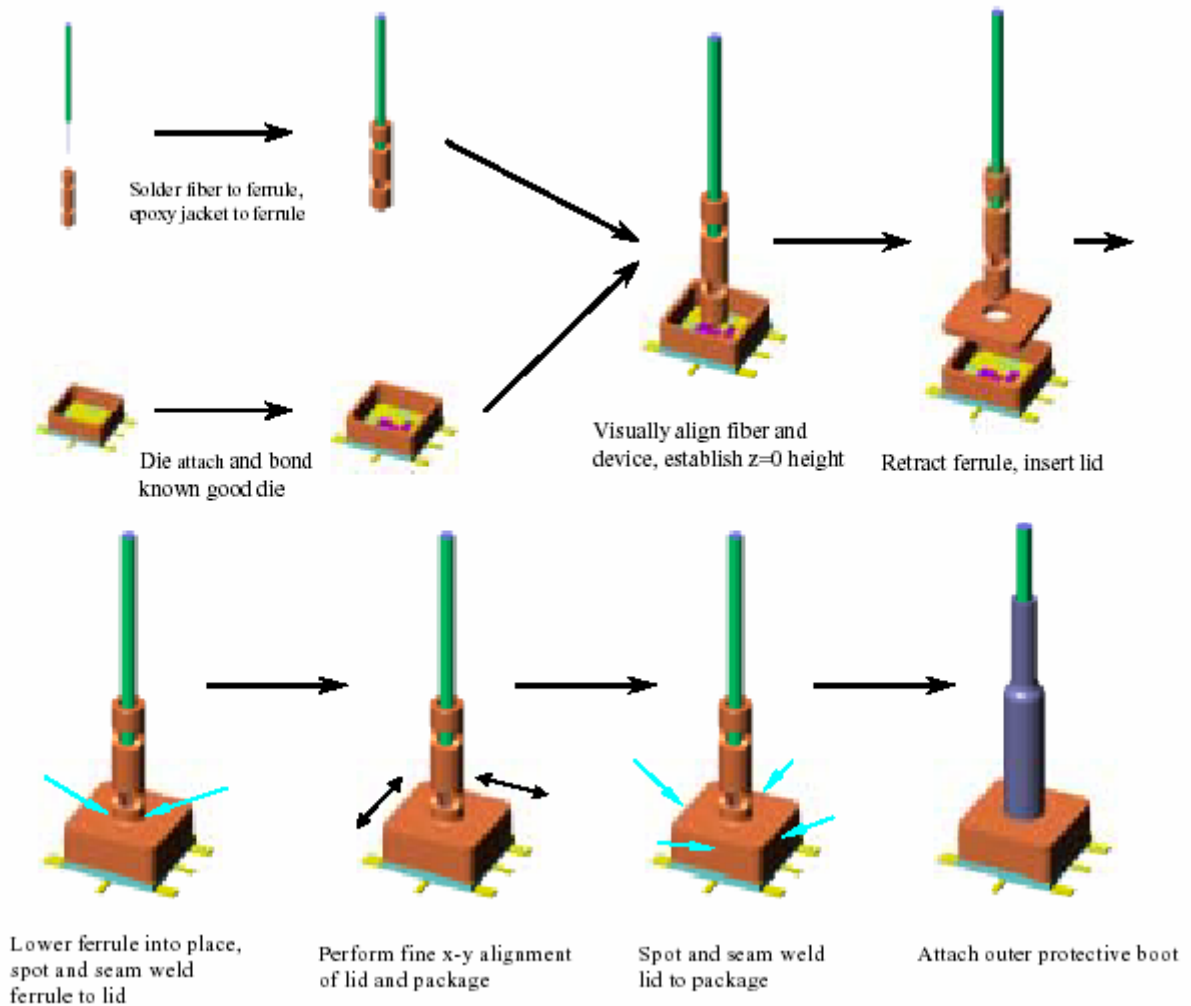
Figure 16. Assembly process sequence.

We are also considering other approaches that require a shorter sequence of steps and allow more parts to be pre-assembled, but they are not as flexible in that they place tighter tolerances on the placement of the die in the package, which is not desirable in our prototyping environment. The introduction of further automation would make these processes more viable.

Welder and fiber aligner tooling

The laser welding system has been designed for the maximum degree of flexibility in package size, shape, and lead configuration. Below we show the overall layout of the welding beam delivery heads, eight axes of weld head motion control, four axes of fiber alignment motion control, and a video microscope. The package is clamped in the middle of the array for welding, but can be easily placed or removed by a human (or machine) operator at the front of the apparatus by actuating a single axis of motion. Furthermore a ferrule/fiber assembly is readily loaded and clamped using the central vertical motion stage. Each laser weld head has two automated degrees of freedom (and one manual DOF), necessary to weld both the ferrule to the lid and the lid to the package. These degrees of freedom are also essential to flexibility to allowing a multitude of package variations while maintaining the same fiber attachment technique.
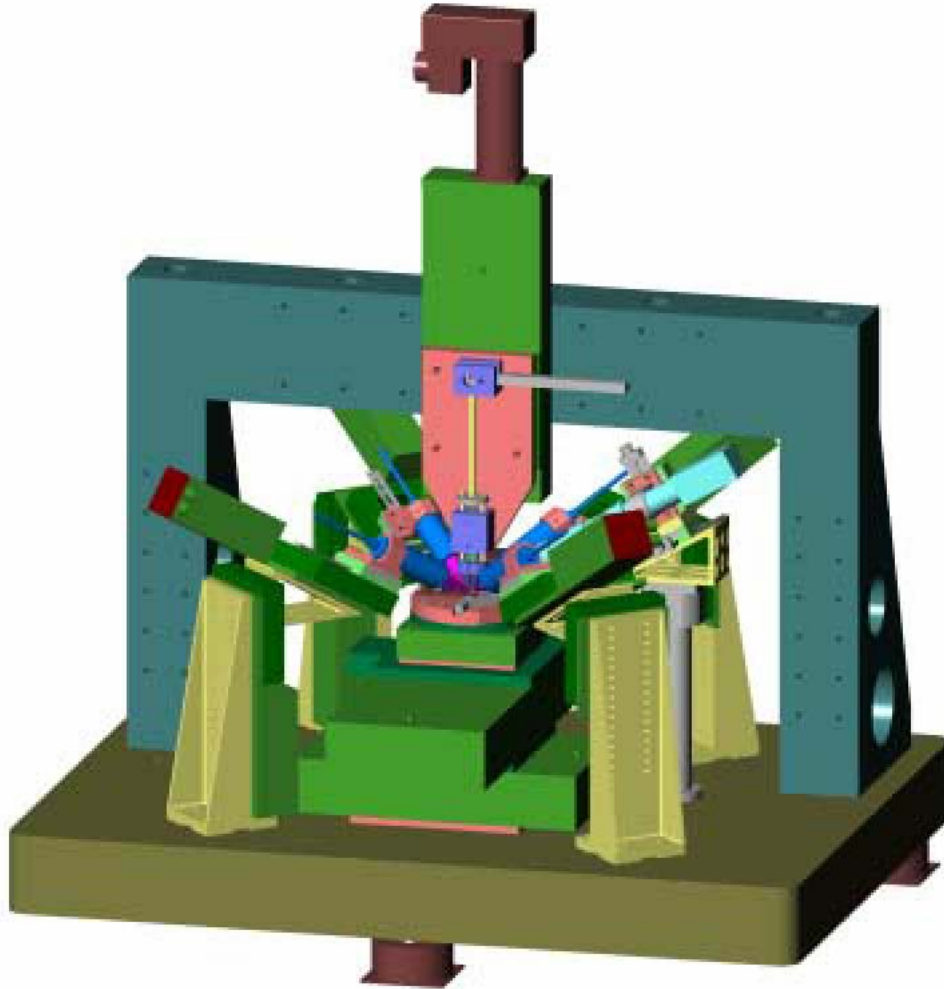
Figure 17. Layout of package welding setup.

All of the hardware needed for the laser welder has arrived and has been assembled, and we have begun preliminary testing. Figure 18 below shows the overall layout of the laser welding and fiber alignment system. At far left is the laser welder head, with the controller, power supply, cavity, and fiber optic delivery in one unit. In the middle is a standard 19" rack containing a passive backplane single-board computer with motion and laser welder control cards, a GPIB interface, and space to add data acquisition and a frame grabber. The welder hardware is at right, with two of the four beam delivery units visible at the front of the pneumatically vibration-isolated optical table. The cream colored stages in the middle are the x-y-z translation stages (those shown are consignment stages lacking linear encoders to give submicron resolution; the final stages arrived after the photo was taken). A granite gantry is mounted atop the optical breadboard to securely suspend the z-axis stage above the x-y-θ stage. The room is secured and the doors interlocked for laser safety.

70

Figure 18. Overview of manufacturing area. At far left is the Unitek-Miyachi LW52 Nd:YAG laser welder, capable of delivering one or four simultaneous beams, with maximum pulse energy of 50J and maximum rep rate of 50Hz (50W maximum power output). In the blue cabinet in the middle are an industrial computer and control/amplifiers for the motion control. The computer contains boards for controlling all 12 motion axes and for controlling the firing of the laser welder; a Windows NT-based interface allows flexible configuration of the welder and weld schedule. At right is the laser welder apparatus, with axes for controlling fiber alignment and the four weld heads. The overall structure is a pneumatically isolated honeycomb optical table with a granite gantry to support the fiber z-axis.

The motion control system is from Aerotech, who makes a computer-controllable driver capable of driving up to 16 axes and a card capable of coordinating the firing of the laser welder with the motion of the stages. The fine linearly-encoded stages for fiber alignment are capable of 20 nm resolution, and the weld head stages are rotary-encoded and have 0.1 μm resolution. The computer will also serve to control the other instruments needed, including a diode driver, optical multimeter, and modulation source, among other things.

Figure 19 shows a close-up of the weld staging area. Here the package, lid, and ferrule are loaded and readied for spot, then seam welding. The ferrule is held in place by a fixed-collet chuck, shown just above the package. To perform a spot weld, all four heads are fired simultaneously to reduce the effects of weld shifts. The beam delivery heads are shown in place to perform the spot welds. To perform the hermetic seam weld, three of the heads are retracted (as is the ferrule chuck) and one head remains in place, while the *x-y-*θ stage moves the part under the beam as the laser is pulsed continuously.
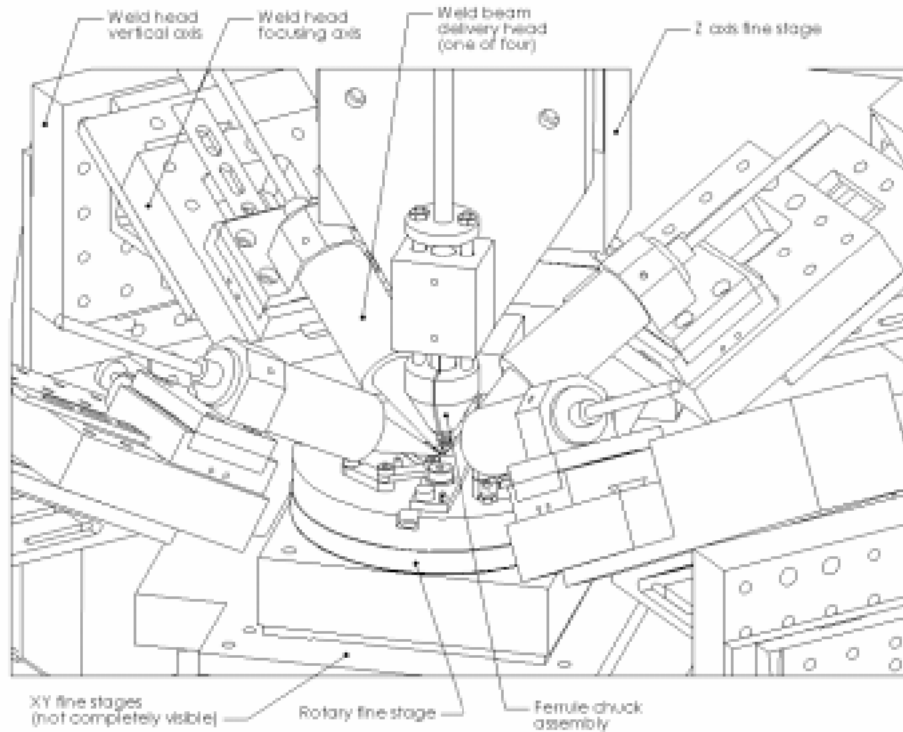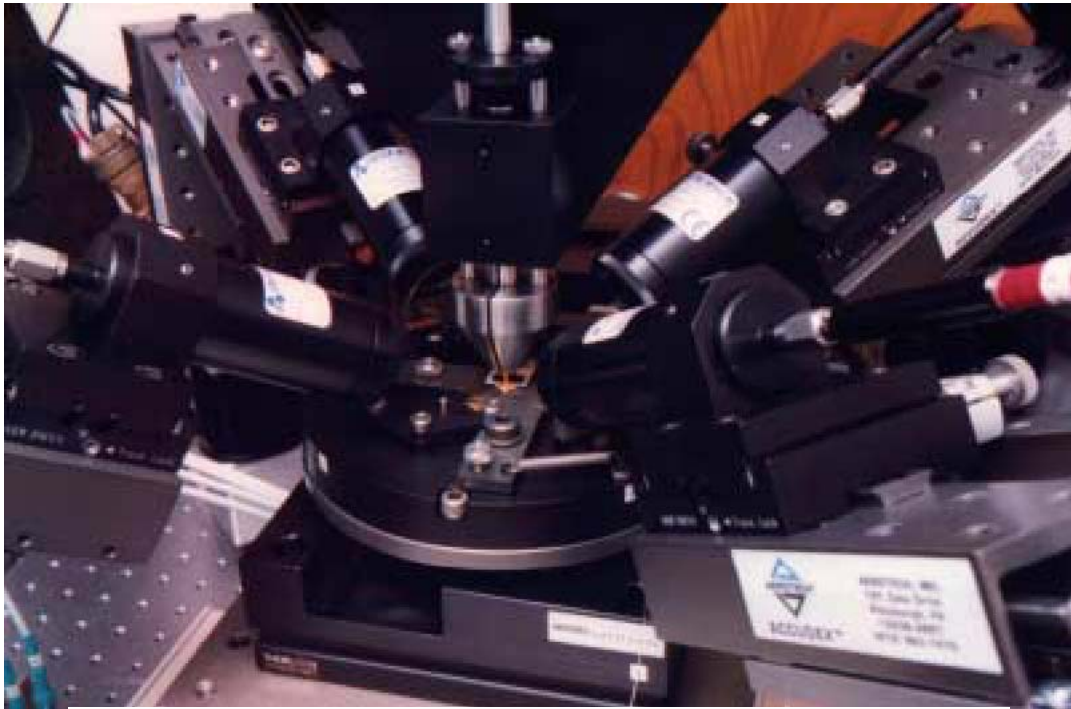
Figure 19. Close-up of the welder / fiber-aligner. At center is the 6.35mm ·6.35mm gold-plated package with lid and 2mm diameter ferrule ready to be spot- then seam-welded. The package is clamped in place by two precision machined torlon arms that both register it laterally and clamp it in place to make electrical contact to a 10GHz fixture. Above the package, holding the ferrule, is a specially machined collet and chuck which allows easy fiber handling and precision loading and re-loading of the fiber ferrule. The package is surrounded by four beam delivery optic modules.

72

Figure 20 shows a detail of the package, lid, and ferrule holding jig. As shown, the package and lid are clamped in place and a fiber and ferrule are loaded, ready to be picked up by the chuck, then aligned. The package is held in place by two torlon arms that laterally locate the package and put vertical pressure on the electrical contacts. At right, a third swinging arm carrying a U-shaped spring steel clamp secures the lid onto the package until it is tacked in place by laser welds. All of the clamps swing away easily to give complete access to the package and lid for loading and unloading, and are designed with a low profile to allow full access to the package both for spot and seam welding.

Hidden by the package and arms is an impedance-controlled circuit board and baseplate, launched from below by four Wiltron K connectors. These are connected to four flexible coaxial cables that exit to the left of the photograph.

At rear of the plate is a small fixture for holding the ferrule to be loaded into the chuck, and at front is a magnetic clamp for securing and strain-relieving the fiber pigtail while the package is welded. Note that the y-axis and weld heads are shown in the retracted state, allowing the operator to easily load and unload the package, lid, and fiber-ferrule assembly without obstruction.
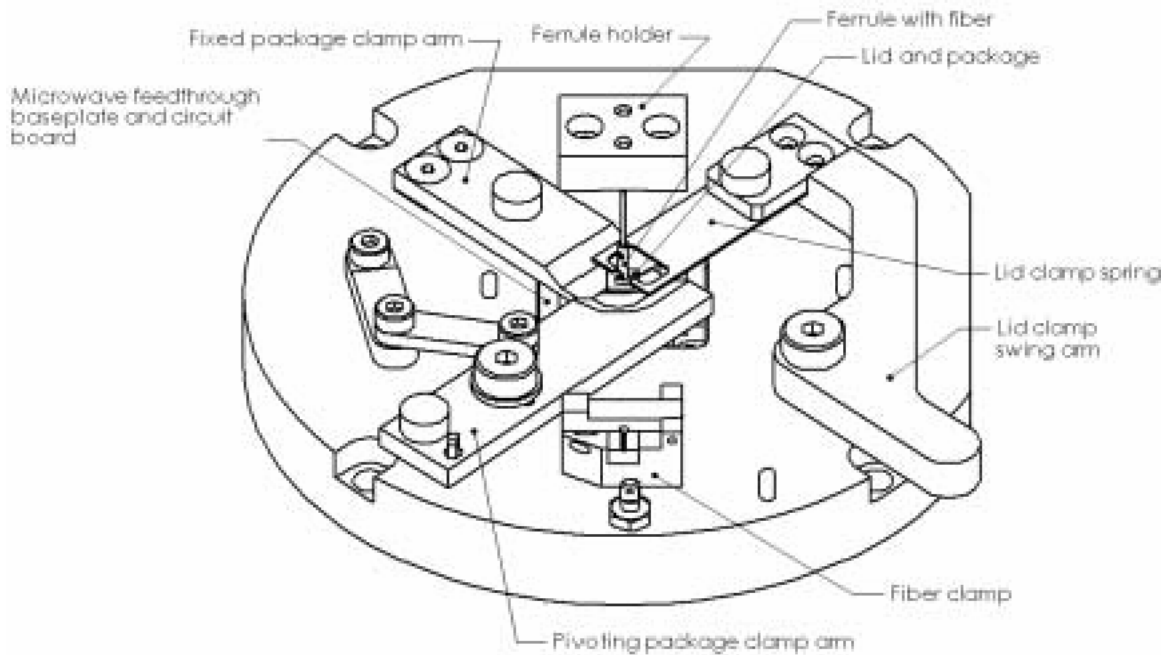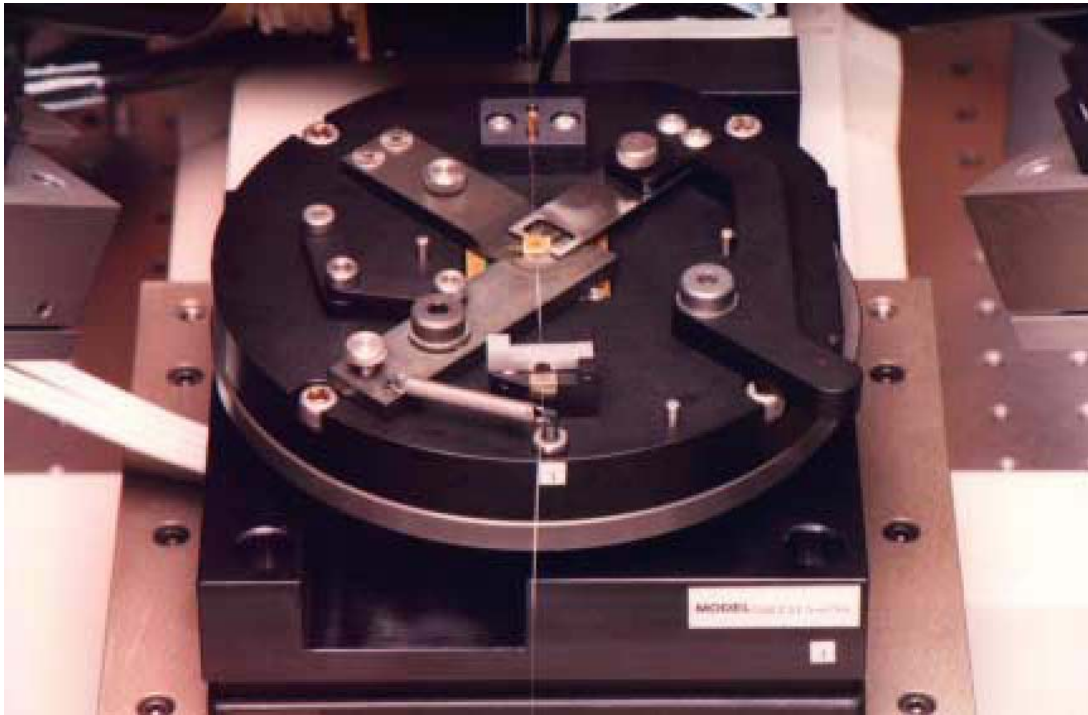
Figure 20. Detail of package and lid tooling. This stage is mounted atop a high-resolution rotary stage that sits on a high-resolution x-y stage with linear encoders.

In Figure 21 we show a detail of the ferrule clamping mechanism, mounted to the z-axis motion stage attached to the granite gantry (partly visible at the top of Figure 19). This is a unique design that relies on a fixed collet and moving saddle, which locates the ferrule in a more repeatable fashion than a traditional moving collet design. The ferrule and fiber are easily loaded into the fixture by lifting the counterweight arm. The fiber slides readily into a slot in the collet and saddle, and emerges out the front, where it is easy to handle.
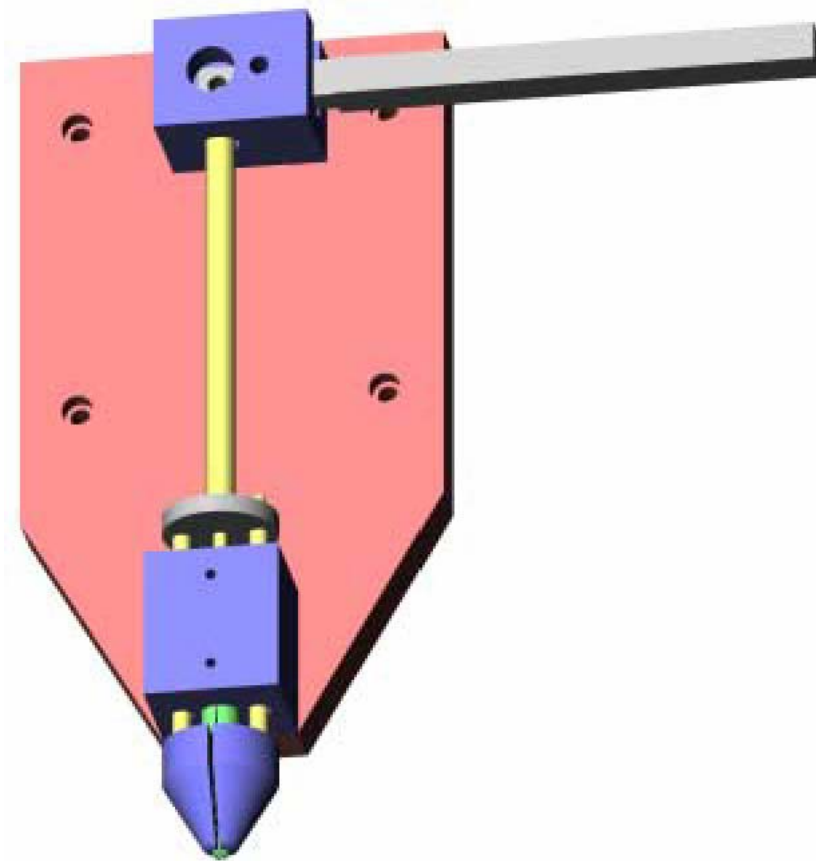
Figure 21. Ferrule clamping mechanism.

To create the soldered fiber/ferrule subassembly that is welded in the previously described photos, tooling is necessary to align and hold the fiber and ferrule. Figure 22 below shows the fixture used to assemble the two parts. A kovar ferrule, bearing two holes for access, is loaded into the right-hand side of the fixture. It is suspended between two thin V-grooves and clamped by the spring-loaded arm shown above it. A gold-metalized fiber pigtail is clamped into a magnetically secured V-groove, then translated into the hole of the ferrule along the rack-and-pinion mechanism. The length of fiber protrusion is precisely controlled by two stops adjusted by ¼"-80 ball-tipped screws. Fluxless solder is added through one of the side holes in the ferrule, and heat is externally applied with a high-temperature hot air soldering gun. While the solder is molten, capillary action and cooling locate the solder blob near the fiber tip, securing it mechanically and forming a hermetic seal.
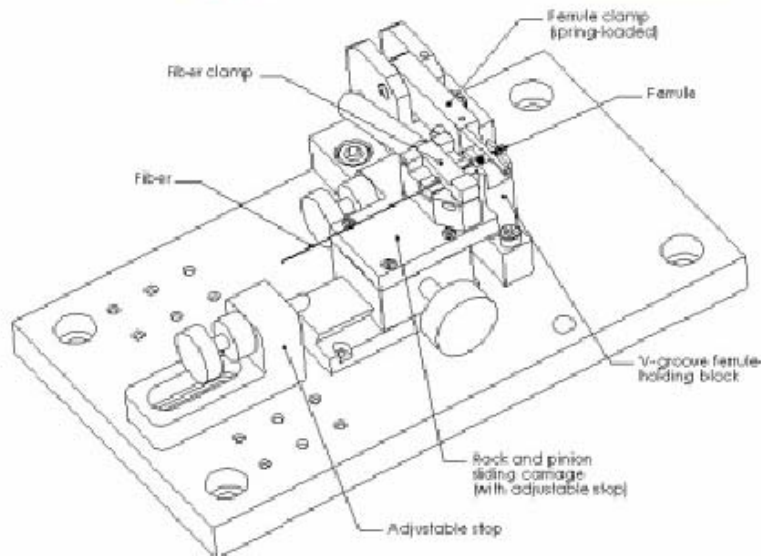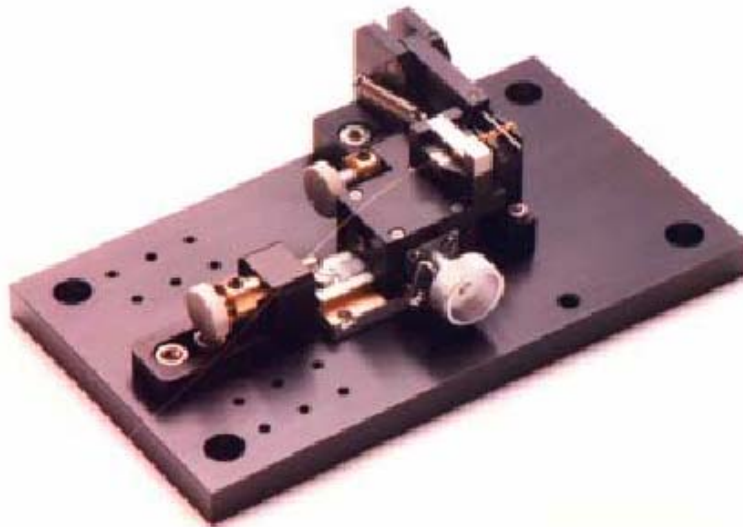
Figure 22. Fiber-ferrule soldering fixture. This jig eases the production of the fiber-ferrule-soldered subassembly. The ferrule is loaded into the right-hand side and held in place with the spring-loaded arm at rear. The fiber is clamped into the holder to the left of the ferrule, and the rack and pinion mechanism is used to place it inside the ferrule. Fluxless solder and a hot-air soldering gun are used to mate the two pieces. These subassemblies are easily made rapidly and in parallel with the lid welding and die attach/bonding processes.

We have assembled and performed initial tests of all of the tooling, and iterated to ensure good solve various small fit-up problems. We have successfully soldered the ferrule to the fiber, and have performed a four-spot simultaneous weld of a lid to the package using our tooling. We have also performed a continuous seam weld of the lid to the package with a manual jig (before the motion control arrived).

76

Package welding

In the process of deciding what laser welding system to purchase, we visited two vendors to test-weld our packages. The first was an applications lab at Unitek Miyachi where they allowed us to test weld lids and ferrules onto our Kyocera packages. While visiting, we determined how weldable our parts are, an appropriate weld schedule, and measured rough cycle times for the welding process. We were also able to learn some about the requirements of our fixture.

At another vendor, MTI, a job shop specializing in laser welding hermetic packages, we tested the hermeticity of the lid seals and refined our lid attach design slightly. The packages we welded using 0.010" thick lids were hermetically sealed and passed the leak test, however the ones with 0.030" lids failed the leak test, showing visible signs of micro-cracking. Based on this knowledge, we have modified our design slightly by acquiring stepped lids and modifying our ferrule design slightly. A stepped lid allows for a thin lip for improved weld geometry, yet has central thickness providing strength against buckling and providing material for the tube-lid seam.

Clockwise from left:
- Lid seal
- Close-up of lid seal
- Lid seal cross-section
- Tube seal cross-section
- Close-up of tube seal

Figure 23. Welded Kyocera package, showing various close-ups of welds from the outside and in cross-section, showing penetration and weld extent. These welds were done using 2-3J pulses from a Unitek Miyachi Nd:YAG laser, at their facility in Monrovia, California.

Conclusions

Component acquisition and characterization

Based on our previous results and measurements of the first-generation VCSEL characteristics, we have created a complete specification for the second generation. Table 3 below summarizes the MODE specification sheet. No major design change in the VCSEL cavity design is expected, but MODE has consistently improved their process reliability and variation across the wafer.

Table 2. Specifications for MODE VCSEL die

Absolute maximum ratings

Parameter	Rating
Storage temperature	-40 to +100°C
Operating temperature	0 to +70°C
Maximum die exposure temperature	325°C for 10 s
Maximum optical output power	10 mW
Maximum reverse bias voltage	5 V
Maximum continuous operating current	10 mA
Maximum instantaneous operating current	15mA

Electro-optical characteristics (T = 0 to 70 °C)

Parameter	Symbol	Units	min	typ	max
Peak wavelength	λ_p	nm/°C	830	850	860
Secondary modes	$\lambda_{1},\ldots$		3	5	
Peak wavelength temperature coefficient	$\Delta\lambda_p/\Delta T$	nm/°C	0	-	0.1
Threshold current	I_{th}	mA	-	2	3
Output power at high current*	P_1	mW	1.5	3	5
Operating voltage at high current*	V_0	V	1.6	2.7	3
Reverse bias for 100 uA leakage	V_{rev}	V	5		-
Differential "on" resistance	R	Ω	40	50	70
Oxide aperture diameter		μm	8		15
Bandwidth at I = $(I_H+I_{th})/2$		GHz	8	10	
Relative intensity noise at I_H	RIN	dBc/Hz		-122	

- High current is I_H = 10 mA

Physical description

Parameter	Symbol	Units	Typical
Die length	L_D	μm	600
Die width	W_D	μm	600
Die height	H_D	μm	150
Bond pad configuration	Ground-Signal-Ground		
Center bond pad width	W_{CF}	μm	80
Center bond pad length	L_{CF}	μm	100
Bond pad to laser aperture*	L_{P-A}	μm	50-100
Bond pad to die edge	L_{P-D}	μm	20-75
Bond pad gap	W_{GAP}	μm	35-50
Ground bond pad length	W_{GP}	μm	100-200
Bond pad pull strength		g	>3.0

- VCSEL in center of die

The major changes from the first generation devices are to provide topside metallization in a coplanar waveguide structure, allowing improved RF coupling. We have added a specification for bond pad pull strength, as this has been a persistent problem among the first generation; they claim that process improvements and a new machine for depositing the polyamide should improve metal adhesion. Absolute maximum ratings should be compatible with solder die attach techniques and our environmental requirements. The other E-O characteristics are matched to current device performance.

We have chosen to put two VCSELs back-to-back on each die, of different diameters. This provides flexibility in two ways: to MODE, since diameter is essentially a derived function of modulation bandwidth and DC operating characteristics (LIV); and to us in making a good couple between the VCSEL and the variety of fiber diameters our anticipated customer base requires. Figure 24 shows the metallization layout for a single die, showing the coplanar waveguide structure, fiducial alignment marks, and location for a serial number.
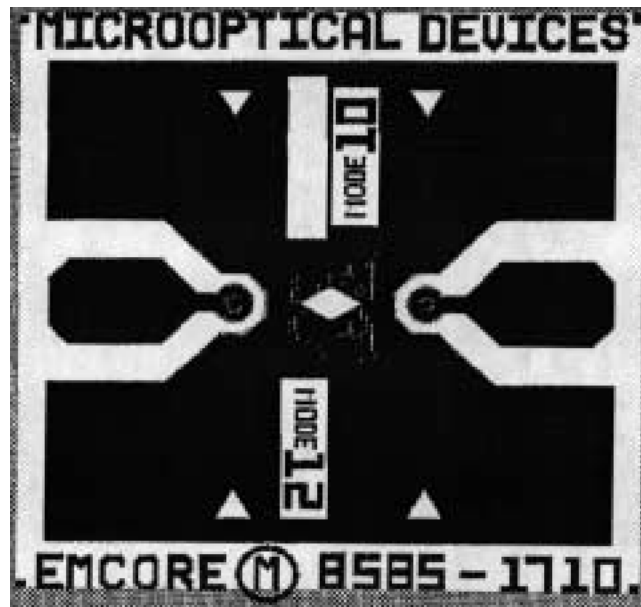
Figure 24. MODE die metallization mask showing two VCSELs back to back, with coplanar waveguide pads and fiducial marks for locating. Nominally the cavities will be 10 μm and 12 μm in diameter, but are subject to the constraints of the other specified parameters.

Link characterization and design

Initial calculations show that the following family of link designs operating at 850 nm would cover all the possible user fiber requirements:

Table 3. Summary 850 nm Link Designs for Various Fibers Core Sizes

Fiber core size, μm	Detector diameter, ∝m	Received power for 10-12 BER in HBT design, dBm	Allowance for plant loss plus link margin	TX min power for 5 dB power margin over life and eye-safety, dB
50	60	-18.5	8.5	-10
62.5	70	-17.5	7.5	-10
100	110	-16	6	-10

Each of the designs in Table 3 would comply with the fiber-channel standards for short wavelength links. However there are two problems with the above designs: First, existing 850 nm sources are not qualified for –40 to +105°C operation. Second, the fiber used in the 777 and F-22 is 100 μm core, and 6 dB is not enough for plant loss with margin in a critical environment.

Plant loss is apportioned between fiber losses (< 1 dB for length less than 300 m), connector loss (1.5 dB worst case for expanded beam connector, 1.0 dB for physical contact connector), and splice losses (0.5 dB worst case). A point-to-point link typically has two connections and no splices for a worst-case total loss of 4 dB for expanded beam connectors. The remaining budget is apportioned between various "penalties" that may be required (Fiber-Channel requires 2 dB for multi-mode links) and safety margin for unplanned splices or component degradation over life.

The ARINC-636 transceiver produced by Boeing for the 777 and F-22 provides 20 dB for plant loss plus link margin. This extra 9 dB compared to a commercial FDDI link is to cover the extra losses of the expanded beam connectors and optical bypass switches used in the Boeing 777 network in addition to added tolerance for aging over a 20-year life. The primary focus of our program is on point-to-point links rather than the bi-directional ring topology assumed for the ARINC-636 devices. Point-to-point links do not require optical bypass switches and have fewer total connectors per link. Therefore, our link specification does not require 20 dB, but is probably more than the Fiber Channel specification of 6 dB. Our working assumption is that an additional 3 dB will be sufficient: 4 dB for plant loss, 2 dB for optical path penalties, 3 dB for unplanned splices and degradation for a total of 9 dB.

Two designs are detailed in Table 4 on the next page. Design "A" is the baseline plan that has the most commercial leverage. Design "B" is an extrapolation of the ARINC-636 requirements. The only major difference between designs A and B is the laser diode and detector elements that are needed to handle the temperature range and higher link-margin requirement of the military application.

Fiber attach and packaging

Using a simple epoxied fiber attachment technique, we have been able to demonstrate that our procedure is robust enough to produce useful prototypes. We have designed and acquired all of the necessary hardware for our automated fiber alignment and welding system, and have created a package profile that is manufacturable. A laser welder and motion control system have been integrated and tested, and all of the custom tooling has been acquired and initially tested.

In the following year we plan to integrate all of the processes and perform most of the welding operations under semi-automated computer control, and determine the best procedural order for the lid attach operation, further determine tooling tolerances and repeatability, and any wear on the tooling caused by the welder. Furthermore, with the arrival of the high-resolution stages we will be able to measure weld shifts and assemble an entirely welded package/fiber combination.

Table 4. Link budget detail for two possible variations

	Specification	A: Commercial	B: Version comparable to ARINC-636 spec
General	Data Rate	10 Gb/s	10 Gb/s [1]
	Wavelength, nm	850	TBD SLM laser [2]
	Optical Fiber Core, µm	50, or 62.5	100
	Operating Temp., °C	0 to +70	-40 to +105
	Hermeticity [3]	<5x10^{-8} atm-cc/s He	<5x10^{-8} atm-cc/s He
Transmitter	Min. Power, dBm	-10	-8 [4]
	Max. Power, dBm	-5	-3 [4]
	Extinction Ratio	10%	10% [5]
	Max. Rise/Fall time, ns	0.045	0.045
	Eye Opening at 10^{-12} BER	57%	57%
	Deterministic Jitter	20 %	20%
	RIN, dBc/Hz	-122	-122
Receiver	Sensitivity, dBm at 10^{-12} BER	-16	-17 [6]
	Overload Power	0	0
	Rise/Fall time, ns	0.035	0.035
	Optical Return Loss	-12	-12 [7]
	Output voltage swing	200 mV differential	200 mV differential

Notes

[1] The ARINC-636 specification is 125 Mbit/s. This program is concerned with 10 Gb/s operation.

[2] There is not presently a commercial VCSEL that covers the full temperature range. The back-up plan is to use a qualified edge emitter on a sub-mount. Longer wavelength can be readily accommodated.

[3] Commercial components for telecommunication applications typically require hermeticity, data-communication applications do not except in special cases. This program is concerned with the cases that do require hermeticity.

[4] ARINC-636 spec. is based on an LED transmitter with −9 and −14 dBm for Max and Min. The proposed version user higher power to improve link margin and achieves eye safety by working at longer wavelength than design A.

[5] The ARINC-636 spec is 5% for an LED transmitter. High-speed laser transmitters will not work well below 10%.

[6] One dB improvement is assumed for >850 nm operation with an InGaAs photodiode.

[7] It is also possible to achieve −27 dB with an angle polished fiber if this is required by laser feedback sensitivity in the chosen laser.

81

Program for Year Two

In the next year we expect new progress in all of the work categories. We plan to ship prototypes with our second generation VCSELs, newly fabricated photodiodes, and receiver/transmitter amplifier/driver chips. Furthermore, we expect to provide welded samples by year-end as well.

In order to do this, we plan to step-up efforts to characterize the individual components, and speed to production of prototypes. On-wafer/on-die characterization will also play a stronger role in determining process quality and improving yield.

Meanwhile the laser welder will undergo development and we will explore the known issues of weld shifts and fiber stability due to solder creep. We don't expect these to be an issue, but they are identifiable hurdles. The fact that our link is multi-mode loosens our tolerances and should make this less of an issue than other groups have found it to be. Furthermore we plan preliminary hermetic testing of the weld and solder seal. At the same time we will examine the tooling reliability and repeatability, and begin to assess production cycle times.

We also plan to revise the package lead frame to accommodate differential inputs. This requirement has been expressed by several potential customers and better fits the specifications of the driver chips. We will also explore the requirements of adding external protocol-specific chips for multiplexing/de-multiplexing and encoding. Although not essential for an application like digital radar, there is strong commercial sentiment that it would be highly appealing to not be required to provide a 10 GHz bit stream to a transceiver, which is typically mounted to a multilayer digital PC board in an environment where impedance is difficult to control. Although a multiplex of only 1:2 or 1:4 would be required, it is unlikely to be economical to place them inside our package.

Overall, we expect the next contract year to be fruitful and exciting!

Year Two Summary

Optical Link for Radar Digital Processor

Terri L. Dooley, Grant R. Emmel, Robert A. Marsland*, Michael P. Nesnidal and Robert S. Williamson III

*Principal Investigator

July 1999

[r] **Focused Research, Inc.**
555 Science Drive
Madison, WI 53711-1060

Abstract

We present our second year of progress toward manufacturing a low-cost, high-speed (10 Gigabits/second), multi-mode fiber optical link based on an 850-nanometer vertical-cavity surface-emitting laser (VCSEL) transmitter and an amplified high-speed gallium arsenide photodiode receiver. Our approach is to combine VCSELs and transmitter/receiver chips built to our specifications by outside foundries, our own photodiodes (based on a proven product) fabricated on-site, and a fiber attachment technique based on a laser-welding approach. A complete, unpigtailed link prototype, using our own custom-designed GaAs transmitter and receiver circuit designs has been built and tested using a psuedo-random bitstream generator, and meets nearly all of our design goals. The link incorporates a mature MODE VCSEL design, a photodiode we designed and fabricated, and a unique differential interface package. We have begun to demonstrate semiautomated operation of our laser-welded lid sealing and fiber pigtailing robot.

Contents

Figures and Tables

Summary

We are developing a high-speed serial optical link suitable for several commercial and military short-haul applications, most notably digital phased-array radar. At the heart of the link lie a vertical-cavity surface-emitting laser (VCSEL) diode transmitter and a gallium arsenide photodetector, coupled by multi-mode optical fiber. The devices are hermetically packaged with basic control circuitry (diode driver and amplifier) and pigtailed in a metal-ceramic surface mount package less than 0.2 cm3 in volume. The link is capable of >8.5 gigabit per second operation, is protocol independent, and can transmit over distances of > 100 meters. Our ability to fabricate photodiodes on-site and our partnership with Micro-Optical Devices (MODE), a VCSEL manufacturer will help make this a low-cost product. Furthermore, under this program we are developing a low-cost automated fiber pigtailing and packaging facility, an essential element to producing inexpensive photonic components.

We have demonstrated a complete link, composed of our receiver and transmitter driver circuitry, a photodiode of our own design, and a mature MODE VCSEL. This link has been tested and functions with a 10 Gb/s psuedo-random data stream. A final link specification, although subject to some revision based on current discussions within the high-speed community, has been settled upon, and we have tested a complete, differentially driven receiver and transmitter pair to compare against this specification. An operational laser-welded packaging system has been demonstrated and several test packages have been sealed.

Optoelectronic device development and characterization. Several batches of devices from MODE have been tested and/or built into transmitters, each batch showing some improvement over the previous one. The most recent parts have shown significant improvements in bondability and frequency response, and have performed well as part of a link. We have fabricated several runs of photodiodes, the final one producing a 6 GHz bandwidth diode, which is marginal for 10 G. Each run has increased our understanding of the complexities of the device, and we expect our next run to produce faster, more sensitive photodiodes.

Link development. We received first-generation SiGe Rx/Tx chipsets from our collaboration with IBM and Mayo, and tested them extensively. A functioning receiver was built using TIA and AGC die and a NF photodiode. The data from these designs were used to design a second-generation GaAs chipset. We demonstrated the primary functionality of our receiver and driver chipset by building a complete link and sending data through it.

Packaging. The robot is operational and can flexibly switch between two styles of package with some minor tooling switchover and re-alignment. A new style of differentially-leaded package and associated tooling has been created. We have successfully welded lids onto both types of package, created a usable welding sequence, and measured weld-induced motion on the order of a few microns. We still need to complete the weld sequence with the aim of minimizing weld shifts, as well as pigtail real receiver and transmitter modules. We are currently seeking a patent on one aspect of the packaging system "Fixture for laser welding fiber tailed surface-mount microwave

packages," and are examining the entire project for other patent-worthy inventions. The link is growing in maturity in all aspects and judging from the widespread interest, shows great commercial promise. Nonetheless, nearly every aspect including the photodiode, packaging approach, and link design will need focused effort in the coming year to produce a usable, reliable design.

Introduction

There is a growing need for high-speed serial communications links that are lightweight, reliable, and cheap, for both commercial and military applications. Copper interconnections are heavy and expensive above speeds of several gigabits per second (Gb/s) even for distances below a hundred meters. Parallel optical connections with a dozen or more fibers have become available, providing speeds of 10 Gb/s and above, but these suffer from high interconnect cost and can be somewhat less reliable since many fibers and devices are required to produce a link. In addition, meeting Class I eye-safety requirements is extremely difficult with 10 850-nm emitters operating at 1 Gbit/s. A much more appealing approach is a higher-speed, single-fiber approach. With the advent and approaching commercialization of reliable vertical-cavity surface-emitting lasers (VCSELs) with several gigahertz of bandwidth, single-fiber multi-mode serial interconnections become a feasible and inexpensive alternative.

We are developing an 850-nm, multi-mode, fiber-optic serial transmitter and receiver, operating at 8.5-12 Gb/s, capable of transmitting over distances of 100 meters. Our design is protocol-independent and can function either with DC-balanced code or in burst mode, making it broadly applicable to virtually any short-haul, high-speed, point-to-point communications application. We expect our highest payoff military application will be digital radar, and commercially, we expect local area networks (LANs), storage area networks (SANs), and telecommunication switch interconnections to be major players. The length and fiber objectives adopted by the Ethernet 802.3 high-speed study group in July 1999 are consistent with our technology's capabilities.

Several elements allow us to make this high-performance link low in cost as well. Using a single inexpensive VCSEL for the transmitter element, designed to operate at high modulation rates and a wide environmental conditions, gives us reliability over competing parallel approaches and considerable cost savings over a traditional edge-emitting laser. The detector in the photoreceiver is similar to an established New Focus design that supports an already successful product family. Also important is a relatively inexpensive, reliable packaging approach; we are using a hermetically sealed, laser-welded package that can be fiber-aligned and sealed automatically with minimal operator involvement. Finally, we are developing a manufacturing process that uses tested devices (known good die), reducing the need for rework and low yield at the end of the assembly process.

This report summarizes our second year of progress in this three-year program. In the following sections, we provide some background motivation and assumptions that have led us to take this approach. Next, we describe the results of our program of component characterization, prototype link development, and packaging/fiber attachment. Finally, we conclude and discuss our plans for the coming year.

Methods, Assumptions, and Procedures

Here we briefly discuss some of the technical rationale behind our approach.

When it is necessary to move large amounts of data very fast over a short (<100 meter) distance, there are at least five possible methods:

- parallel copper wires,
- parallel fibers driven from logic levels,
- parallel fibers driven by separate serial interfaces,
- parallel serial interfaces wavelength-multiplexed on one fiber, and
- a single serial interface on one fiber.

The single serial interface will be the optimal solution in many applications where reliability, robustness, size, and cost are the major considerations. A single fiber interface can incorporate controls on average laser power and receiver DC levels that would be too costly if repeated 12 or more times for a given link. Wavelength division multiplexing relies on the data being divisible into separate data streams. This is not the case for the digital radar application where the data is originating from a single A/D converter.

All things being equal, a single fiber is preferable to 12 and any fiber is preferable to a massive copper cable, which becomes too heavy and costly when sending data more than a few meters at >1 GByte/second. The pressure on the serial link is to demonstrate cost and power requirements comparable to the other approaches. Table 1 summarizes this comparison, based on a 5 meter link with an aggregate bandwidth of 12 gigabits (transceiver and cable only). Clearly, the case for fiber solutions gets better as for lengths >5 meters.

Power and cost estimates for parallel optical approach very widely because these units are only now going into production. For the purpose of comparison, 1 W was chosen as the power since this is the minimum power necessary to drive twelve 50-ohm lines at ECL levels from a 5V supply. The multiplexer/demultiplexer price is not included in Table 1. Since the data channel widths do not match the word length from the A/D, each technique compared in Table 5 will require a mux and demux although the 12 Gb/s parts will be the most expensive. For reference, a 10 Gb/s mux/demux including the phase detector and timing circuitry is available from Vitesse for $2500 in a prototype package and dissipates 5 W. They expect this device to fall below $100/ea in quantity as yields improve.

Table 1. Transceiver approach comparison

	Single Fiber 12 Gb/s	Parallel Optical Link, 12 Parallel, 1 Gb/s	Serial Copper Link	Parallel, Copper Link, 41 diff-parallel, 250 Mb/s
Power (W)	1 (2.5) [1]	1	1 (2.5) [1]	2
Cost Projection ($/Transceiver)	200	610 [2]	800	600 [3]
Diameter of cable(s) (mm)	0.125	3	7 [4]	100×10 [5]
Weight (5 m cable, kg) [6]	0.008	0.1	0.51	0.5
Reliability (MTTF hrs, VCSEL, 25°C)	$1.0 \cdot 10^7$ [7]	$0.75 \cdot 10^7$ [8]	N/A	N/A

(1) 2.5 W includes serializer/deserializer circuitry
(2) Based on $10 per Gb/s as target price of parallel optical link plus cable and connector cost
(3) Based on cost of 5 meters of W.L. Gore "RIBBON-AX" cable at $120/meter (no connectors)
(4) Based on UFE 276B high-isolation cable
(5) Based on bundle of 2, 2.25" wide "RIBBON-AX" cables
(6) Based on weight of cable only, no armor
(7) Based on 1E7 hour MTTF number from Honeywell preliminary data sheet
(8) Based on 12 VCSELs, log-normal distribution, $\int$ = 0.225

Technical Approach

Presently, high-speed (~10 gigabit/second) fiber optic transmitters and receivers rely on singlemode long-wavelength laser diodes aligned to single–mode fibers. The alignment and packaging process is time-consuming, labor-intensive, and relatively low yield (<50%). Furthermore, it requires an expensive package that is prohibitively large for many applications.

We will build 12 gigabit per second transmitter and receiver modules that are inexpensive and substantially smaller in size (cubes less than 0.25 inches on a side) by taking advantage of multi-mode VCSEL laser chips, state-of-the-art foundry services, and, most importantly, a fast, low-cost, high yield fiber attachment technique. This fiber attachment technique will also be flexible and amenable to customization: it will allow us to accommodate different package styles or different fibers without dramatically increasing costs.

Constructive Plan

The fiber attachment technique will involve the following steps:
   • bonding the fiber to the lid, using a tool to align along the *z*-axis, and strain-relieving the fiber
   • aligning the lid-fiber subassembly to the transmitter or receiver package, and
   • welding the lid in place.

Results and Discussion

Opto component acquisition and characterization

VCSELs

Introduction

Over the past year we have received several generations of oxide-confined multi-mode VCSELs from MODE (now Mode/Emcore). The MODE VCSELs have shown consistent improvement over the past year in improved frequency response and wirebondability and we are working with them to make further improvements. In this section we discuss the critical VCSEL parameters we have measured and compare them with the specifications listed in Appendix B.

We continue to receive new VCSELs from MODE and, more recently, from Gore Photonics. Both of these companies want to see their product succeed and so are providing these additional samples and detector wafer samples free of charge or for nominal charge.

Testing methodology

The VCSEL and photodiode on-die testing procedures have been documented and we have written LabView code to assist in the data-taking process. The LabView application that helps automate the testing of VCSELs controls the diode driver, signal generator, and high-speed oscilloscope to give a calibrated bandwidth profile of the diodes. A power/wavelength meter is also used to measure LIV curves and wavelength. This suite enables us to perform complete testing on each device and determine consistency as we take time to test more devices.
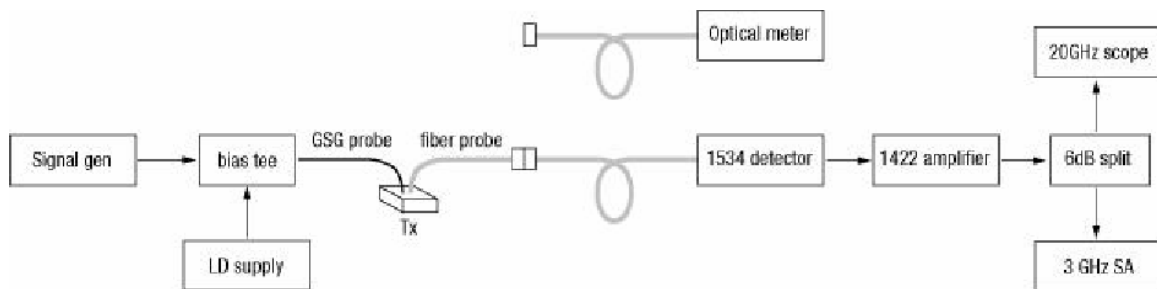

Figure 1. Block diagram of setup used to test VCSELs.

Our testing scheme is diagrammed in Figure 1. The die are placed on the probe station and electrically probed with a GGB ground-signal-ground probe rated to 40 GHz. The VCSEL is driven by a Newport model 5005 laser diode drive through a picosecond pulse labs bias tee; AC signal comes from a Wiltron signal generator. The output of the VCSEL is captured through a 50 μm multimode fiber probe and delivered either to an ILX Lightwave meter or a New Focus model 1534 detector. To measure LIV curves, the LD supply and optical multimeter are monitored. Then, to measure bandwidth and RIN, the output is switched to the 1534. We can observe a spectrum from 0-2.9 GHz on the HP spectrum analyzer, and beyond that we use the HP 20 GHz scope and our LabView application.

DC Response

Measurement technique

The electrical input end of this setup is identical to that in Figure 1, except that the RF modulation is disabled, and the optical fiber is routed to the ILX Lightwave power and wavelength meter ("Optical meter"). The LD supply current is adjusted and forward voltage is monitored.

Results

We tested a sample of the second-generation multimode devices (batch of 100 devices) to see if they meet specifications. The DC LIV characteristics are as expected, with a lasing threshold of about 0.5 mA, and a dynamic impedance of 50 ohms. The DC impedance measurement was confirmed by a TDR measurement. We also performed TDT measurements using a NF 1534 detector; these measurements showed good step response, although the coaxial cable degrades the stimulus risetime to 55 ps before it reaches the VCSEL.

The DC results for one VCSEL are shown below in Figure 2, showing power output and drive voltage versus current, as well as the AC impedance as measured by TDR. These tests show the device meets specifications for output power, threshold current, operating voltage, and differential "on" resistance. Note that the impedance measured via TDR correlates well with the slope of the I-V curve.
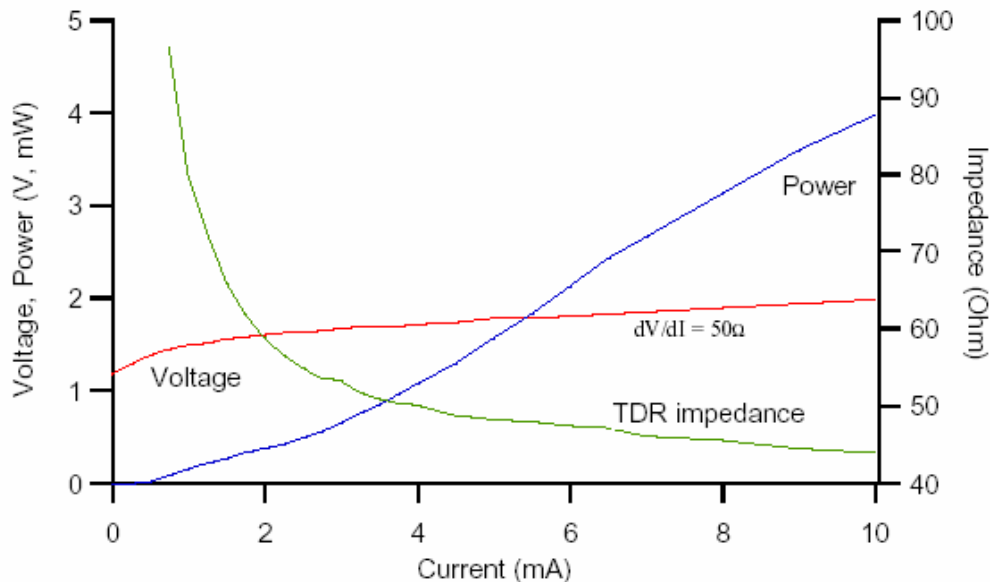
Figure 2. LIV and AC impedance characteristics of a second-generation 10mm GSG VCSEL. The TDR impedance is measured by applying a 40 ps risetime step to the input of the VCSEL.

AC Response

Measurement technique

The bandwidth is measured by driving the VCSEL with a sinusoidal source provided by a Wiltron function generator (with leveling set to manual, pivot at 6 GHz, slope 172) that goes into a Picosecond Pulse Labs 5545A bias tee. The Wiltron leveling function provides

approximately constant amplitude drive to the VCSEL ensuring optimal signal to noise while maintaining small signal drive conditions at all frequencies. DC bias is provided by a Newport 5005 diode driver. This passes through a 4 foot cable and SMA elbow into a Picoprobe GSG-40 for on-wafer (on die) probing of the VCSEL.

The multi-mode and single-mode setups are identical, save for a short wire that provides a separate direct DC connection from a gold-plated mount that the DUT sits upon to the outside of the coax connected to the Picoprobe. This adds some filtering near 1 GHz, but we can account for this during testing. The reason for this extra connection is that this particular batch of singlemode devices suffers from a very thin oxide layer between the topside ground pads and the internal cathode connection, providing only an AC connection from the chip topside.

The output of the VCSEL is collected by a 50 μm lens-tipped fiber (approximately 140° angle) which helps reduce the effects of back-reflection by presenting a non-planar surface as well as allowing the tip to sit farther above the VCSEL while still collecting a majority of the light. The fiber tip is adjusted to be 50-100 μm above the surface, which generally collects only about 80% of the light, but by careful lateral and vertical adjustment, reduces back-reflections and interactions that lead to high RIN.

The probe and its several inches of fiber are connected to a 2 m patch cord of 50 μm MM fiber. This is detected by a Newport D-15 detector which has about 29GHz 3dB bandwidth, and amplified by a New Focus 1422 with 20 GHz bandwidth. We measure the RMS value of the signal on a HP54750 scope with 20GHz head, and subtract in quadrature both instrumental and RIN noise to arrive at the effective response.

We calibrate the electrical portion of the system simply by bypassing the probe, VCSEL, and D-15 detector and measure the response. We remove this response from the device response. Newport has provided the response of the D-15, and we account for this also. In the range of 0- 15GHz, the Picoprobe response is flat to a few tenths of a decibel, so we do not correct for this. Furthermore, there is a short cavity formed between the output of the D-15 (which is internally unterminated) and the input of the 1422 amp, which causes some variation in the system response. We have estimated this variation to be a few dB, as measured by Fourier transforming the impulse response of the D-15/1422 system as compared with the D-15 response directly measured by the scope head; however, we do not include this as part of our calibration.

Note also that because of the relatively low average power limit of the D-15 detector (due to the thin interdigitated metal contacts), at VCSEL output levels much above 1 mW we purposely attenuate the optical output (by loosening an FC/FC connection). This affects only the absolute signal level, but not the relative, since this misalignment reduces both the DC level and carrier signal equally.

Results

Second generation devices

We received 100 of these devices, nominally manufactured to our specifications. Figure 3 shows the optical AC response, normalized to the RF input power, so the nominal 3 dB electrical rolloff is occurs at 1.5 dB, which we see is at about 7 GHz, below the typical specification of 10 GHz and even the minimum of 8 GHz. There is a 1-dB ripple in the frequency response that is probably due to a calibration issue.
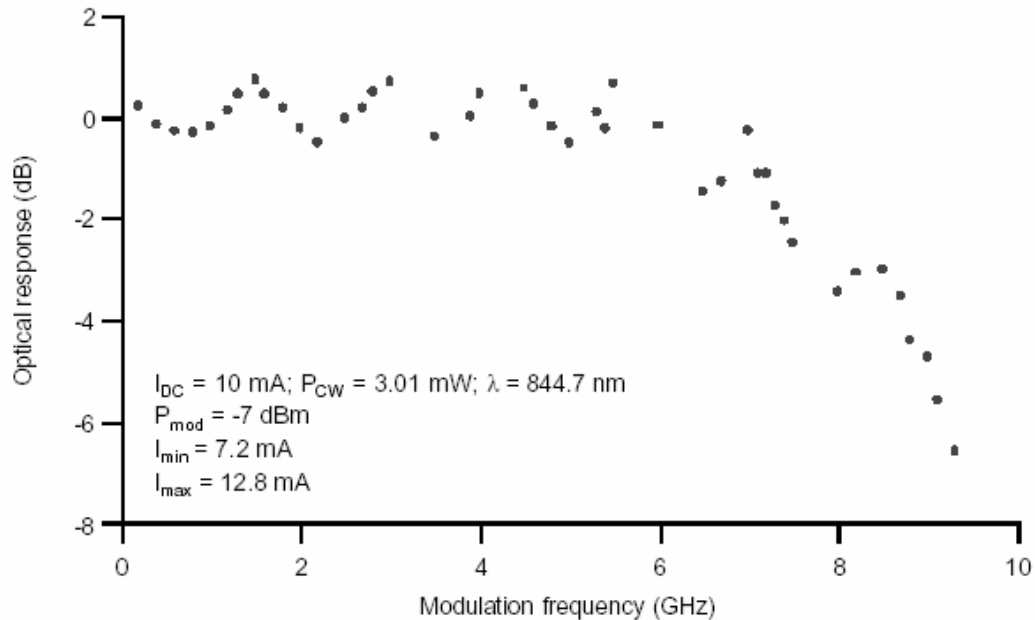

Figure 3. Frequency response of MODE VCSEL, probed with a GGB picoprobe.

At high bias, (8-10 mA), both the 10 μm and 12 μm diameter VCSELs show similar bandwidth, between 6 and 7 GHz. This is below the specification of 10 GHz and below the minimum specification of 8 GHz. We carefully examined the response of three devices and observed similar results in several more devices using a more limited test (by measuring the location of the 3 dB point). The results of these measurements are shown in Figure 4.

We also examined the dependence of bandwidth on drive level. In Figure 5 we show the spectra for three different 10μm diameter devices, each at four drive levels. Note the pronounced oscillations in the spectrum at 4 mA; this is due to the fact that at this low bias, the minus 10 dBm modulation level over-modulates the laser, driving it below threshold. It is clear that for best bandwidth the devices like to be driven at high current, although even at the maximum recommended drive level of 10 mA, the 3 dB point is still about 7 GHz.

We shared this data with MODE, who responded with several more batches of devices, each using an improved process.
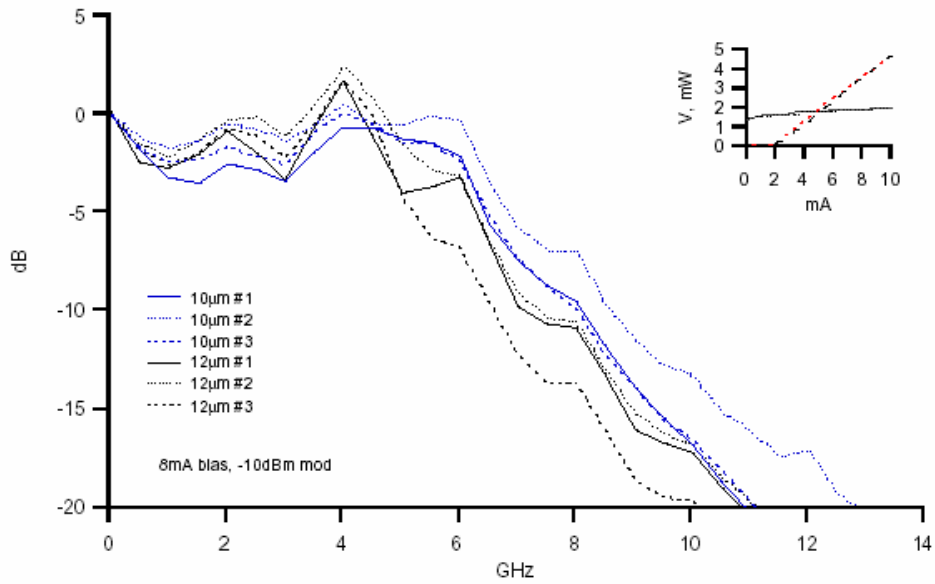
Figure 4. Relative frequency response of MODE GSG multimode 10- and 12-mm VCSELs; these curves have been normalized to 0 dB at 50 MHz. The 3-dB rolloff occurs at 6-7 GHz for high bias levels. The inset shows an LIV curve for "device #1."
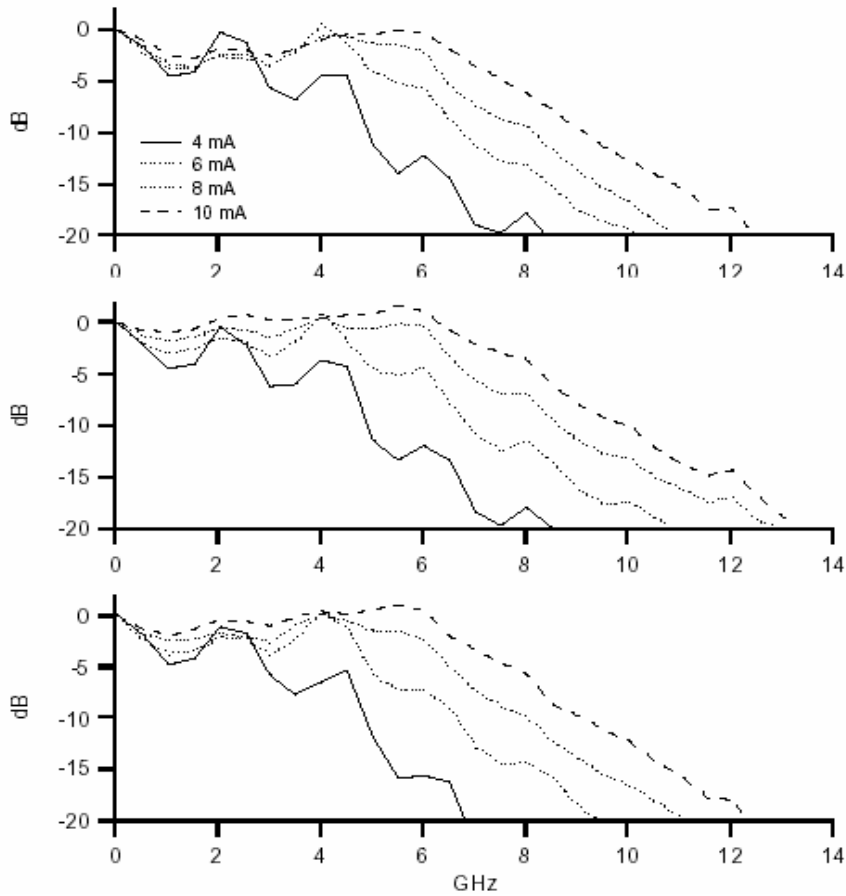
*Figure 5. Relative frequency responses of three different 10mm diameter GSG VCSELs, each operated at four different bias levels. The pronounced wiggles in the response at 4 mA drive is due to the fact that at this low bias, the –10 dBm modulation level over-modulates the laser, driving it below threshold.*

98

Single-mode devices

MODE provided us with a small sample of single-mode VCSELs that were processed similarly to the multi-mode devices to help us understand the bandwidth limitations. Figure 6 and Figure 7 summarize the results of the measurements we made on these devices. They show similar operating characteristics, except having a much higher dynamic impedance of 120Ω. These devices had incomplete front-side ground contacts, leaving a fairly high-capacitance connection. We successfully probed the devices using a Picoprobe GSG-40 as usual, but added a DC ground wire to make contact with the substrate backside. The filter formed by this procedure accounts for the pronounced dip near 1 GHz in both responses. The layout of these devices is quite similar to the multimode devices, although the contact surface area is larger.
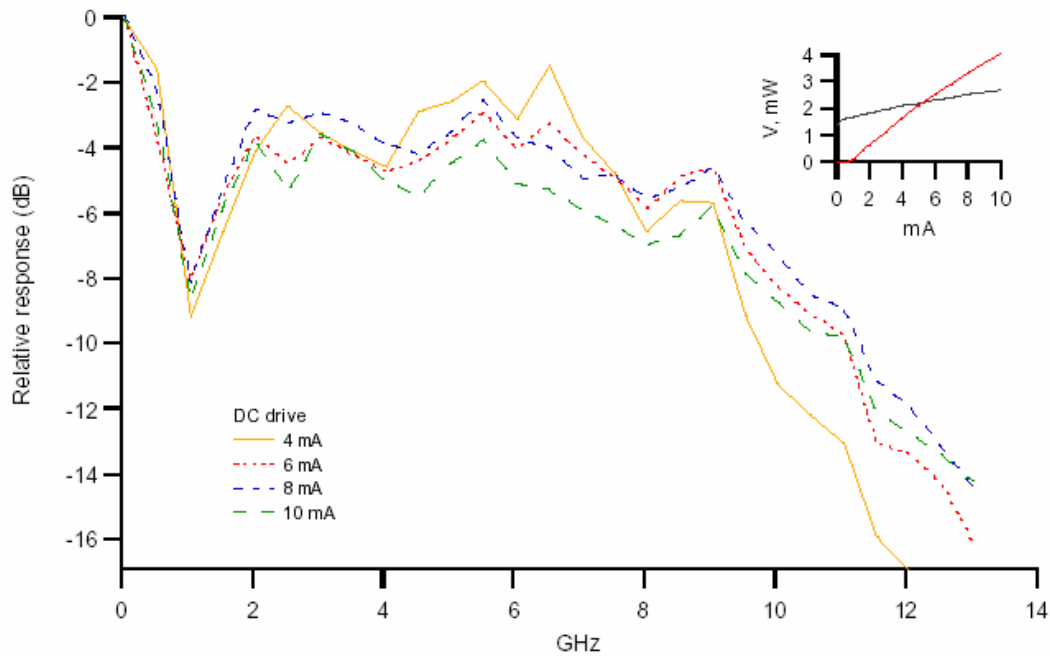

Figure 6. Single-mode VCSEL from MODE (s/n 8585-1400), showing relative response to a –10 dBm sinusoidal drive at various bias levels. The inset shows the LIV characteristics of the device.

The 3 dB bandwidth falls just below 10 GHz. Ideally, a single-mode device with such a small aperture (about 5 μm) would possess somewhat more bandwidth than this, since 10 GHz is our target for the larger-diameter, slower multimode device. This bandwidth was consistent among several sample devices, and they all showed some reduction in bandwidth at lower drive levels.

These single-mode results led us to think that the bandwidth limitation is inherent to the device design and is not caused by the contact area. After sharing these results with MODE, we received several more batches of multi-mode devices with improved response.
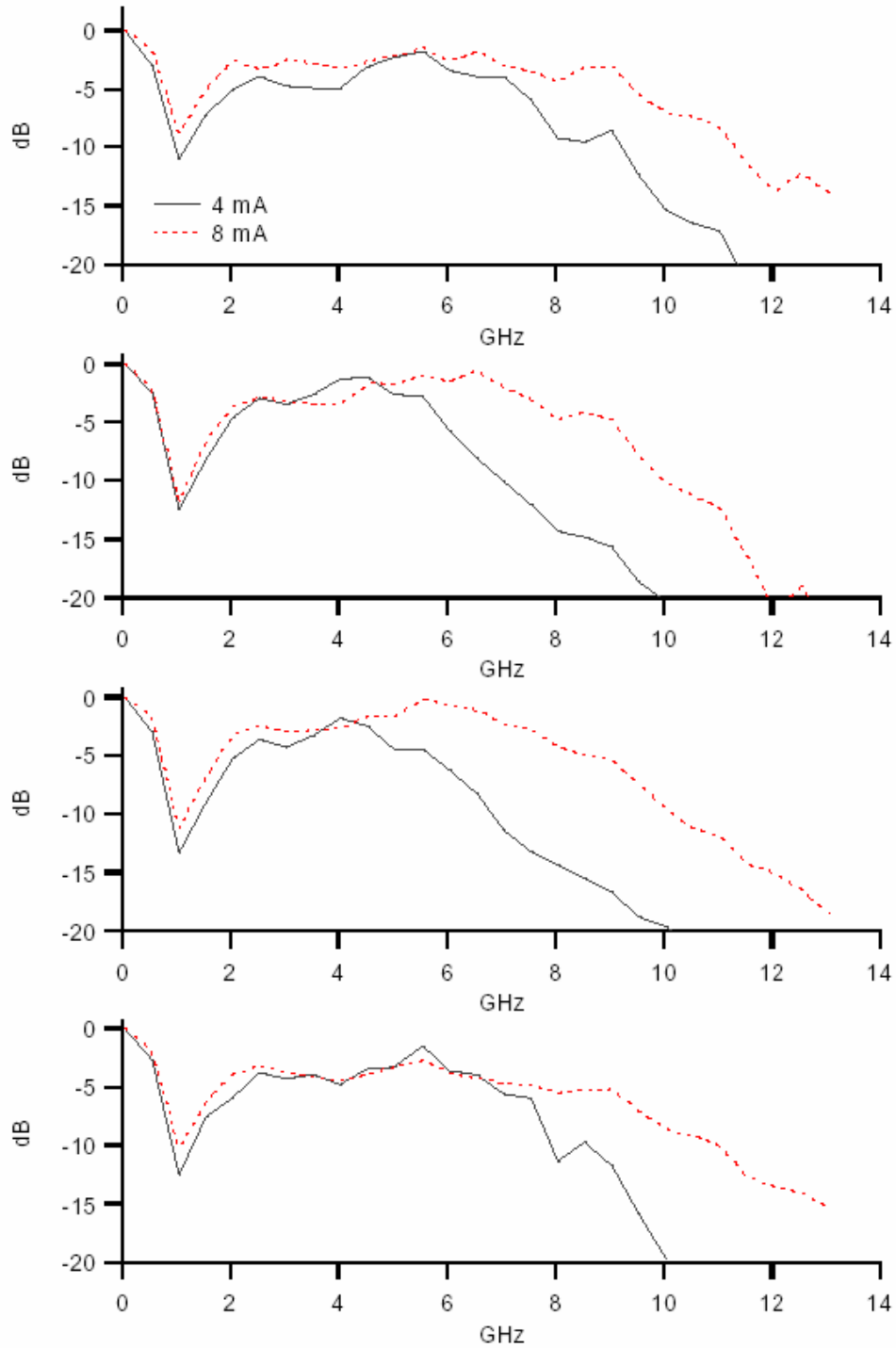
Figure 7. Frequency response of four different single-mode VCSELs, operated at two different drive levels. For the higher drive level of 8 mA, the 3 dB rolloff point appears at roughly 10 GHz. The pronounced dip at 1 GHz is an artifact due to capacitance between the topside metallization and internal cathode contact, caused by not etching through the oxide layer; DC contact is made via the substrate through a separate wire, forming an LC-section filter at low frequencies. The top two plots are for device 8585-1440; the bottom for 8585-1500.

Third generation devices

We have received several more devices in small sample quantities this period. The first batch was a mixture of single and multi-mode devices whose frequency response we measured and display in Figure 8. The top two panels are two different 10 μm MM devices, with roughly 8.5 and 9.5 GHz rolloff respectively. The small sample of devices showed a broad range of dynamic resistance from 50-100 Ω with the lower resistance devices giving better performance. The bottom panel shows the response of a single-mode device processed in a similar manner.
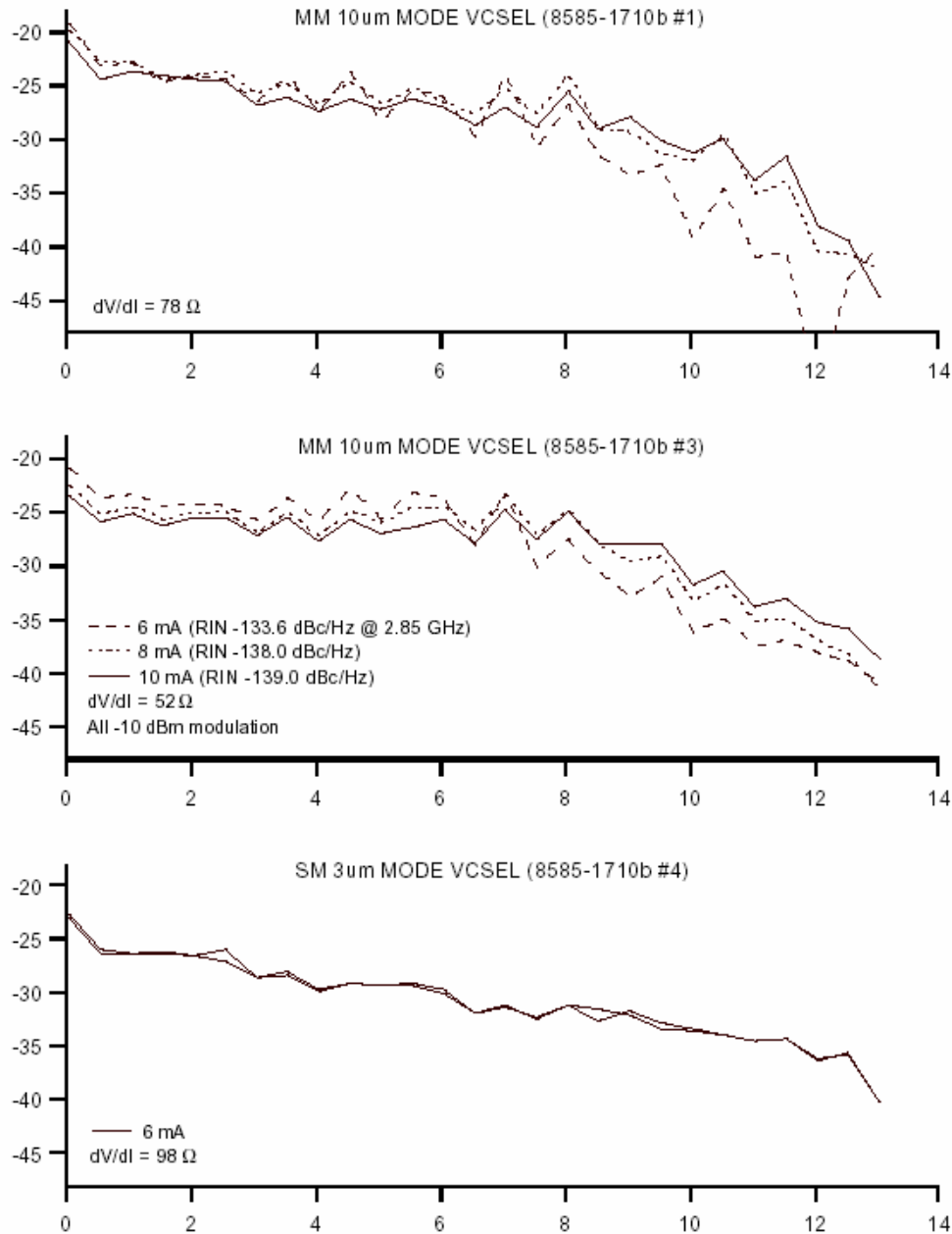

Figure 8. Response of improved MODE VCSELs.

RIN

Measurement technique

This arrangement follows Figure 1, except that the output of the 1422 is observed on an HP 8560E spectrum analyzer, which has a bandwidth of 3 GHz. In addition, to reduce etalon effects which influence the shape of the RIN spectrum, a 50-m length of fiber is used to couple the detector and fiber probe.

Results

We have measured the RIN spectrum of the "second generation" devices up to 3 GHz, and RIN over an integrated 12.4 GHz bandwidth as a function of optical output power. This data is summarized in Figure 9 and Figure 10. The devices meet the RIN specification at just over 6 mA of drive current, or 1.5 mW of output power, and shows signs of becoming more flat with rising drive current.

As seen in Figure 9, below an operating current of about 6 mA the spectrum is fairly flat, which we can safely extrapolate all the way up to the full VCSEL bandwidth. No significant resonances are visible here, however we have observed etalon effects with moderate optical feedback from an FC-FC connector interface. Using a long (50 m) length of fiber, as was done in taking this data, nearly eliminates these effects.

From Figure 10 we see that to get a RIN of –122 dBc/Hz or less the VCSEL must operate at a minimum of 1.5 mW optical output. Since the maximum eye safe limit at 850 nm is –5 dBm (0.3 mW), this suggests that we will need to optically attenuate the light between the VCSEL and the fiber. To a limited extent, this can be accomplished simply by purposeful misalignment of the fiber. Achieving the required attenuation may require optical coating of the VCSEL or fiber. The roll-off in RIN at higher power is due to compression near the system noise floor and is not characteristic of the devices themselves.
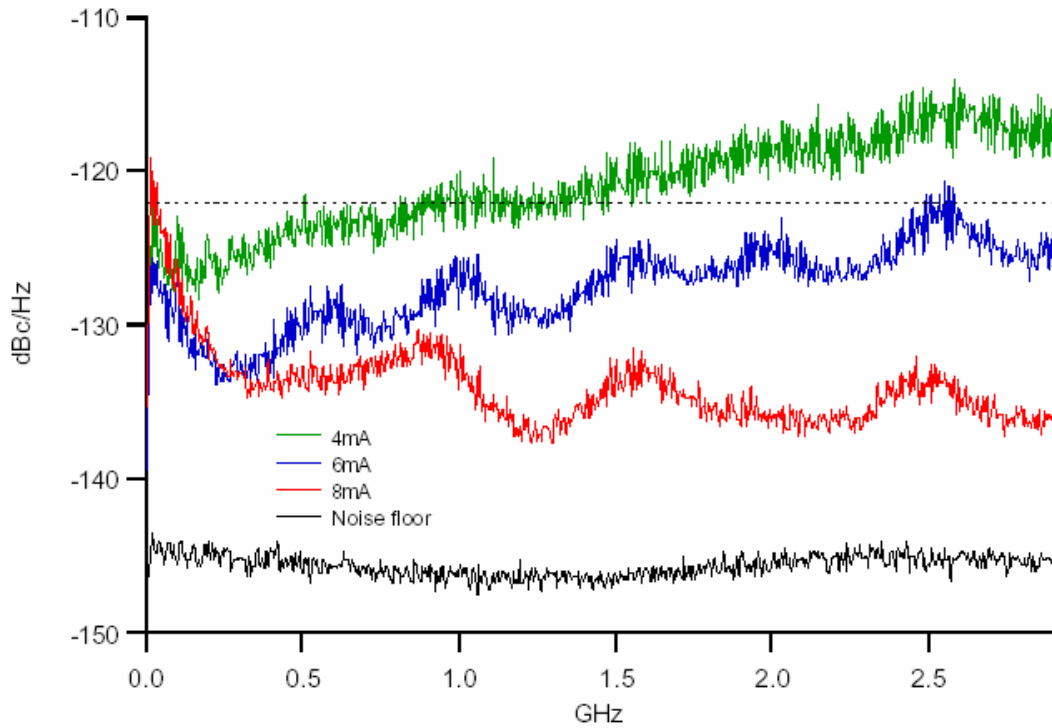
Figure 9. Spectrum of RIN from 12mm diameter VCSEL, up to 3 GHz. The dashed line indicates the specification of −122dBc/Hz. To reduce etalon effects from fiber back reflection, a 50-m length of fiber was used between the detector and fiber probe tip. This data reflects an average of 100 analyzer sweeps.
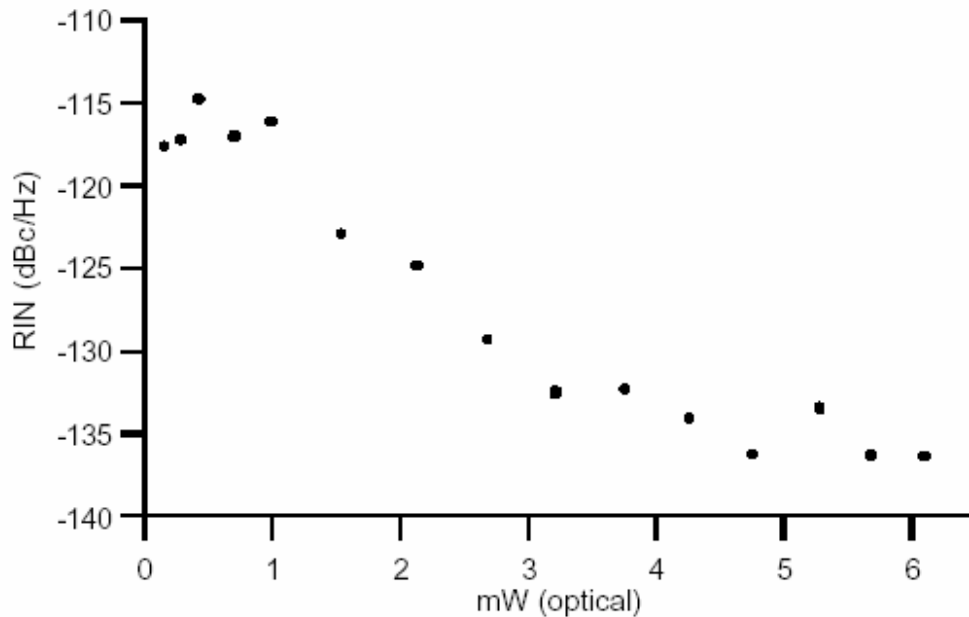

Figure 10. RIN, measured at 2.8 GHz vs optical power for a 12mm VCSEL. Above about 4 mW, the RIN is limited by the detection system noise floor. The D-15 detector is limited to approximately 1 mW of optical input, so above this limit, the optical power is attenuated by frustrated coupling.

Wire bonding

To keep capacitance low in order to maintain high speed, the MODE VCSELs are made with a polyimide layer beneath the top-side metallization. Typically, this structure produces bond pads that are more fragile than those placed over harder materials, and can tear easily requiring good control over bonding parameters. Our experiences with all batches of devices up to and including the "second generation" have shown them to be nearly impossible to make a bond to using conventional techniques. We developed an *ad hoc* technique that has helped us in building prototypes, however, this is not acceptable for a mature device.

MODE worked closely with an independent micro-assembly facility (Analytical Solutions) to improve the bondability of these 2nd-generation devices. Their report showed poor results using wire bond and ball bond techniques, with yields in the 20-50% range. In-house, using a ball bonder, MODE reported 100% bondability with 5.6 g average pull force. Results at FRI have been in the 50% range, although we have just begun using a manual technique with ribbon that has given good results.

With the 3rd generation of devices, MODE has greatly improved metal adhesion, enabling us to do "traditional" manual bonding with gold ribbon, automated wire feed, and a large-area wedge. We got 11 of 12 bonds to stick without difficulty; an impromptu bond pull test using tweezers pulled the ribbon off the substrate bond before the VCSEL bond. Bonding to the signal pad was a bit less reliable than to the ground plane metal (one pad pulled up during bonding), but better than we've observed on any previous devices. We feel confident using these new devices for all of our prototypes.

Photodiodes

Several fabrication runs have been performed that have elucidated some difficulties in the design, stemming from the high sheet resistance of the p-layer and difficulty isolating the thick photodiode structures.

Design and fabrication

The devices are *p+-i-n+* (PIN) photodiodes, designed for top-side illumination. The p+ upper contact layer is 0.1 μm-thick GaAs, doped with beryllium to 1.5×10^{19} cm^{-3}; the intrinsic layer is 1.5 μm-thick undoped GaAs; and the n+ lower contact layer is 0.6 μm-thick GaAs doped with silicon to 8.0×10^{18} cm^{-3}. The optically active region consists of a mesa formed by proton bombarding the surrounding field region. A 1.8 μm–thick gold mask is used to protect the mesa from the bombardment. Contact is made by selectively etching the field through the intrinsic layer, exposing the n$^+$ layer.

Two fabrication runs were performed, and both encountered high series resistance. Measurements of p$^+$ sheet resistance are approximately four times the expected value, confirming a problem with the doping of the p$^+$ layer, namely that the doping level was far too low.

We then redesigned the photodetector epitaxial layers to yield a structure that should reach 10 GHz. In addition, we added a secondary current collection ring to the *MET1* mask

level to reduce p+ layer resistance. The nominal p+ doping and thickness were increased to 1×10^{20} cm^{-3} and 0.15 μm, respectively, and the intrinsic layer thickness was increased to 1.75 μm. These changes were introduced to decrease the *RC* time constant and push the frequency response closer to the transit-time limit. Not much could be done to improve the responsivity of the device, however without compromising speed. The essential speed trade-off between transit time and *RC* time constant is illustrated in Figure 11.
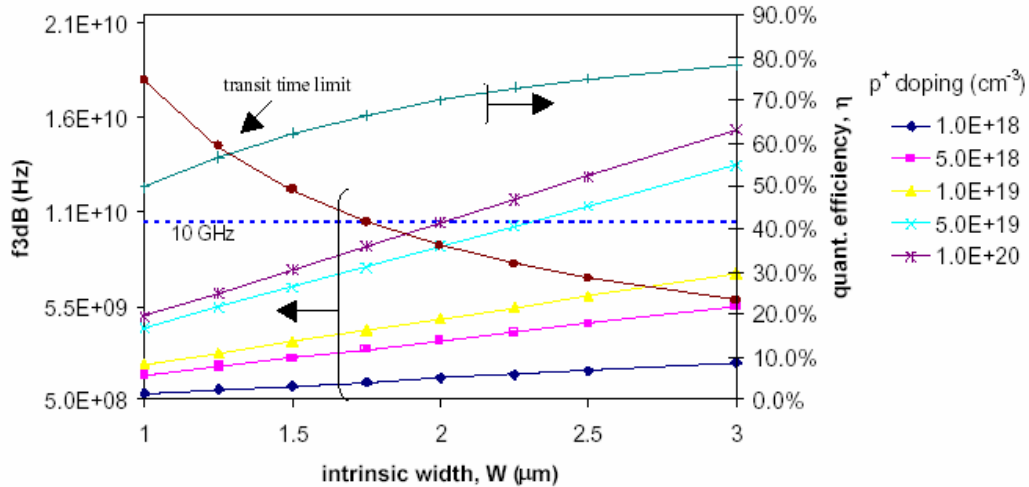

Figure 11. Photodiode frequency response and quantum efficiency versus intrinsic layer thickness for various doping levels.

We worked with two collaborators to get the GaAs material quickly. MODE delivered a structure grown by MOCVD, and device processing and testing were completed. These devices demonstrated only a marginally improved frequency response, on the order of 6 GHz. The frequency response showed improvement with increasing reverse bias voltage up to 23 V, indicating incomplete depletion of the intrinsic region at the nominal drive voltage. Clearly the background impurity level of the intrinsic layer had increased over the previous run.

Litton recently delivered an MBE-grown wafer of the specified design and processing is underway. We are hopeful that improved results will be obtained from this material since MBE growth can achieve lower intrinsic layer impurity levels.

Photodiode testing

While the photodiodes are still in process (after *MET1*), the diodes are checked by measuring forward and reverse *IV* curves, giving a measure of leakage current and the contact resistance. After final processing and dicing, the photodiodes are impulse tested with our 130 fs laser and high-speed sampling scope. Smaller samples are checked for responsivity by applying signal from a fiber-coupled 850 nm VCSEL.

Diode test structures incorporated into the mask design are used to characterize the device integrity during the processing sequence. These structures indicate a highly resistive p^{+} contact for this first iteration of photodiodes. Measured I-V curves show a PIN

diode knee at approximately 0.9 V, while the Schottky diode knee appears at about 0.45 V, with low reverse bias current of roughly 40 nA at 10 V in both cases. Measurements of p$^+$ approximately 4 times the expected value, confirming a problem with the p$^+$ layer; n$^+$ sheet resistance measurements agree with expected values.

Several devices on the mask were designed with very small bond pads and lack bias circuitry, and thus do not rely upon the isolation step. We performed a modified fab run using our original wafer design, producing several of these 65 μm diameter devices. They show good reverse leakage current of about 20 nA and breakdown in excess of 10 V. Using a modulated MODE VCSEL, we measured photodiode bandwidth of just over 5.5 GHz with responsivity of 0.35 A/W.

In Figure 12 we show the response of the photodiode and VCSEL together, and below, the VCSEL alone. The photodiode and VCSEL combination shows about 5.5 GHz response, whereas the VCSEL alone shows a 6.5 GHz roll-off. This speed, although below our target, is in agreement with the measured and calculated sheet resistance of the p$^+$ layer.
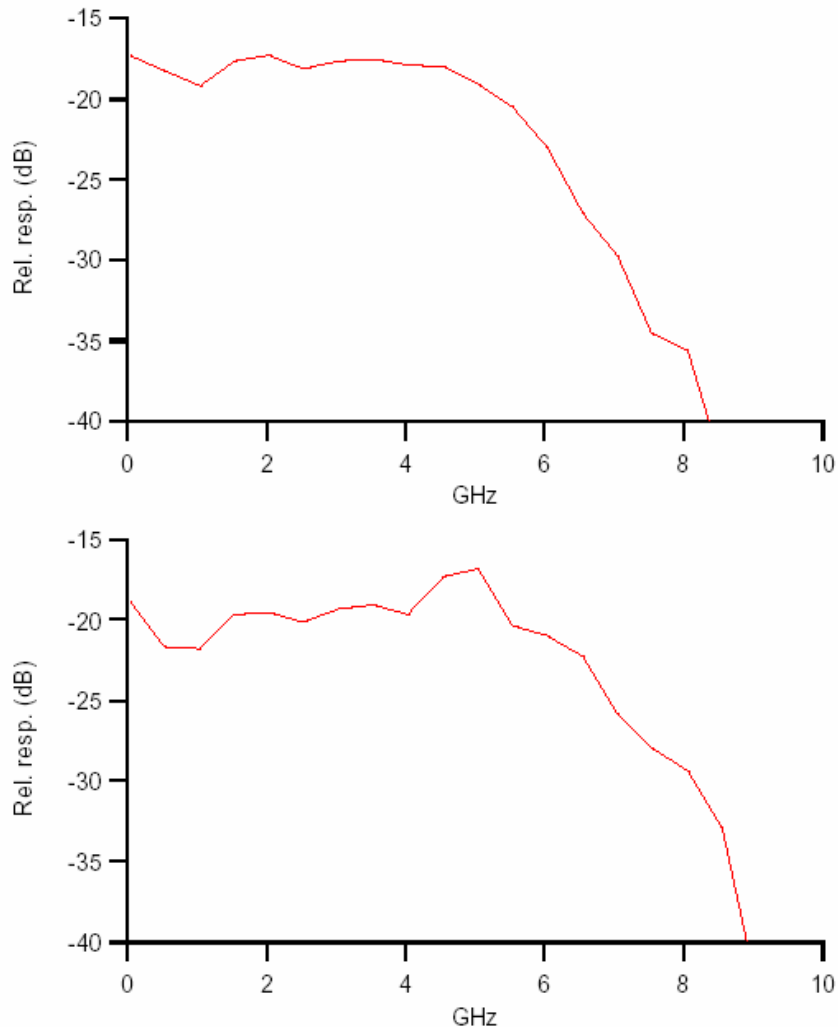

Figure 12. Frequency responses of (top) VCSEL and 'DARPA 70' photodiode, (bottom) VCSEL alone.

Link evaluation

**First-generation Rx/Tx drivers (SiGe)**

Introduction

We designed these circuits in collaboration with consultant Prof. Mark Rodwell at UCSB. Mask layout was done by Greg Fokken and his group at The Mayo Foundation. The devices were fabricated by IBM using the new SiGe BiCMOS process, piggybacking a run with devices from others on a multi-user mask set. Mayo provided several sample die each of four circuits: a transimpedance amplifier with differential output, a differential gain block, a differential AGC amplifier, and a laser driver with differential inputs. Furthermore, with some difficulty they were able to thin the millimeter-sized diced wafer pieces, allowing us to test them while bonded into a package with our opto devices. Mayo provided device models and measured all four Sparameters of each die using a network analyzer and has provided us this data.

Testing methodology

We show the test fixture used to test the receiver in Figure 13. The laser produces a 130 fs long pulse, but the photodiode limits us to 25 GHz bandwidth, which is plenty to test our nominal 10 GHz bandwidth amplifier. The test setup includes a Time-Bandwidth Products semiconductor saturable-absorber 1.06 μm laser, the HP digital scope, and an HP DC power supply and Keithley 6-digit digital meter. We integrate the stored pulse off-line on a computer.
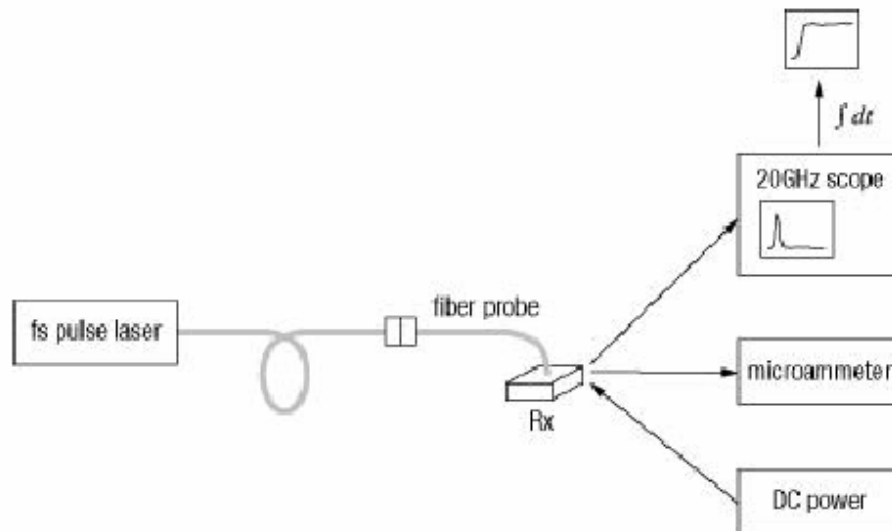
Figure 13. Setup used to impulse-test receiver module.

TIA (and Receiver Test)

A sample of one device's S-parameters, taken on the TIA, is shown below in Figure 14. This data was taken using only one "leg" of the differential output; the other output was terminated.
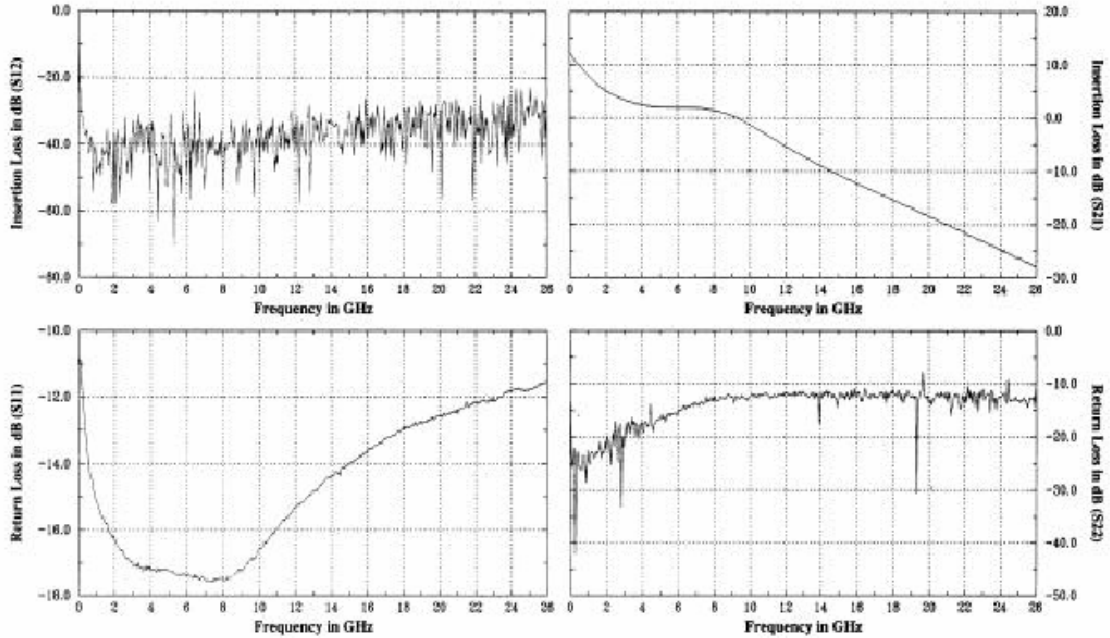
Figure 14. Sample S-parameter test data (for TIA) measured by Mayo.

Below we show a measured dc transfer characteristic of the TIA. We discovered that the biasing of the input transistor and resistor was done incorrectly in the chip design, rendering the range of the input offset pin so limited that the amplifier could not be put into the middle of its operating range using the pin alone. To get around this problem, we drive dc current directly into the input to see the effect. The measurements displayed in Figure 15 closely match our SPICE model of the device.
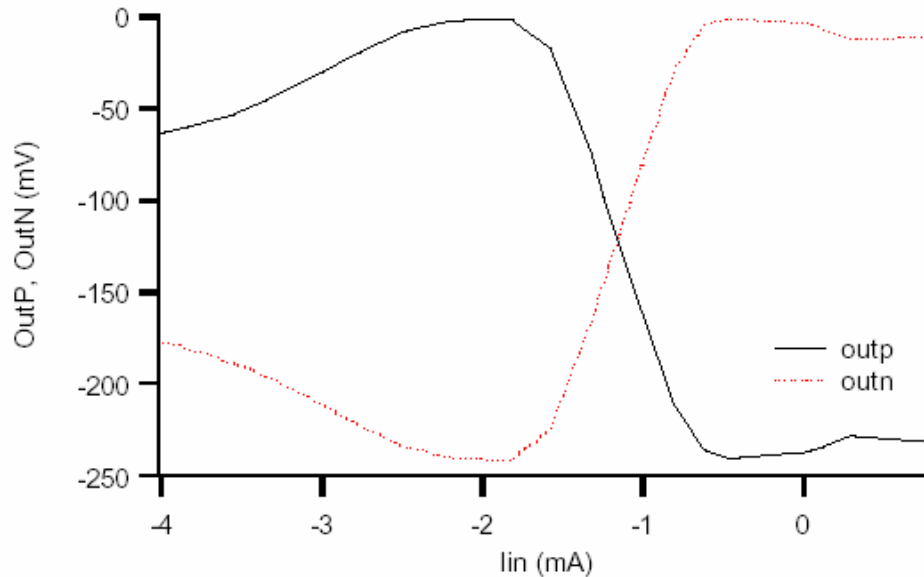

Figure 15. Measured DC transfer characteristics of Mayo/IBM/FRI SiGe TIA.

Now able to properly bias the TIA, we bonded the unthinned die and a photodiode into a package and illuminated it with a 150 fs, 1060 nm pulse. This is similar to the

108

measurement taken last quarter and is still using the unthinned die bonded into the four-pin Kyocera package, resulting in very long input and output bond wires, contributing to poor speed. Nevertheless, the impulse response of this properly biased system is shown below, showing the TIA output OUTP. Here the TIA was operated at $V_{EE} = -3.3$ V, with 1.1 mA DC added to the input to bias it properly. The DC current is summed with the photodiode output at the TIA input pad by bonding two wires to that pad, with the extra wire connected to a supply via a 500 Ω die resistor in the package.

We were able to bond an unthinned transimpedance amplifier and a standard New Focus 102140 photodiode (used in our 25 GHz photodetectors) into our package to perform impulse testing. The TIA was operated at $V_{EE} = -5.2$ V, and we found that setting $V_{offset} = -5.4$ V produced best results (minimal offset, good signal size). The receiver consumes 200 mW while operating.

Below in Figure 16 (blue trace) we show the output of the receiver in response to a 130 fs, 57 fJ pulse (repetition rate 100 MHz, average power 5.7 μW). The pulse is 60 ps wide, corresponding to a bandwidth of about 5 GHz, although it shows some definite ringing. We believe the primary limitation is the inclusion of a filter capacitor (discussed later) but the thickness of the die might also play a role in that it requires the use of longer bond wires.
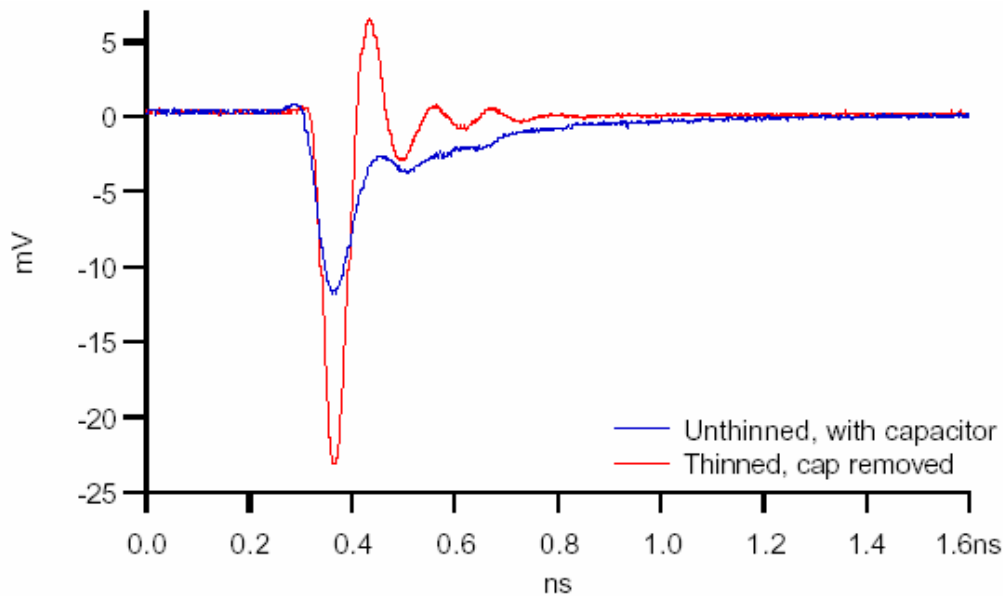

Figure 16. Impulse response of SiGe TIA and NF 25 mm diameter InGaAs photodiode bonded, illuminated by a 150 fs, 1060 nm pulse, showing both before and after thinning and removing spurious capacitor on input stage

By monitoring the photocurrent on a micro-ammeter, we deduce a photodiode sensitivity of 0.21 A/W at 1060 nm (typical of these diodes). Integration of only the first peak of the pulse gives a transimpedance gain of about 100 V/A, but if we include the energy of the ringing following the pulse, we find it to be about 270 V/A. These results are roughly consistent with estimates made by Mayo deduced from the measured S-parameters in Figure 14: about 375 V/A near DC, about 100 V/A below 4 GHz, and dropping off rapidly above that.

To confirm the operating range of the TIA, we measured the pulse height from the TIA as a function of input bias current, as shown below. This also gives a good idea of how this design, which lacks a dc restore circuit, will handle variation in the optical dc level as the input is degraded or the laser output decays over time. This indicates that a dc restore circuit is indeed necessary.
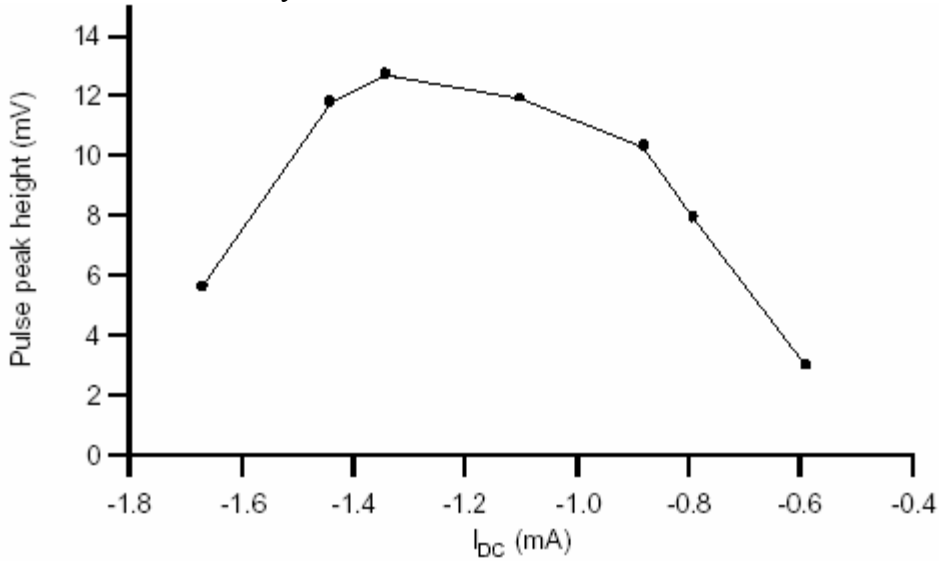

Figure 17. Impulse response peak height versus input DC bias current.

We then discovered a design error in the TIA, namely a large capacitor in the differential input stage. The Mayo foundation has access to an excimer laser with the capability to drill into semiconductor substrates. They were able to repair our die by removing the spurious capacitor on the input that was severely limiting the response of the TIA. The red trace in Figure 16 also shows the results of this operation, showing a higher, narrower peak and ringing rather than a broad piled-up tail.
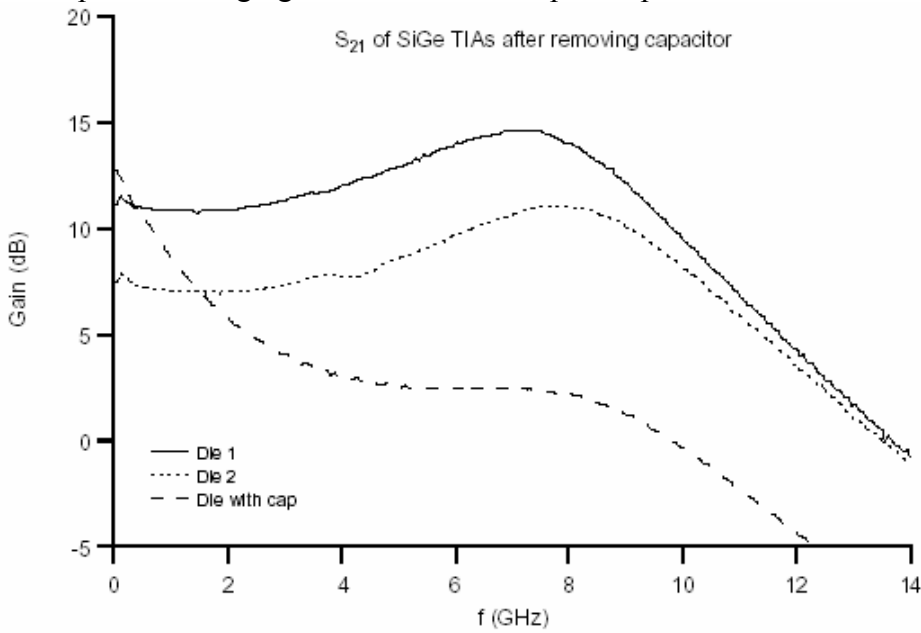

Figure 18. Single-ended response of SiGe TIA with and without the spurious input capacitor.

110

Note that the gain at very low frequencies is unchanged, but now we have significant high frequency response. Note that "Die 1" and "Die 2" are both lasered, but differ in gain by about 3 dB. We suspect that the lasering operation may have some deleterious effect on surrounding components and is responsible for the gain difference. One other possibility is that the removal of the capacitor has a slight destabilizing effect on the circuit. The original purpose of the capacitor, albeit with a much smaller value, was to provide gain stabilization.

We bonded one of these newly repaired TIAs into a package with a New Focus 102140 photodiode (25 μm diameter, roughly 25 GHz bandwidth) and illuminated it with a 1060 nm, 150 fs impulse. The TIA was operated at $V_{EE} = -4.2$ V and the photodiode was biased with $V_{PD} = 3.0$ V.

The photodiode was illuminated with a single-mode fiber, and the output of the TIA was collected using a GGB-40A GSG probe. The impulse response shown in Figure 16 gives a clean pulse of 49.7±.5 ps FWHM. The moderate ringing afterwards is due to the slight gain peaking of the TIA at 8 GHz. We Fourier-transformed this pulse to estimate the frequency response, which is shown in comparison to the VNA measured response in Figure 19. The impulse-measured response shows approximately 9.5 GHz of 3 dB bandwidth.
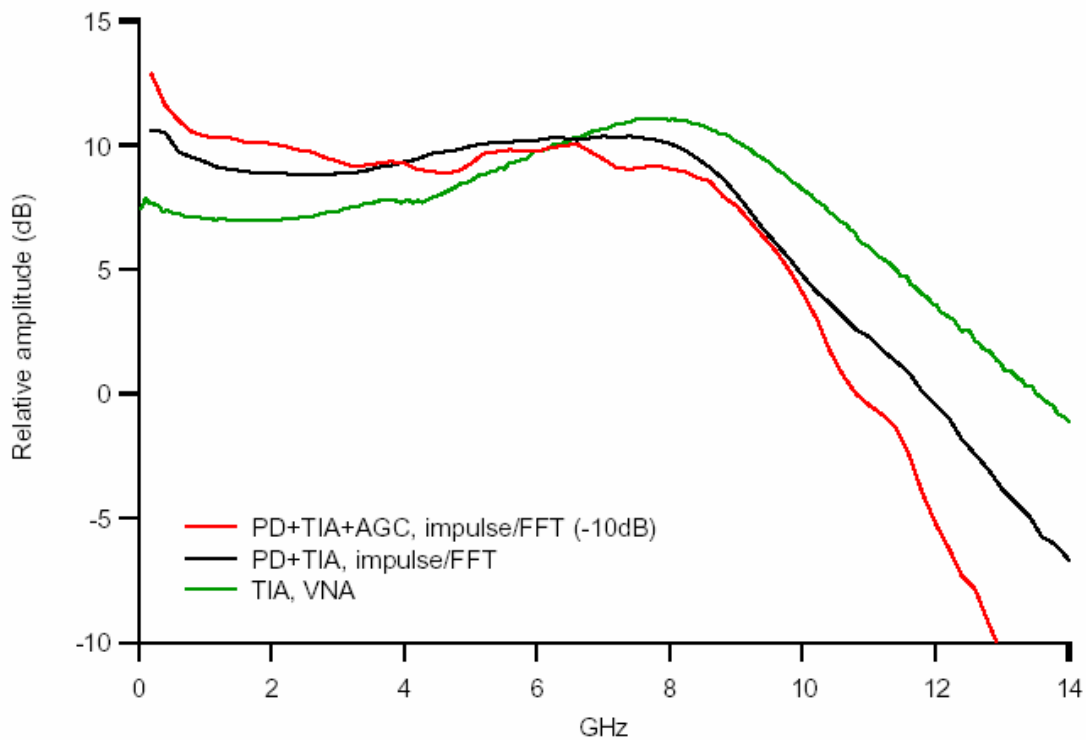

Figure 19. Frequency response of thinned TIA with emitter capacitor removed, and of TIA amplified by AGC stage.

AGC

Below in Figure 20 we show the response of the AGC amplifier tested at low signal levels in a single-ended, probed configuration, operated at $V_{EE}=-3.3$ V with a variety of AGC control inputs. Figure 21 shows the broadband response for one particular AGC setting. These measurements were made by Mayo on the thinned die we received at the end of this quarter. At high frequency it shows gain control operation of nearly 15 dB at 5 GHz, but much reduced response at DC. This poor response is likely due to operation of the AGC in a single-ended configuration. The two parts that were tested had very similar responses, within 1 dB of one another.
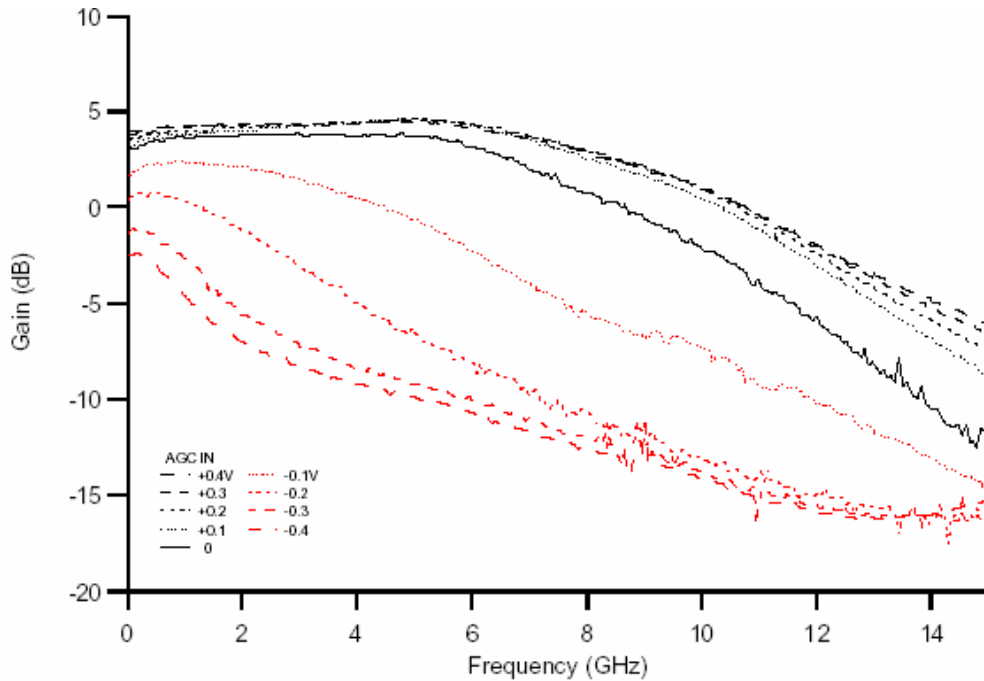

*Figure 20. Small signal gain (S21) of the SiGe AGC at various AGC drive levels. (Dice W14-F8)*
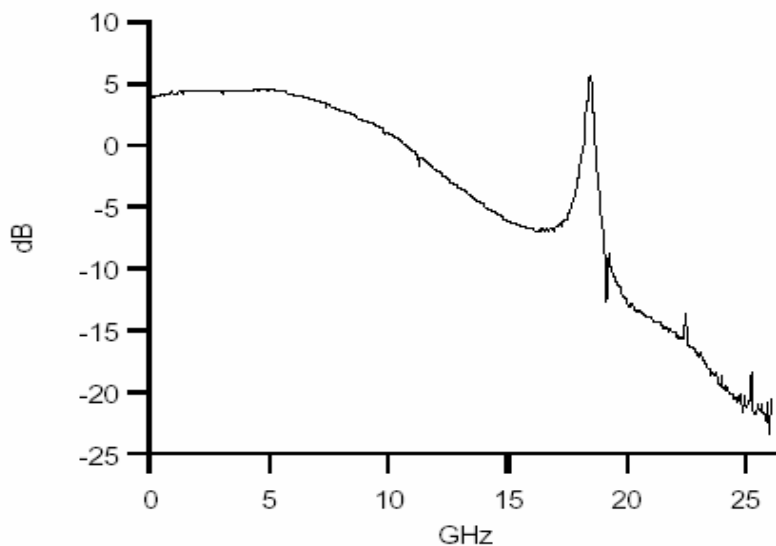
Figure 21. Broadband VNA measurement of AGC S21 response.

112

We then bonded a thinned repaired TIA and a thinned AGC into a package. To optimize operation of both the TIA and AGC, we split the supplies and operated the TIA at $V_{EE} =$ -4.3 V ($I_{EE} = 20$ mA) and the AGC at $V_{EE} = -2.3$ V ($I_{EE} = 30$ mA). Although the AGC was designed to operate at -3.3 V, it would oscillate at any voltage below -2.3 V. Figure 22 shows the measured gain of the AGC at a variety of AGC control currents, operated with a TIA and photodiode as a complete receiver, and we look at only one of the differential outputs, the other one terminated by 50 ohms to ground. Again, for these measurements, the photodiode was illuminated by a 150 fs pulse and a FFT was taken of the response to give these spectra. The gain ranges from about -7 to $+7$ dB and maintains over 9.5 GHz of 3-dB bandwidth over that entire range. This performance would indicate that a receiver based on this design could operate well over 10 Gb/s.
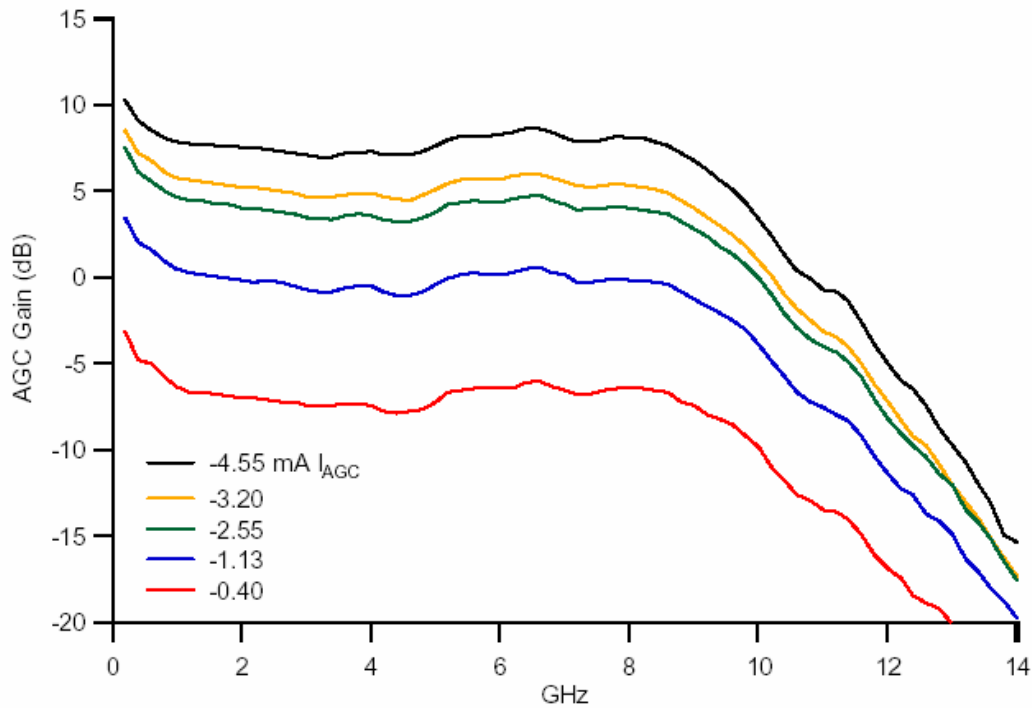

Figure 22. Measured AGC gain variation with impulse test and TIA.

Laser Driver (LD)

The small-signal response of the laser driver is shown in Figure 23. Although the response is fairly flat (less than 3 dB drop at 6 GHz), the overall level is very low.
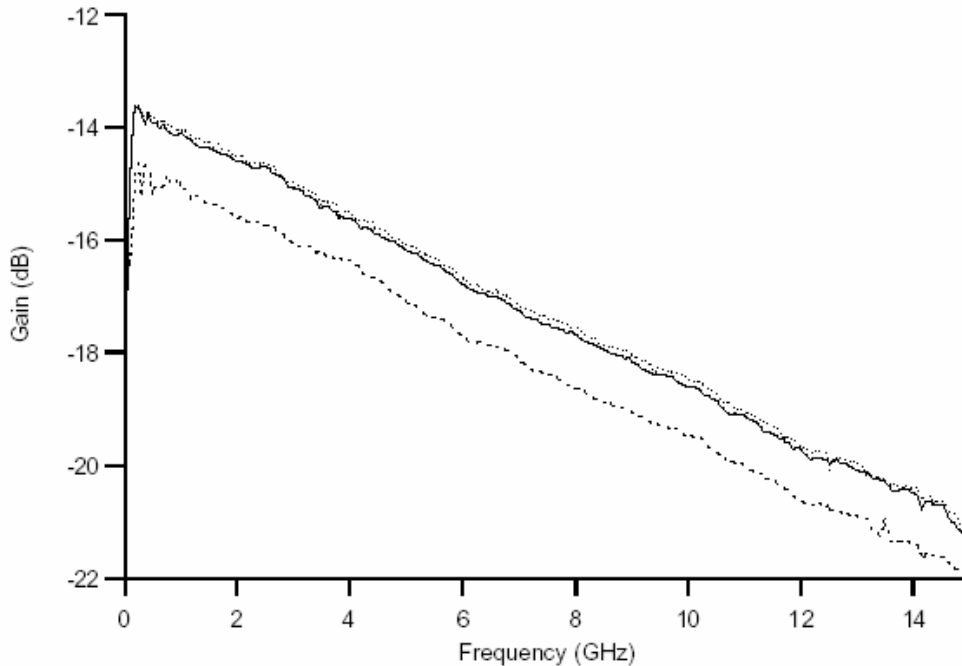

Figure 23. Response (S21) of SiGe laser driver, probed on-wafer. (Die W14-F7,8,9)

We bonded up a transmitter in the original four-lead package using a 10 μm VCSEL and the fairly simple SiGe laser driver chip. However, we were provided with only a couple of good LD chips, and the one we were able to fully test we suspect suffered ESD damage to the output bias FET. We were able to work around this by adding a bias-tee to the output of the driver which we suspect induced resonances in the frequency response. From this data, we estimate the rolloff to be roughly 5 GHz. The GaAs design we use is a significantly different design and thus data from this chip is less critical to the design review process.

Second-generation Rx/Tx drivers (GaAs)

Design

Based on our measurements of the first-generation chipset, we began design of the receiver and transmitter chipsets. Simulations were done in MicroSim Pspice using models provided by the foundry.

We chose a GaAs foundry called EIC, Inc. in California because of their low price, fast turnaround, and full heterojunction-bipolar transistor (HBT) monolithic microwave integrated circuit (MMIC) capability including plated via holes and semi-insulating substrate for low-loss microwave transmission lines.

114

Receiver testing

Specifications

Prior to completing the Rx and Tx designs, we settled on a link specification, included here as Appendix A. Table 2 below lists the relevant goals along with the measured performance. Optical return loss was not measured since these units were not fiber pigtailed. The basic circuit design is illustrated in Figure 24. In addition to meeting the link design specs, the receiver design included the following features:

- Automatic Gain Control
- DC level restore
- DC coupled signal path
- Differential inputs and outputs
- Insensitivity to PD capacitance < 0.5pF
- Minimum external components
- Portable to other bipolar technologies
- 200 mA, 5.2V operation w/ GaAs HBT process

Table 2: Receiver design goal from the final link design document

Parameter	Goal	Meas
Sensitivity (dBm at 10_{-12} BER)	-16	-10.5
Overload Power (dBm)	0	Not meas
Rise/Fall time 20 - 80% (ns)	0.035	0.032*
Optical Return Loss (dB)	-12	Not meas
Output voltage swing (mV differential)	200	200

*Based on $t_r(20/80) = 0.221/f_{3dB}$

The receiver chip takes a photocurrent from a 70-µm diameter GaAs PIN detector, amplifies the signal and converts it from single-ended to differential. The differential signal is amplified through a six-stage adjustable gain amplifier chain. The chip is designed to drive 50-ohm loads directly with no external components required for dc bias or ac coupling the outputs. The receiver is integrated with a microwave detector for AGC control and a dc differential amplifier for dc level restoration.
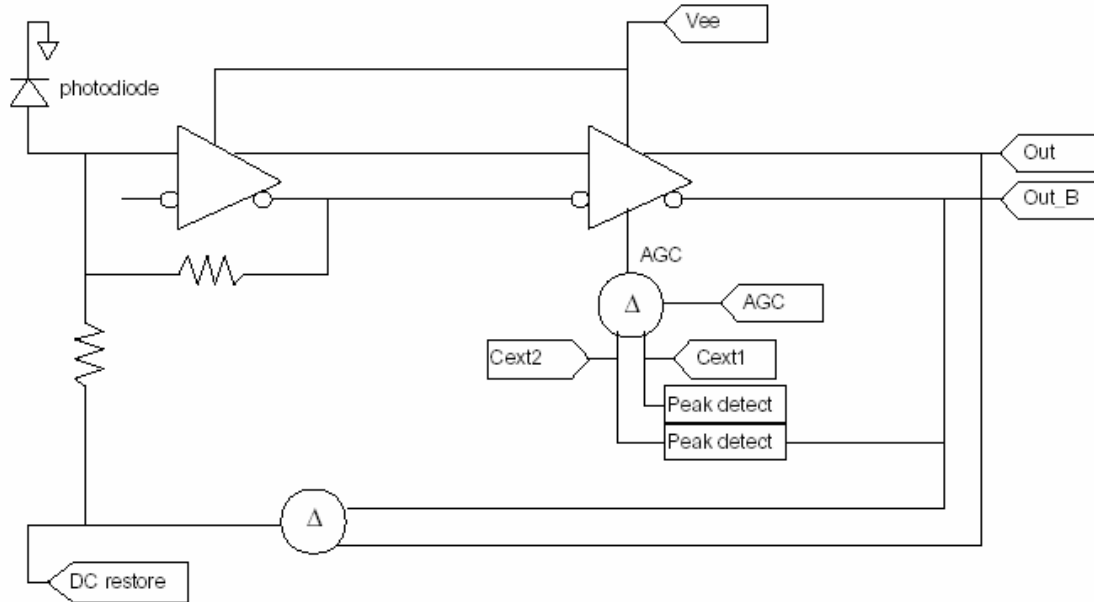
Figure 24 : Simplified schematic diagram of the receiver design.

Measurements

The RX chip conditions the photodiode output to provide an amplified constant amplitude differential output while the TX chip interfaces current mode logic (CML) signals to the VCSEL laser. We achieved 7 GHz 3 dB electrical bandwidth, >30 dB gain, and >20 dB gain control on the receiver. There was good agreement with simulations. We would prefer electrical bandwidth closer to 8 GHz, but this is as good as we expected to do in this first iteration. The dc-restore circuit worked as expected. The AGC control worked as expected, but the AGC detector had a mask error. We fixed the mask and the foundry delivered two new wafers this quarter but we haven't tested them yet.

The initial part check out was performed using a Giga 10 Gb/s MUX/DeMUX evaluation board driven by a Vitesse pattern generator. This allowed us to qualitatively screen and optimize the prototype operation before going to the Mayo Foundation for full BER measurements.
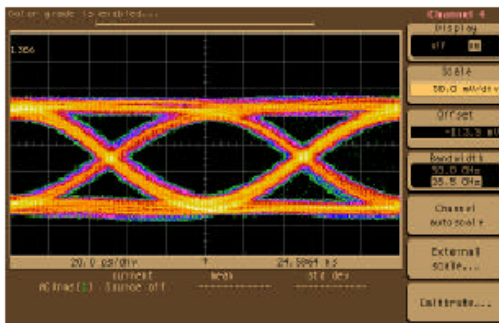
Figure 25: Output of Giga mux/demux evaluation board fed by Vitesse 622 Mbit/s PRBS generator used for prototype checkout.
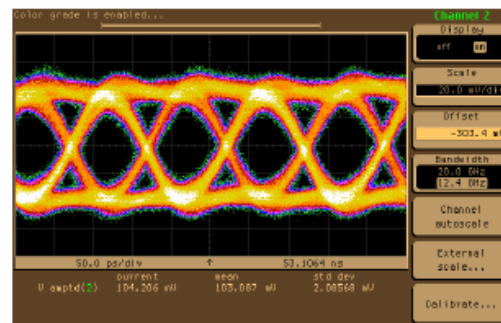
Figure 26: Wafer-probed RX chip output when driven with 10mV p-p 10 Gbit pattern.

Transmitter testing

116

Specifications

The transmitter design goals from the final link design spec are repeated below (Table 3) along with the measured values. The basic circuit design is shown in Figure 27. In addition to meeting these design goals, the transmitter design included the following features (characteristics):

- Differential CML input
- DC coupled
- Plus and minus supply
- 40 mA supply current
- Present design runs at 5.2 V

Table 3 : Transmitter design goals from the final link specification document.

Parameter	Goal	Meas
Min. Power (dBm)	-10	-*
Max. Power (dBm)	-5	0
Extinction Ratio	12%	25%
Max. Rise/Fall time 20 - 80% (ns)	0.045	0.020/0.035**
Eye Opening at 10_{-12} BER	57%	Not meas
Deterministic Jitter	20 %	20% ***
RIN (dBc/Hz)	-122	-122

Min and Max apply only to fully pigtailed modules
**Based on measured eye diagram and removing 35 ps receiver response.*
***Total deterministic jitter for the link at 125m*

The Tx driver interface chips takes current-mode logic inputs and drive the VCSEL laser including constant power control and resistor-programmed modulation depth on the transmitter side.
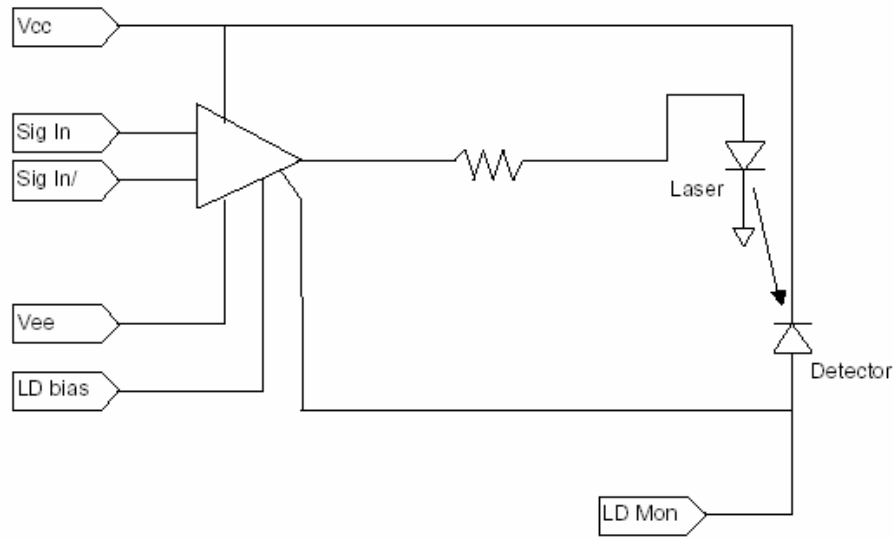
Figure 27 : Simplified schematic diagram showing transmitter operation.

Measurements

The TX achieved 10 GHz of 3-dB small-signal bandwidth and was able to modulate 10 mA of current into a 50 Ω load with the two CML logic inputs receiving 100 mV$_{p-p}$ each. Drive capability improved with 400 mV$_{p-p}$ drive and remained nearly constant for drive levels above 400 mV. The exact sensitivity to logic drive and the optical power control circuit have yet to be tested.

Using the same PRBS generator discussed above, we performed initial checkout and optimization of the TX performance. The resulting eye diagrams are shown in Figure 28 and Figure 29.
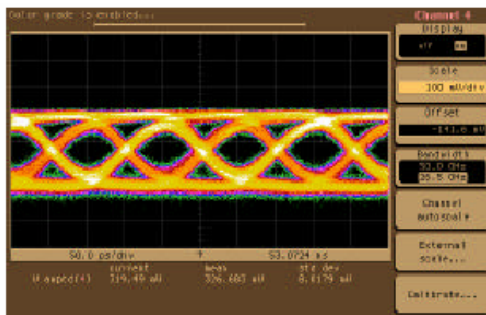

*Figure 28. Preliminary TX testing 200-mV differential TX drive at 10 Gbit/s.*
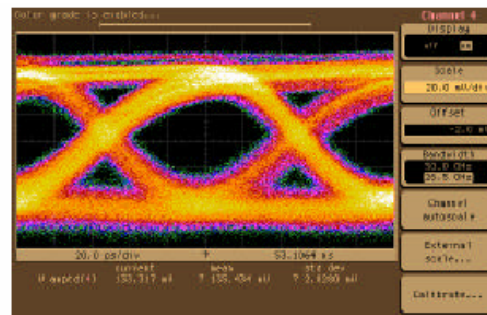
Figure 29. Close-up of eye diagram shown in previous figure.

Detailed link evaluation

In-house testing

Once the Rx and Tx chips were evaluated with small-signal swept-sine measurements, we packaged a receiver and transmitter prototype for BER testing. The transmitter package

contained a 10 μm MODE VCSEL and the Tx chip with differential input and wired to allow external control of modulation depth and laser bias. The receiver package contained an 80 μm GaAs detector along with the Rx chip with differential output. The receiver was wired to permit external control of AGC gain, but dc restore was performed internally.

In addition, to make more realistic measurements on the complete link, we have investigated several low-cost approaches to creating some type of eye diagram. We considered purchasing a pulse generator, but this provides limited capability that does not justify the cost, and renting a BERT is still very costly while providing only a short-term solution.

Instead, we purchased a 16:1 mux/demux evaluation board from Giga that can be configured to generate a differential 10Gb/s data stream from a 622Mb/s source. We combine this with a 622Mb/s BERT evaluation board from Vitesse to build a 10 Gb/s pattern generator suitable for generating eye diagrams at our facility. This was constructed under a related contract (DAAH01-97-C-0139).

This simple system provides an attenuated CML drive signal while we monitored the device output on a sampling oscilloscope. Once we achieved an open eye-diagram using this test setup, we were ready to perform full bit-error-ratio (BER) characterization of the link.
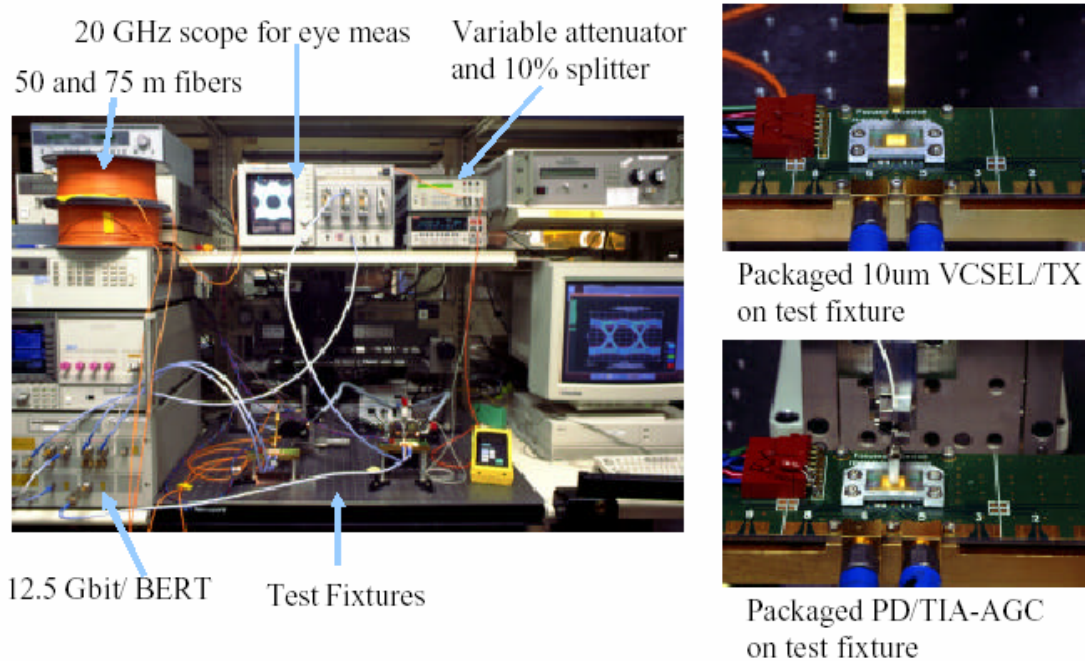

Figure 30. Photograph of experimental test set-up at the Mayo Foundation used for BER characterization of the link prototypes.

Mayo testing

Once the receiver and transmitter prototypes and test fixtures were functioning well, we moved the units to the Mayo Foundation for complete BER evaluation. The experimental test setup is shown in Figure 30. Here a 12.5 Gbit/s PRBS generator and error detector

replaced the simple MUX, and an in-line variable attenuator with a 10% splitter allowed accurate power monitoring.

We collected data over a range of optical power levels, data rates, and fiber lengths. The performance demonstrated meets our design goals with the exception of receiver sensitivity. We designed for –16 dBm. We are investigating this discrepancy, but it is at least partially due to imperfections in the transmitter eye. We achieved approximately –10 dBm sensitivity at 10 Gbaud and –13 dBm sensitivity at 8.5 Gbaud. The overall summary is presented in Figure 31.
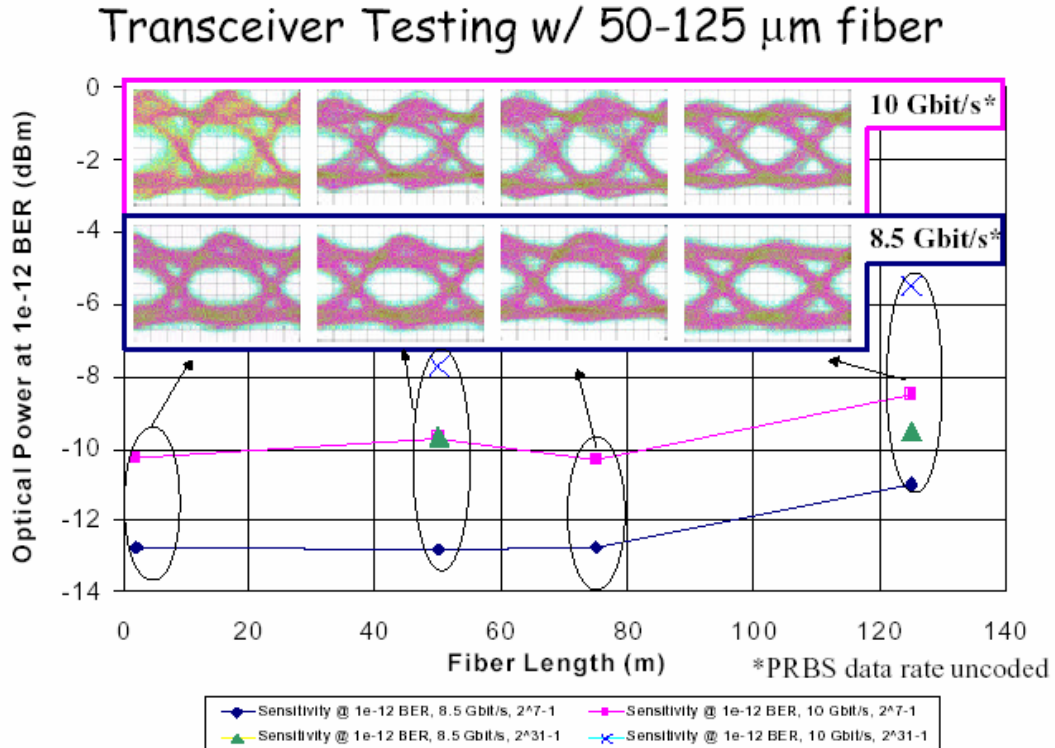

Figure 31. Final summary of BER results.

Packaging

Introduction

The laser welder and motion control systems have been fully debugged, integrated and the motion is programmed to operate with a minimum of operator interaction, and is capable of attaching a fiber ferrule and lid to two different types of package. The software performs seam and spot weld under automatic control and prompts the operator for action, such as loading and unloading of the packages and fiber ferrules.

The code that drives the laser welder has been refined considerably and is now largely a menu-driven system. We have also added a set of routines that aid in automating the alignment of the weld heads to the package, which was previously a lengthy and iterative manual procedure. This aids in recovering from tooling changes or upgrades as well as switching from one type of package to another.

Using a quad-cell bonded into our package and a single-mode fiber pigtail, we have demonstrated the ability to measure lateral motion with a resolution of about 0.25 µm. Using this measurement technique, we have tracked the motion of the fiber tip relative to the detector as the packaging system progresses through its steps. It appears that the initial spot weld shifts are less than one micron, which is acceptable for our multimode fiber. However, the fiber moves several microns during seam welding. We expect that a modification of the weld schedule will readily solve this problem.

A new, differentially-leaded package, designed to operate with the optical fiber both perpendicular and parallel to the circuit board plane, and with an interface designed to work to 18 GHz, has been fabricated, and tested. Compatible electrical test fixtures were also created, as was tooling to facilitate precise die placement within the package.

The welder package nest was revised to accommodate the differentially leaded package, and some improvements were made over the previous design. Similar to the previous design, this nest passes low-frequency control signals as well as a high-frequency differential signal. The tooling is readily changed to accommodate both package types, and the motion control software now facilitates tooling changeovers.

We have built a simple fluid immersion / bubble emission gross leak testing system that should be sensitive down to 10_{-5} std cc/s according to ASTM E515-95. The system consists of a beaker filled with leak checking fluid, a bell jar, and a diaphragm pump. The packages are immersed and bubbles are observed with a magnifying glass and strong light source. We have written a procedure for proper testing. Once the packages pass in-house gross leak test, we can send them out for fine helium leak checking. We have sealed a few packages with a simple lid (no ferrule hole) attached, and several of these have passed this gross leak test.

A revised lid design using a machined rather than etched lid, resulting in closer tolerances and better tube-lid and lid-package fit-up. A sacrificial boss on the lid at the tube-lid interface provides a much stronger weld between the ferrule and lid. Using a quad

cell in the new differential package, we have done additional weld shift measurements and are in the process of perfecting the weld schedules and weld process sequence to reliably minimize weld shifts. We will pigtail several working transmitters and receivers next period.

A detailed procedure for building epoxied ferrules has been worked out and we have debugged the tooling for making these ferrules. However, we are exploring a ferrule design that is structurally stronger (lacking side cutouts) and easier to assemble, both for epoxy and soldered approaches.

Motion control / measurement

Using a quad photodiode cell mounted in the Kyocera package we measured the motion of the fiber with relatively high accuracy in x-, y-, and z-axes. A single-mode fiber is mounted in a ferrule and the uniform Gaussian beam from the fiber tip is used to illuminate the quad cell. As the spot moves over the quad cell, more or less light illuminates each quadrant. By appropriately summing and differencing the quad cell voltages, and normalizing this to the total signal illuminating all four quadrants, we produce a signal that is proportional to the distance that the beam spot is away from the exact center of the cell. A small amplifier box is used to measure the four photocurrents and to generate two difference signals (horizontal and vertical) and a sum signal. The ratio is taken in software after the photodiode signal is digitized; the motion control boards have several 12-bit A/D converters available.

Figure 32 shows the value of the ratios a_0 and a_1 versus motion across the quad cell taken over a range of 10µm. This technique can be used over a much wider range, but to get 0.25 µm resolution requires a slightly more sophisticated technique that relies on mapping a_0 and a_1 over the x-y plane. We have tried this technique, but don't expect to need it since weld shifts should not be any more than 5-10 µm in magnitude.
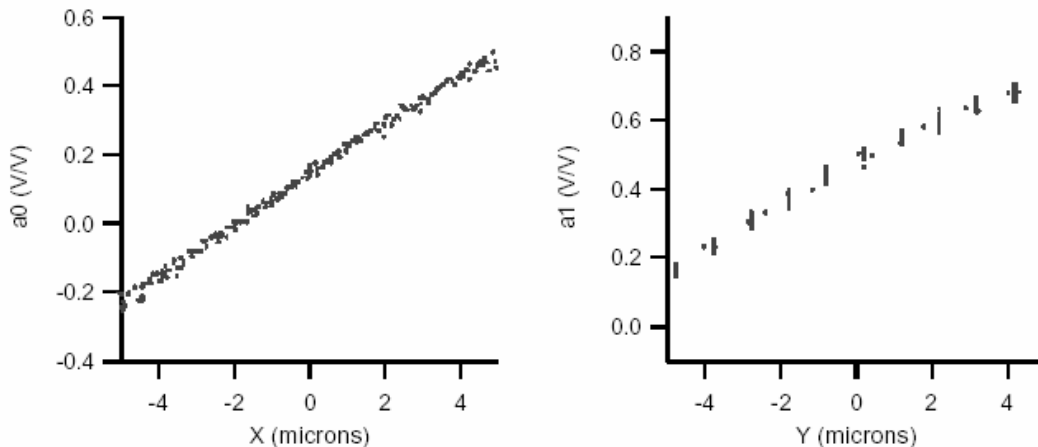
Figure 32. Quad ratio signals versus transverse fiber location.

We can also measure motion of the fiber in the z-direction, albeit with less resolution. However, the required resolution in the z-direction is much less. Figure 33 shows the response of the sum voltage on the quad cell to vertical motion of the fiber in blue and the slope of that signal in red; in this case, the fiber is well-aligned laterally with the center of the quad.

122
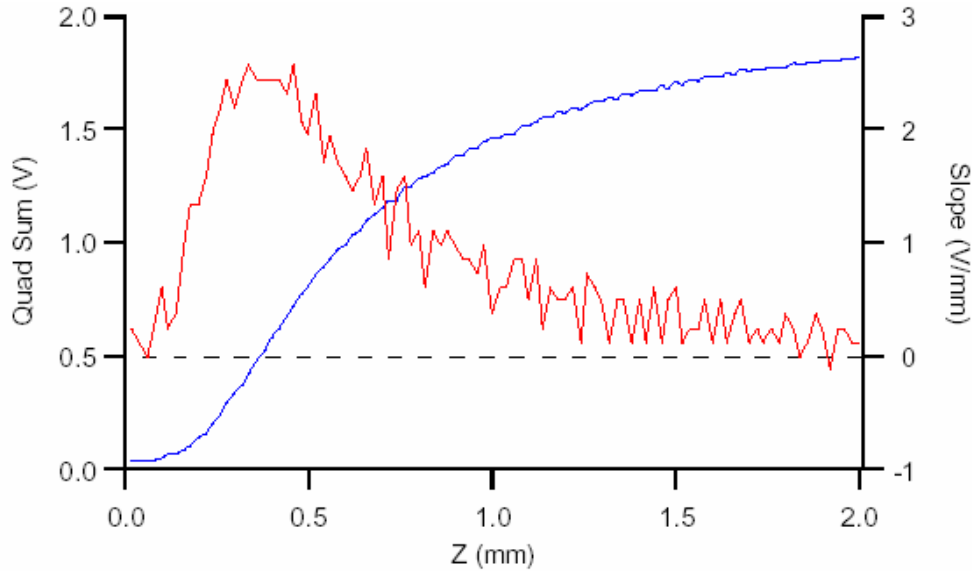
Figure 33. Response of quad-cell to vertical fiber motion, fiber well-centered on quad.

The shape of this curve can be readily explained. The quad cell has a cross-shaped "dead zone" consisting of two lanes approximately 20 μm wide where no light is detected. When the fiber is nearly touching the quad cell, the dead zone obscures the light coming from the core of the fiber, blocking light from reaching the detector's light sensitive quads. In fact, for a singlemode fiber that is well-centered laterally, it does a very good job, since the fiber core is 5 μm in diameter and the lanes are 20 μm wide. As the fiber is retracted from the surface of the detector, the diameter of the Gaussian spot grows until it extends beyond the insensitive cross region and signal falls on the detector area, causing the total signal to rise. As the fiber is raised even more, the Gaussian spot grows to become larger than the entire quad cell area and the total detected signal falls off again (this regime is outside the range shown in Figure 33).

The only shortcoming of this technique is that the vertical measurement is sensitive to the absolute level of light coming from the laser driving the fiber, and we have observed fluctuations of several percent in our source. If we determine that we want to use this technique, we can easily add a splitter and reference detector to the setup. For now, the measurement of z is not critical.

We have used the quad-cell to automatically align the fiber with the center of a quad-cell using a simple hunting algorithm. The result of one particular hunt is shown in Figure 34; the inset shows a blow-up at the end of the hunt, showing roughly 0.25 μm resolution. This hunt procedure, starting several millimeters away from the center of the cell, took less than two seconds. This could be reduced even further through better optimization of the hunting routine. We will use a modified motion procedure can be used to align to a photodiode, which does not provide the direct location feedback that a quad cell does.
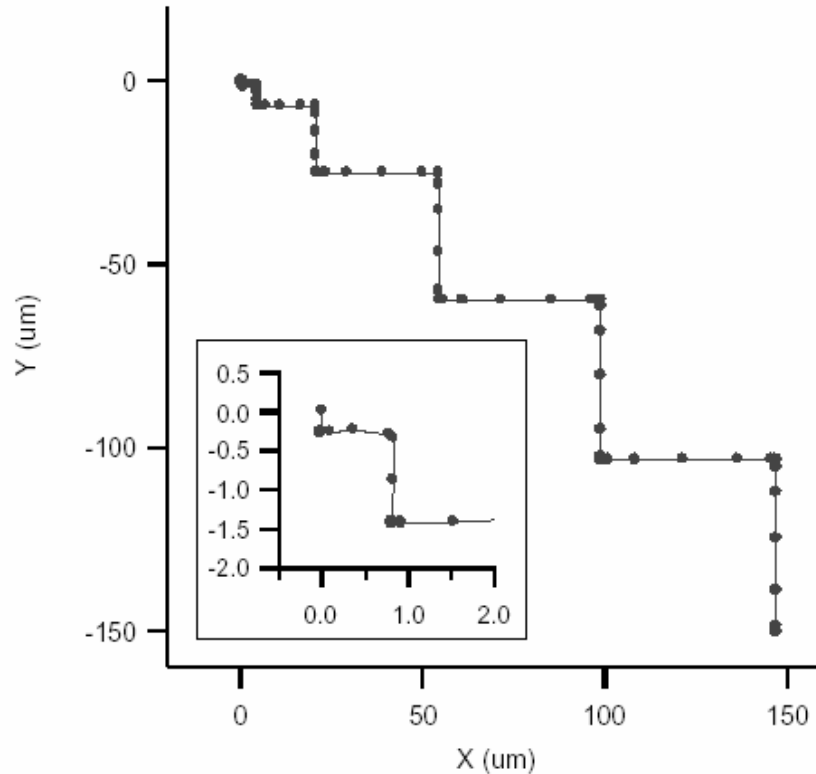
Figure 34. Path of fiber tip as it homes in on a quad photodiode cell; note 200 nm resolution.

Differential package design

We have received the differential input metal-ceramic packages from Kyocera and have begun testing them. To this end we have designed a test fixture and PC board with a target of nearly 20 GHz in order to evaluate the package performance. This will also serve as something that we can easily send out to Mayo and to prospective customers for testing and evaluation. Preliminary TDR results of the connector-board-package interface look promising, and VNA data will come early next quarter.

The differential input package design is nearly complete and we expect to have parts by the end of next quarter. Kyocera has performed full EM simulation of the package and provided a full report, including modeled S_{11} and S_{21} parameters for the differential input. They are also providing the board layout so that we can rapidly revise our test fixture to accommodate the new package.

In order to accommodate the differential input/outputs of our amplifiers and drivers, we need a differential input package. None of the package vendors we contacted carry an off-the-shelf differential input part. This gives us the opportunity to design a package that better fits our needs and the needs of our commercial customers. The main paradigm shift is that the fiber remain in the plane of the circuit board. This means we want to keep the package short (low component height to pack boards together). After several iterations we settled on the design shown below in Figure 35 as serving all of our needs.

124
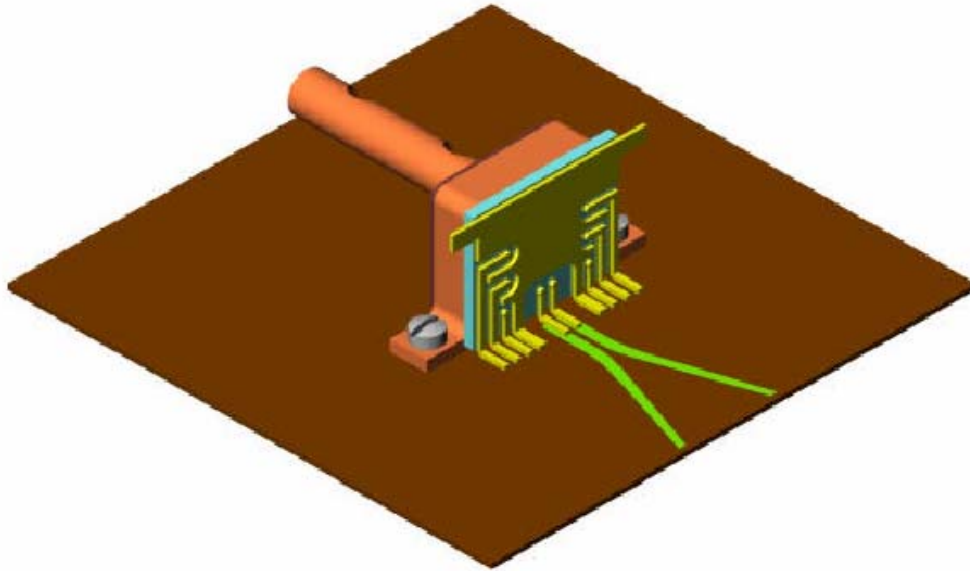
Figure 35. Rendering of package redesigned to accommodate differential inputs and an in-plane fiber configuration.

We have tested the thermal capabilities of the package in the more demanding in-plane configuration. For a package firmly attached to a circuit board with 1/2oz. copper over 0.010" duroid and 0.052" of FR4, we measured a temperature rise inside the package of 34 °C/W in still air and 27 °C/W in moving air. A package poorly mounted (no solder or heatsink grease) to the circuit board resulted in a rise of 52 °C/W. For the <1 W we expect the receiver to dissipate, these numbers are acceptable; the transmitter will likely dissipate only 200 mW.

Interface performance

Kyocera simulated the performance of the package and modified the differential pin and surrounding ground placement to meet our design specifications of >18 dB of return loss and <1 dB insertion loss from 0-12 GHz. The geometry they used in their simulations is shown below in Figure 36. Port 1 is a thin trace on a duroid board, and port 2 is a microstrip transmission line wire-bonded to the port with a 1.5 mil wire, inside the package. Figure 37 shows the results of the simulation, and that they do meet specification. Kyocera has also simulated the package in the flat configuration, and it appears to have similar performance, and thus the differential package can be used both for horizontal and vertical orientations of the fiber with respect to the circuit board.
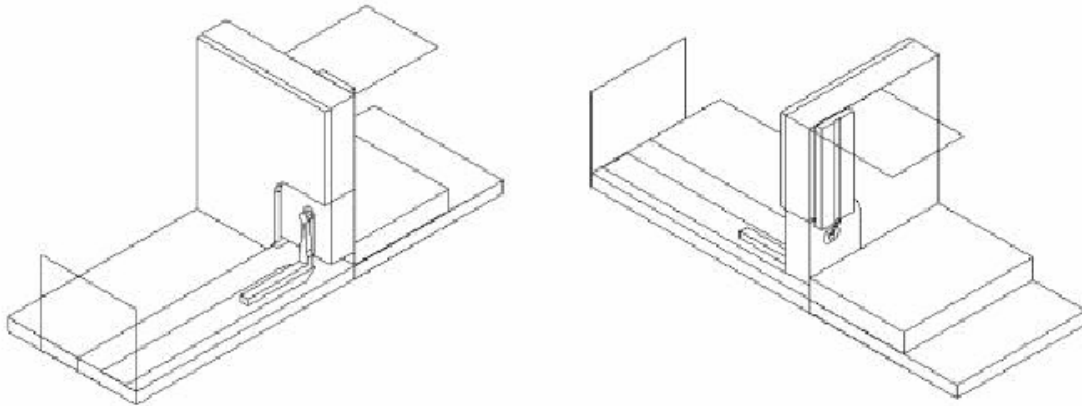
Figure 36. Package simulation geometry used for right-angle configuration by Kyocera.
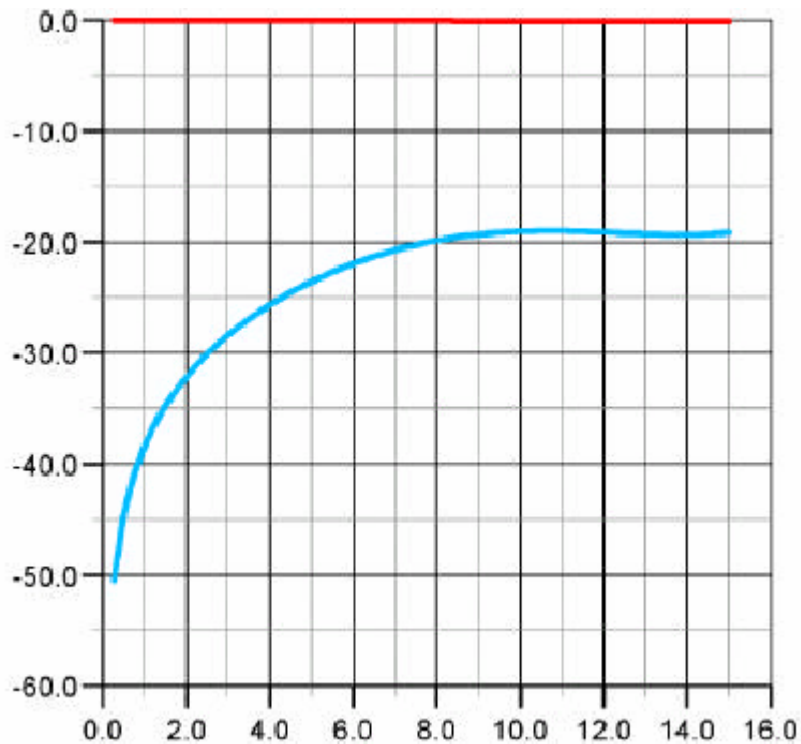

Figure 37. S11 and S21 versus frequency for package in right-angle configuration.

Initial measurements of the package interface in our electrical test fixture using a TDR and with a Rx and Tx indicate acceptable performance. We are working to test the interface more rigorously using a VNA.

Tooling

We have designed and constructed tooling to accommodate the new differential package in the welder. With just a few modifications, this nest drops right into the current tooling, allowing us to change between both styles of package relatively easily. Below in Figure 38 we show a rendering of the nest with callouts and an exploded view.
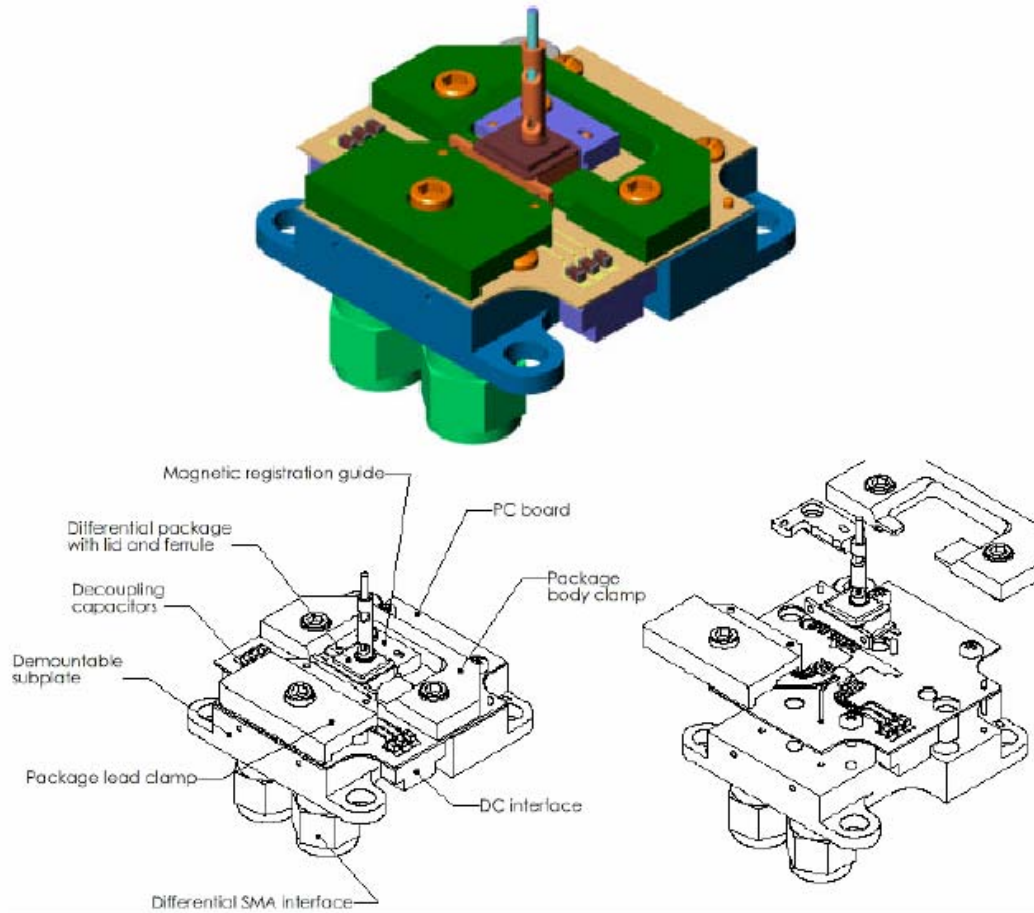
Figure 38. The welder package nest used for the new differential package.

The nest allows the package seal ring to be registered with the nest and the rest of the welder to within approximately one-thousandth of an inch. The package is lightly held against a magnetic registration guide, then the body is clamped into place atop the circuit board. A separate clamp makes good electrical contact between the package leads and the gold-plated circuit traces. We designed this interface to operate up to about 10 GHz.

Conclusions

The link is rapidly approaching maturity, as demonstrated by the ability to reach 10^{-12} BER with -10 dBm sensitivity at 10 Gb/s and -13 dBm sensitivity at 8.5 Gb/s. This test, where the link was driven directly by CML logic levels and detected with no post-amplification, is 3-dB better than our prior results where a good part of the link was composed of high-performance test equipment. Although, this does not yet meet the link sensitivity specification of -16 dBm at 10 Gb/s, this is mostly limited by photodiode sensitivity. We have fabricated several runs of photodiodes and feel confident that our final run will produce diodes that meet bandwidth and sensitivity specifications.

MODE has demonstrated the ability to produce fast VCSELs, and with our input have improved their fabrication process considerably. Although the bandwidth of 8-9 GHz at $I_{op}=10$ mA falls a bit short of specification, we have demonstrated that their bandwidth is sufficient for a 10 Gb/s link. The RIN and DC response have been consistently well within specification, and the wire bondability of the devices is now quite good. We still need to determine that the device dynamic resistance is consistent from device to device, but we are confident that the yield of low-resistance devices is high enough that we could select them through testing. MODE's commitment to improvement even after delivering their "final" batch gives us confidence to have them as a supplier partner in the long-term.

After fabricating several runs of photodiodes, our latest one produced a 6 GHz bandwidth diode, which is marginal for 10 Gb/s operation. We learned that we need not only a very high p+ doping concentration, but that the high purity provided by an MBE growth is also necessary. Having learned this, we expect to fabricate a faster photodiode with higher sensitivity next period.

The first-generation SiGe receiver and transmitter chips have demonstrated in part how fast the SiGe process is. Although the receiver TIA and AGC were both of relatively straightforward design, their bandwidth was nearly 10 GHz and we were able to build a functioning receiver prototype. Through our tests, we also confirmed the validity of IBM's device models. We suspect the AGC design, with 14 dB of dynamic gain range and nearly 10 GHz of bandwidth, is the first such circuit ever to be fabricated.

Gallium arsenide was used for the second-generation circuit design because of its low cost and rapid turnaround, although we will likely use SiGe for the next-generation and production parts because of its intrinsically higher speed and lower power dissipation. We demonstrated the primary functionality of our receiver and driver chipset by building a complete link, although the secondary functions, receiver peak detect, DC restore, and transmitter power control have not yet been tested.

We have demonstrated a simple two-piece lid using a laser-welded attachment technique, and observed weld shifts on the level of 2-5 μm. With further development in the next year we expect to reach micron-level shifts. The package is hermetically sealed on the gross leak level, and has yet to be tested for fine leaks to reach true military-specification hermetic sealing. Our simple ferrule design has served the purpose

of these demonstrations, but to reach a fully hermetic soldered ferrule will require a redesign of the ferrule as well.

The final link design was submitted on 8 April 1999 and is included in Appendix A. However, in light of recent technological developments and activity in the development of a high-speed 10 Gb/s standard, we are considering the following revisions:

1) Revise specification to reflect newly available fibers from Corning and Lucent. These multimode fibers, trade named Infinicore and Zeta, respectively, offer higher and more consistent modal bandwidth.

2) Revise spec for anticipated increase in eye-safe limit. It is projected that the exposure time used in eye-safety calculations will be decreased from 100s to 10s. The reduced exposure time should translate into a 1.5 dB increase in allowed optical power level for Class I operation.

3) Tighten transmitter power variation allowance. Specification currently allows 5 dB. This could be tightened to 4.3 dB according to one presentation at a recent IEEE 802.3 meeting.

These changes would allow 2.2 dB to be added to the link margin while keeping the same sensitivity, or permit a less sensitive receiver. The new fibers will extend the reach of the link. A recent demonstration by Lucent achieved 300 meters at 10 Gb/s and 850 nm.

We feel that the commercial viability of these parts is quite high, judging from our demonstration successes and great interest from the data communications community.

Program for Year Three

In the next year we plan to build several fiber-pigtailed prototype links, with hermetically welded lids. This will help us to refine our fiber alignment techniques and explore any issues that might arise with coupling the fiber to the VCSEL or detector. The fabrication of a final, higher sensitivity GaAs photodiode that overcomes the doping and isolation issues is imminent, and will be used to build these links. This will also entail final characterization of the photodiodes and optical characterization of the complete link. We are also discussing the potential of revising the Rx and Tx circuit designs one more time.

There are some final steps to fully automate each step of the packaging process with intervention required only to load and unload parts and possibly to do some final alignment step or placement verification. This would entail taking final steps to integrate the laser welder and the computer control, as well as adding some additional motion control to grab and release the ferrule. We also plan to house the robot in a glovebox to control the humidity and environment inside the package. Furthermore, the ferrule design will likely have to be revised to strengthen the fiber strain relief to meet Bellcore standards and to ensure a hermetic soldered seal between the package and metalized fiber.

In addition, the next year will include a great deal of documentation, including documenting the chip, tooling, and manufacturing specifications, as well a detailed demonstration plan.

We plan to ship several complete links to the Mayo Foundation for full BER testing as we continue to improve our link performance. Furthermore, we expect to supply parts for the Harrier datalink flight testbed under a related contract, which will provide a very realistic and demanding operating environment for our parts.

We are actively involved in the IEEE 802.3 Higher Speed Study Group, which is responsible for developing a standard for data transmission at rates of 10 Gb/s and beyond. We presented the results of this quarter's link test and received great interest from a range of companies. We plan to stay closely involved with the standards committee to help develop a meaningful 10 gigabit standard.

Because of the growing commercial interest in these parts, we are carefully studying the market and plan to submit a commercialization plan to our parent company, New Focus, to provide funding to help us turn this link into a real product.

Appendices

Appendix A: Link specification

Introduction

The purpose of this report is to document the link design that is guiding the component development efforts under this program. The link design that guided our initial efforts was reported in the first-year annual report. This report is an update and first formalization of that link specification. There are a number of variants discussed here. We are trying to design such that all variants will be producible with modest investment in tooling. However, the primary focus of this program is on the multi-mode 850-nm vertical cavity surface emitting laser (VCSEL) based links.

Link Budget

Initial calculations show that the following family of link designs operating at 850 nm would cover all the possible fiber requirements of users:

Table 4. Summary 850 nm Link Designs for Various Fibers Core Sizes

Fiber core size, μm	Detector diameter, μm	Received power for 10_{-12} BER in HBT design, dBm	Allowance for plant loss plus link margin	TX min power for 5 dB power margin over life and eye-safety, dB
9	12	-19	9	-10
50	60	-18.5	8.5	-10
62.5	70	-17.5	7.5	-10
100	110	-16	6	-10

Each of the designs in Table 4 would comply with the fiber-channel standards for short wavelength links. However there are two problems with the above designs: First, existing 850 nm sources are not qualified for –40 to +105°C operation. Second, the fiber used in the 777 and F-22 is 100 μm core, and 6 dB is not enough for plant loss with margin in a critical environment.

Plant loss is apportioned between fiber losses (<1 dB for length less than 300 m), connector loss (1.5 dB worst case for expanded beam connector, 1.0 dB for physical contact connector), and splice losses (0.5 dB worst case). A point-to-point link typically has two connections and no splices for a worst-case total loss of 4 dB for expanded beam connectors. The remaining budget is apportioned between various 'penalties' that may be required (Fiber-Channel requires 2 dB for multi-mode links) and safety margin for unplanned splices or component degradation over life.

The ARINC-636 transceiver produced by Boeing for the 777 and F-22 provides 20 dB for plant loss plus link margin. This extra 9 dB compared to a commercial FDDI link is to cover the extra losses of the expanded beam connectors and optical bypass switches used in the Boeing 777 network in addition to added tolerance for aging over a 20-year life. The primary focus of our program is on point-to-point links rather than the bi-directional ring topology assumed for the ARINC-636 devices. Point-to-point links do not require optical bypass switches and have fewer total connectors per link. Therefore, our link specification does not require 20 dB, but is probably more than the Fiber Channel specification of 6 dB.

131

Our working assumption is that an additional 3 dB will be sufficient: 4 dB for plant loss, 2 dB for optical path penalties, 3 dB for unplanned splices and degradation for a total of 9 dB.

Table 5 details two designs. Design A is the baseline plan that has the most commercial leverage. Design B is an extrapolation of the ARINC-636 spec. The only major difference between designs A and B is the laser diode and detector elements that are needed to handle the temperature range and higher link-margin requirement of the military application. It should be noted that lasers that operate at 10 Gb/s to 105°C are not readily available. Significant additional development will be required to produce a link that operates over the B temperature range.

Table 5. Link budget detail for two possible variations

	Specification	A: Commercial	B: Version comparable to ARINC-636 spec
General	Data Rate	10 Gb/s	10 Gb/s [1]
	Wavelength, nm	850	TBD SLM laser [2]
	Optical Fiber Core, μm	9, 50, or 62.5	100
	Operating Temp., °C	0 to +70	-40 to +105
	Hermeticity [3]	$<5\times10^{-8}$ atm-cc/s He	$<5\times10^{-8}$ atm-cc/s He
Transmitter	Min. Power, dBm	-10	-8 [4]
	Max. Power, dBm	-5	-3 [4]
	Extinction Ratio	12%	12% [5]
	Max. Rise/Fall time, ns	0.045	0.045
	Eye Opening at 10^{-12} BER	57%	57%
	Deterministic Jitter	20 %	20%
	RIN, dBc/Hz	-122	-122
Receiver	Sensitivity, dBm at 10^{-12} BER	-16	-17 [6]
	Overload Power	0	0
	Rise/Fall time, ns	0.035	0.035
	Optical Return Loss	-12	-12 [7]
	Output voltage swing	200 mV differential	200 mV differential
Notes	[1] The ARINC-636 specification is 125 Mbit/s. This program is concerned with 10 Gb/s operation.		
	[2] There is not presently a commercial VCSEL that covers the full temperature range. The back-up plan is to use a qualified edge emitter on a sub-mount. Longer wavelength can be readily accommodated.		
	[3] Commercial components for telecommunication applications typically require hermeticity, data-communication applications do not except in special cases. This program is concerned with the cases that do require hermeticity.		
	[4] ARINC-636 spec. is based on an LED transmitter with –9 and –14 dBm for Max and Min. The proposed version user higher power to improve link margin and achieves eye safety by working at longer wavelength than design A.		
	[5] The ARINC-636 spec is 5% for an LED transmitter. High-speed laser transmitters will not work well below 10%.		
	[6] One dB improvement is assumed for >850 nm operation with an InGaAs photodiode.		
	[7] It is also possible to achieve –27 dB with an angle polished fiber if this is required by laser feedback sensitivity in the chosen laser.		

Appendix B: VCSEL specification

Based on our previous results and measurements of the first-generation VCSEL characteristics, we have created a complete specification for the second generation. Table 6 below summarizes the MODE specification sheet. No major design change in the VCSEL cavity design is expected, but MODE has consistently improved their process reliability and variation across the wafer.

Table 6. Specifications for MODE VCSEL die

Absolute maximum ratings

Parameter	Rating
Storage temperature	-40 to +100°C
Operating temperature	0 to +70°C
Maximum die exposure temperature	325°C for 10 s
Maximum optical output power	10 mW
Maximum reverse bias voltage	5 V
Maximum continuous operating current	10 mA
Maximum instantaneous operating current	15mA

Electro-optical characteristics (T = 0 to 70°C)

Parameter	Symbol	Units	min	typ	max
Peak wavelength	λ_p	nm/°C	830	850	860
Secondary modes	$\lambda_{1,...}$		3	5	
Peak wavelength temperature coefficient	$\Delta\lambda_p/\Delta T$	nm/°C	0	-	0.1
Threshold current	I_{th}	mA	-	2	3
Output power at high current*	P_1	mW	1.5	3	5
Operating voltage at high current*	V_0	V	1.6	2.7	3
Reverse bias for 100 uA leakage	V_{rev}	V	5		-
Differential "on" resistance	R	Ω	40	50	70
Oxide aperture diameter		μm	8		15
Bandwidth at I = $(I_H+I_{th})/2$		GHz	8	10	
Relative intensity noise at I_H	RIN	dBc/Hz		−122	

* High current is I_H = 10 mA

Physical description

Parameter	Symbol	Units	Typical
Die length	L_D	μm	600
Die width	W_D	μm	600
Die height	H_D	μm	150
Bond pad configuration	Ground-Signal-Ground		
Center bond pad width	W_{CF}	μm	80
Center bond pad length	L_{CF}	μm	100
Bond pad to laser aperture*	L_{P-A}	μm	50-100
20Bond pad to die edge	L_{P-D}	μm	20-75
Bond pad gap	W_{GAP}	μm	35-50
Ground bond pad length	W_{GP}	μm	100-200
Bond pad pull strength		g	>3.0

 * VCSEL in center of die

The major changes from the first generation devices are to provide topside metallization in a coplanar waveguide structure, allowing improved RF coupling. We have added a specification for bond pad pull strength, as this has been a persistent problem

among the first generation; they claim that process improvements and a new machine for depositing the polyamide should improve metal adhesion. Absolute maximum ratings should be compatible with solder die attach techniques and our environmental requirements. The other E-O characteristics are matched to current device performance.

We have chosen to put two VCSELs back-to-back on each die, of different diameters. This provides flexibility in two ways: to MODE, since diameter is essentially a derived function of modulation bandwidth and DC operating characteristics (LIV); and to us in making a good couple between the VCSEL and the variety of fiber diameters our anticipated customer base requires. Figure 39 shows the metallization layout for a single die, showing the coplanar waveguide structure, fiducial alignment marks, and location for a serial number.
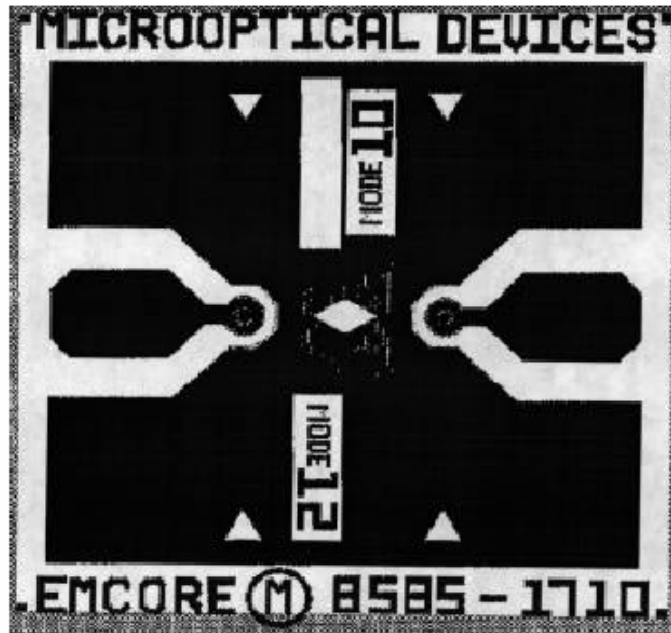
Figure 39. MODE die metallization mask showing two VCSELs back to back, with coplanar waveguide pads and fiducial marks for locating. Nominally the cavities will be 10mm and 12mm in diameter, but are subject to the constraints of the other specified parameters.

Intellectual property summary

Patents filed during the course of this effort

"Method and apparatus for optically aligning optical fibers with optical devices,"
Robert S. Williamson III and Robert Marsland, New Focus, Inc., serial 09/457756,
filed December 8, 1999.

"Method and apparatus for optical transmission," Robert S. Williamson III,
Robert A. Marsland, and Mark Rodwell, serial 09/553,591 filed April 20, 2000.

"Method and apparatus for optical reception," Michael P. Nesnidal,
Robert S. Williamson III, and Robert A. Marsland, serial 09/552,894, filed April 20, 2000.

"Method and apparatus for packaging high frequency components,"
Robert S. Williamson III and Robert A. Marsland, serial 09/552,893, filed April 20, 2000.

IP for 10 G Datalink

Patent portfolio covers all aspects of design:

Method and apparatus for packaging high-frequency components
- high-speed OE package

Method and apparatus for optical reception
- photodiode design
- transimpedance amplifier

Method and apparatus for optical transmission
- Automatic power control of VCSEL
- Laser driver
- Optical coupling technique

Method and apparatus for optically aligning optical fibers with optical devices
- Packaging process
- Four-fold symmetric welding station

Focused Research, Inc.   [r]

Laser welding system
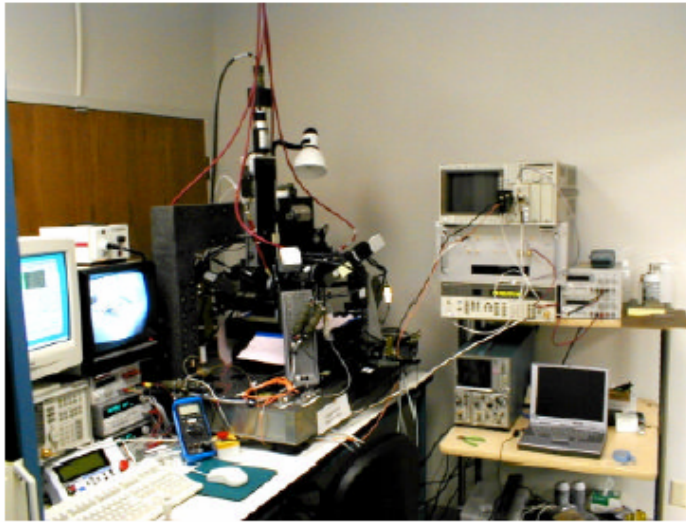
Fourfold symmetric, 12-axis motion control system

Computer-driven with prompted operator interaction
- Welding completely automated
- Alignment and parts loading requires operator

Readily configured for receiver or transmitter pigtailing

Complete cycle time approximately 25 minutes; has approached 15 minutes

Station cost <$200k, 10k parts/year double shift

Focused Research, Inc.

[*r*]

137

Differential package nest tooling

Magnetic registration guide

Differential package with lid and ferrule

Decoupling capacitors

PC board

Package body clamp

Demountable subplate

Package lead clamp

DC interface

Differential SMA interface
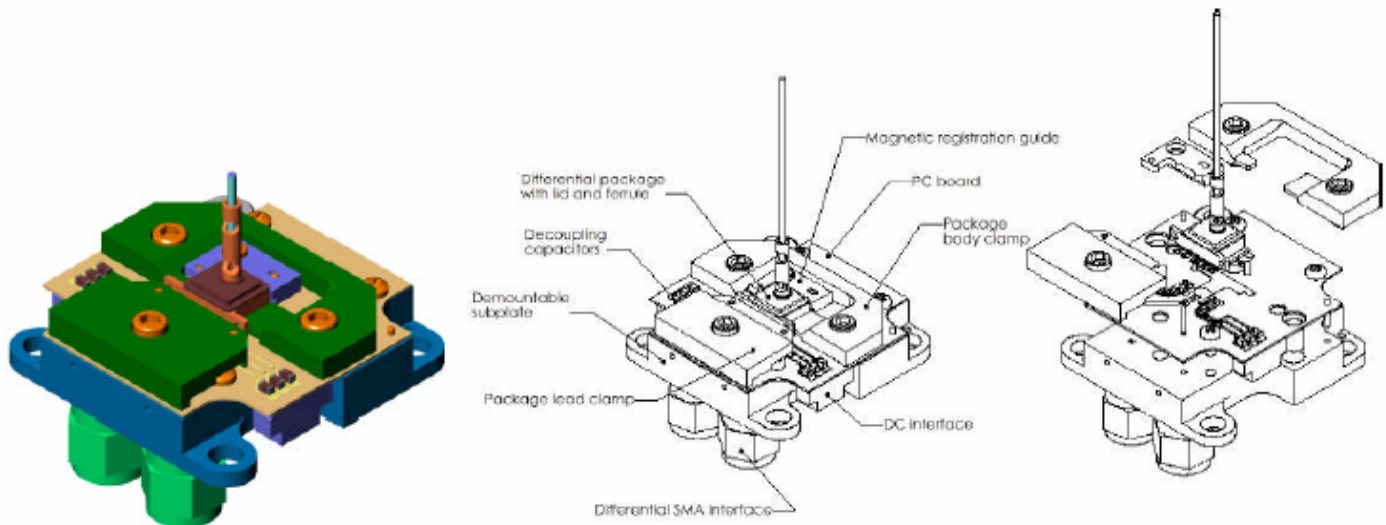
- Interface capable of operating module at speed (10 Gb/s)
- Fully accessible for laser welding
- Fast manual loading and unloading of modules

Focused Research, Inc.

【*r*】

138

Pigtailing process sequence (1/2)

Solder fiber to ferrule, epoxy jacket to ferrule

Die attach and bond known good die

Visually align fiber and device, establish z=0 height

Retract ferrule, insert lid

Focused Research, Inc.

[*r*]

139
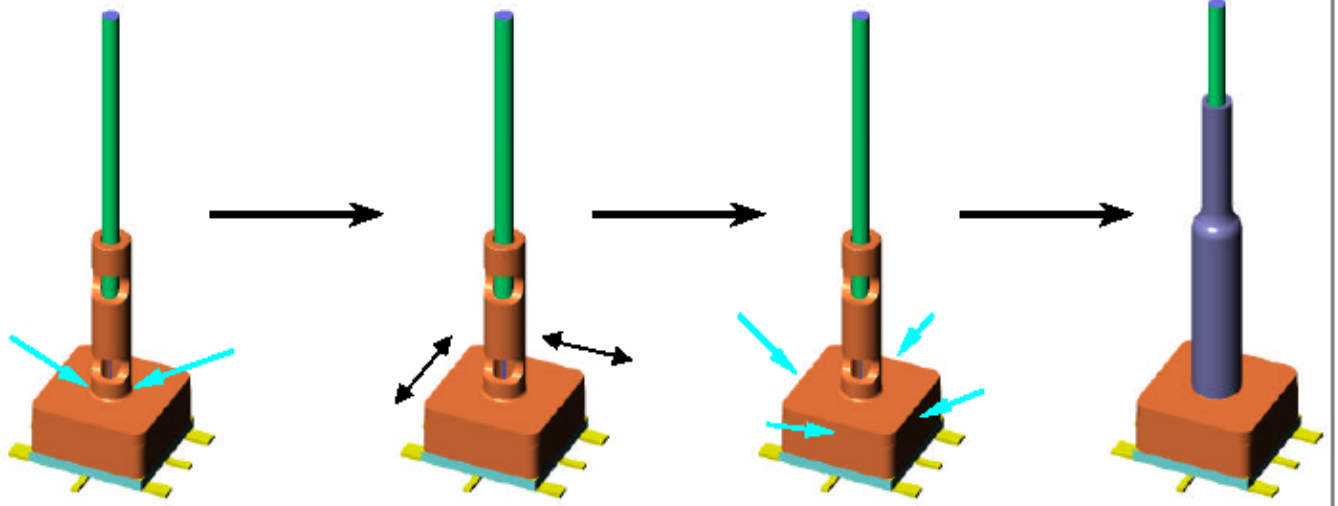
Lower ferrule into place, spot and seam weld ferrule to lid

Perform fine x-y alignment of lid and package

Spot and seam weld lid to package

Attach outer protective boot

Focused Research, Inc.

[r]

Module layout detail
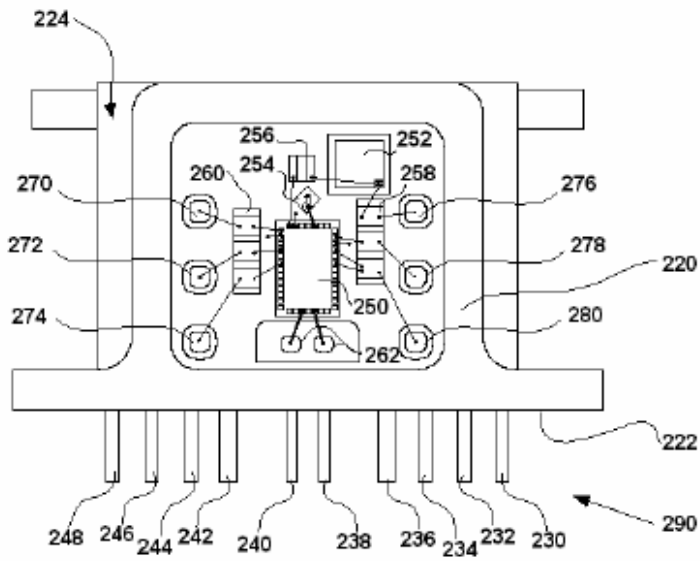
Transmitter
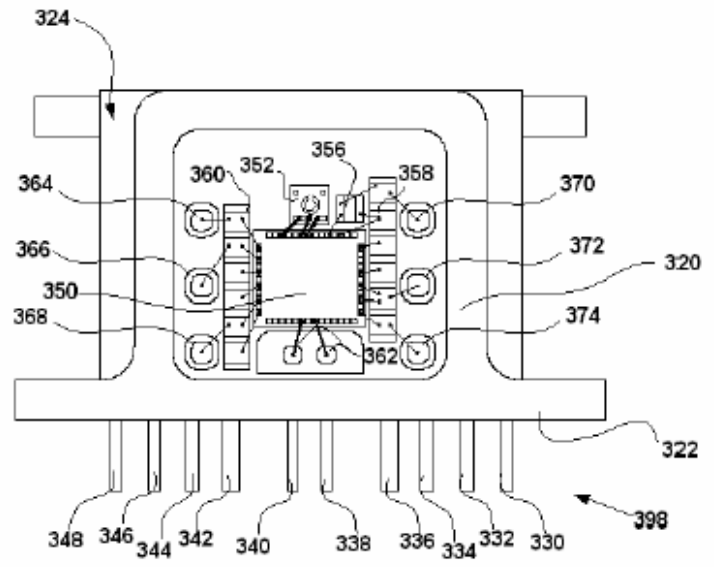
Receiver

Focused Research, Inc.

[r]

141

Package interface simulation

[r]

FIG. 2E

FIG. 2D
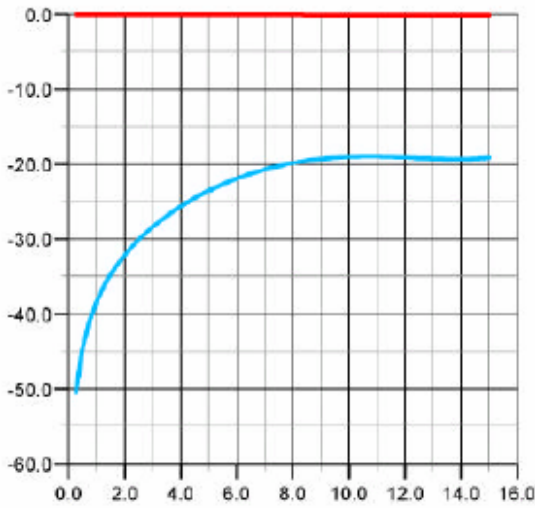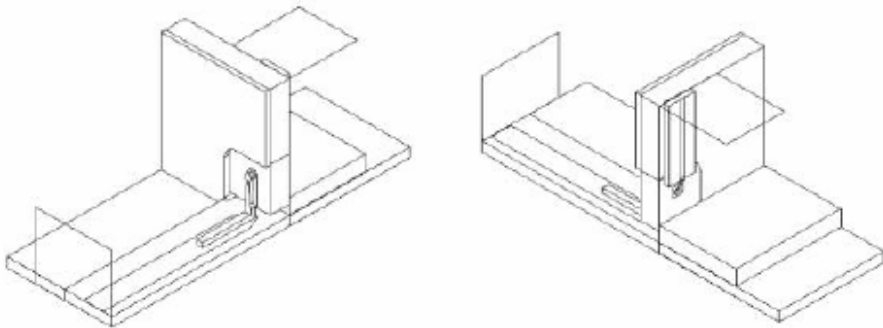
Focused Research, Inc.

【r】
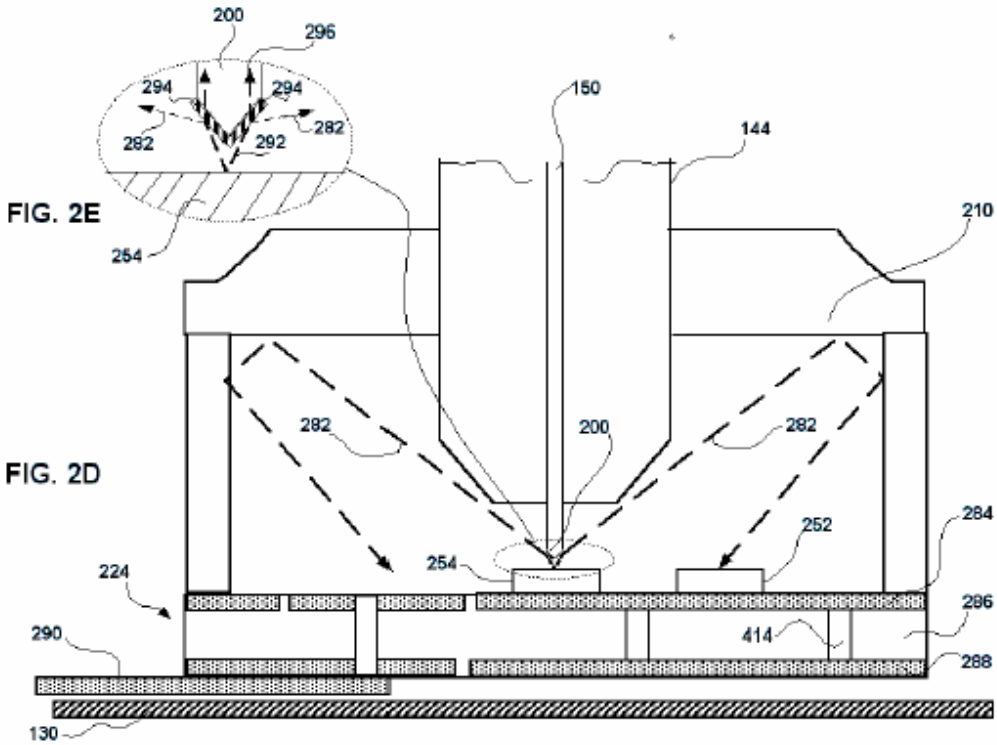
Tx power control circuitry (patent pending)
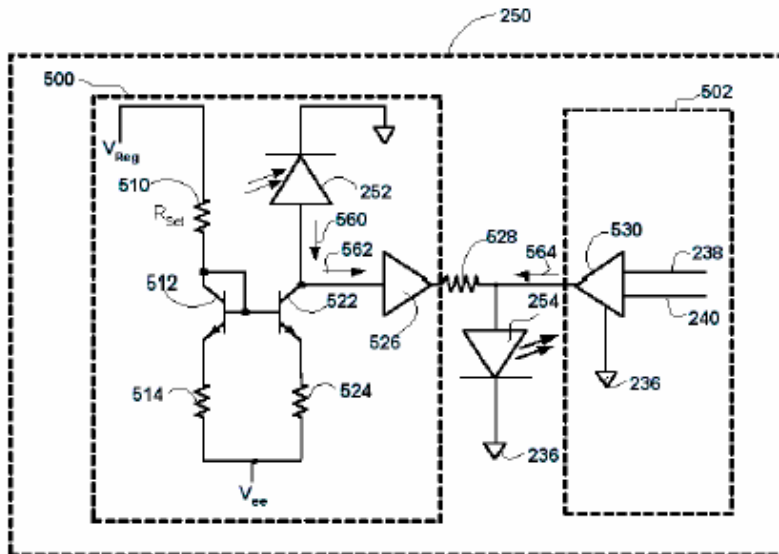
252: Monitor PD
254: VCSEL
526: DC driver
530: AC driver
528: Isolation R

Current mirror 512/522 provides a simple high-gain current to voltage converter for the APC loop

500, 528, and 502 are on the same chip.
254 and 252 are separate chips

Focused Research, Inc.

[r]

144

Photodiode design (patent pending)

FIG. 3D

352

378
376
390
384
386
388

FIG. 3E

392

FIG.3C

352

386
384
382
380

378

378
376

P
+ ++ +++
I
N

FIG.3F

392
394
382

Focused Research, Inc.

[*r*]
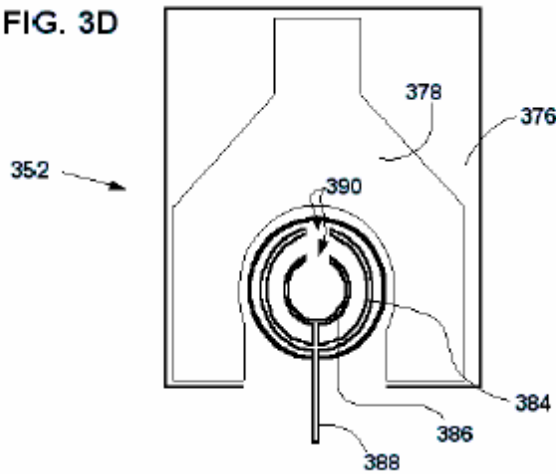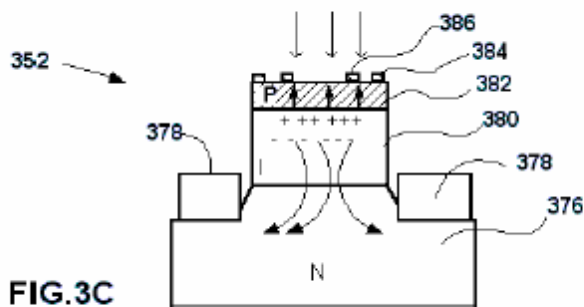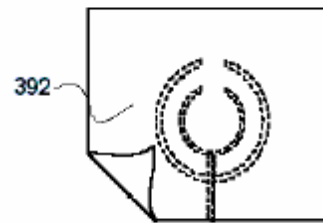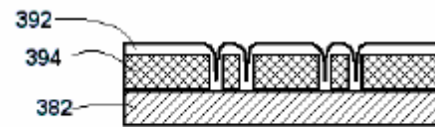
Module Layout Detail
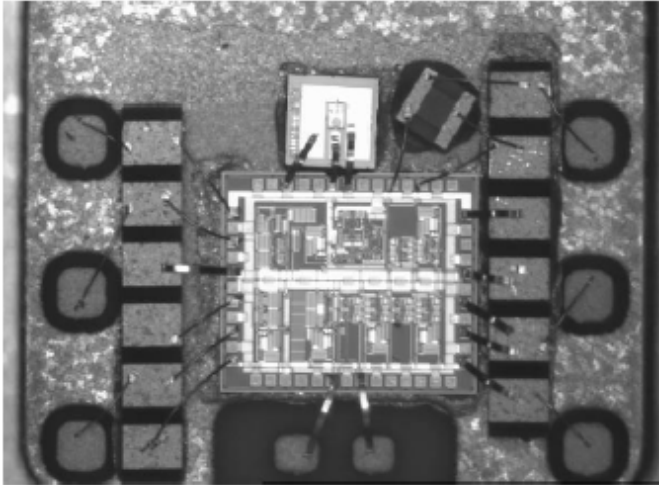
Custom Package

Proprietary RX & TX

Custom Photodiode

Critical Placement
Tolerance for
PD/VCSEL/RX/TX
+/- 0.002 inch

Default: +/- 0.005 inch

Focused Research, Inc.

【*r*】

Photodiode Detail
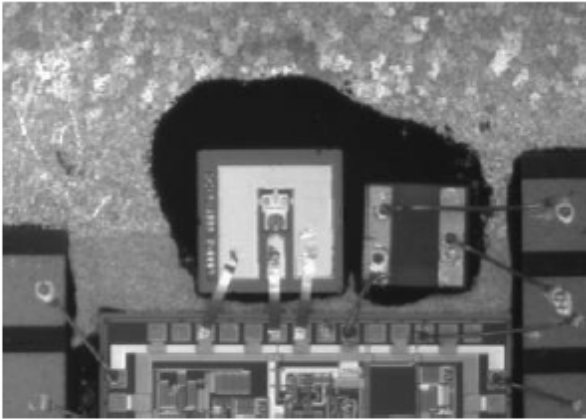
GaAs PIN structure

750 um square die

65 um active area
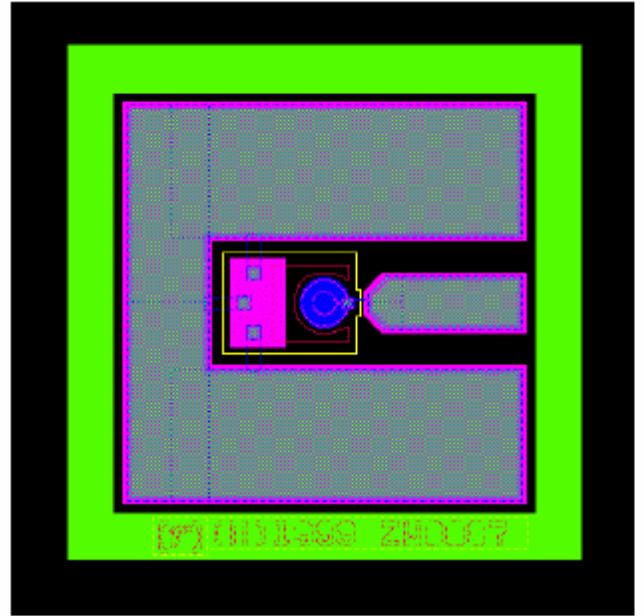
Focused Research, Inc.

[r]

10 Gig Package Electrical Analysis & Optimization
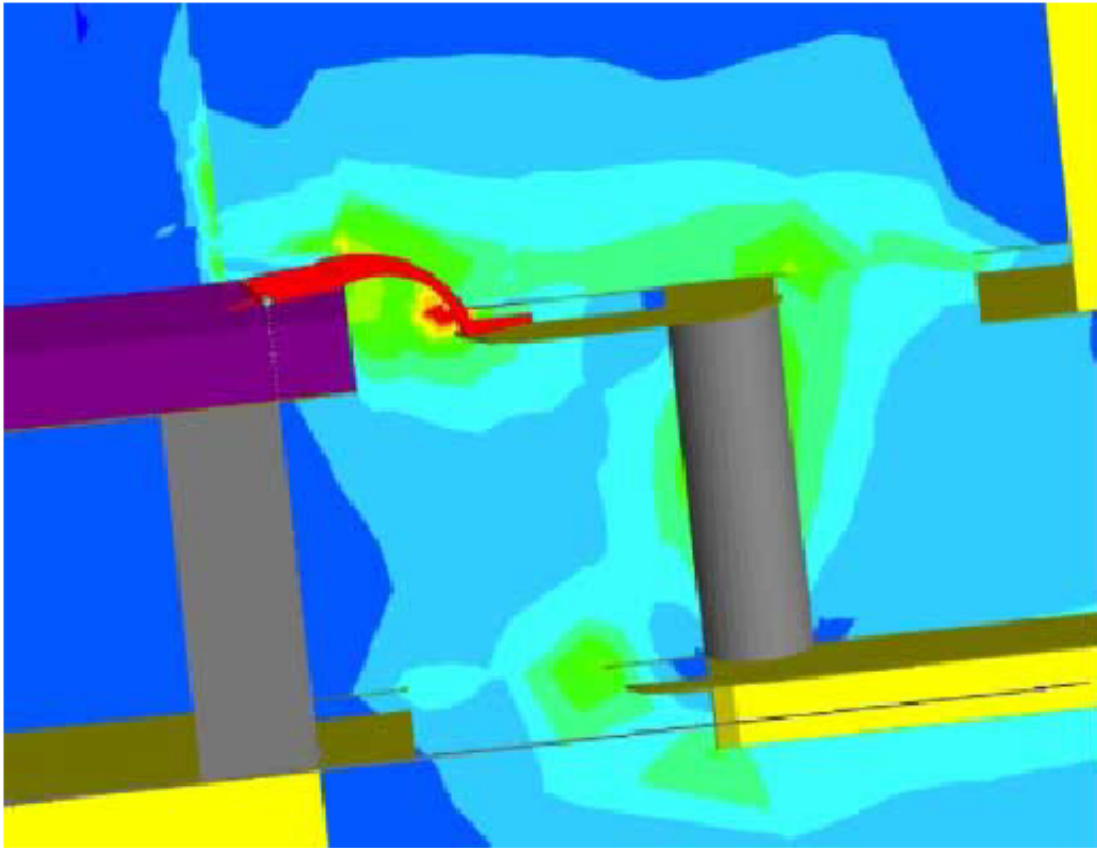
Brent Harper
Focused Research
January 31, 2001

NTK Package Simulations

Brent Harper
Focused Research
January 31, 2001

NTK was contracted to build the 10 Gig Optical Link packages for Focused Research. They were also required to predict the electrical performance of the design. Using the drawings furnished to NTK, the performance of the package with bent leads was evaluated and then optimized here at Focused Research using Ansoft's High Frequency Structure Simulator (HFSS) version 7.

Simulated NTK Package (As-Built)

The NTK package as drawn (and built) does not satisfy the input reflection requirement of a return loss, S_{11}, < -18 dB for the frequency range 0 to 15 GHz. Figure 1 (a,b,c, & d) show images of the NTK package. The NTK version of the simulation seemed to meet the spec, but they did not include correct placement of the chips and did not use a ribbon. Figure 2 shows NTK's simulation results. A more realistic model of the NTK package has S_{11} < -18 dB for frequencies up to only 11 GHz (fig. 3). The package was cut in half and a virtual ground plane was inserted to reduce computation time and to force differential mode operation. (Common mode operation can be simulated using a virtual magnetic symmetry plane.)
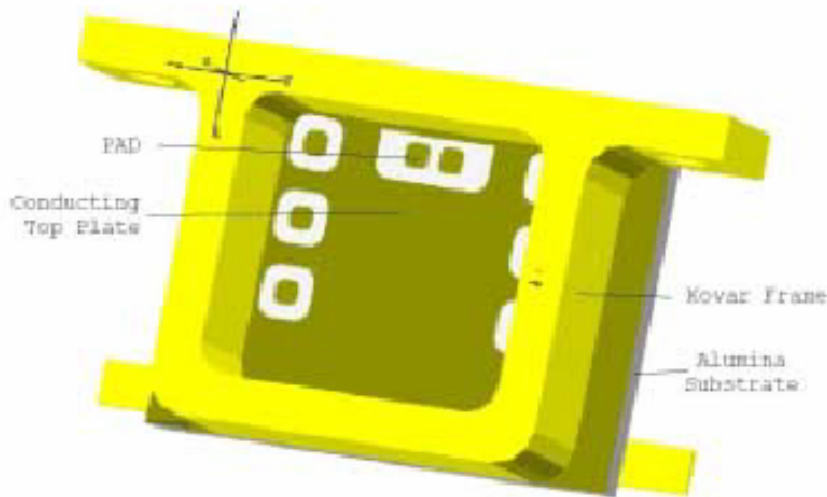

**Figure 1a**. NTK package without hybrid board, lid, or dice (top view with bent leads).

149
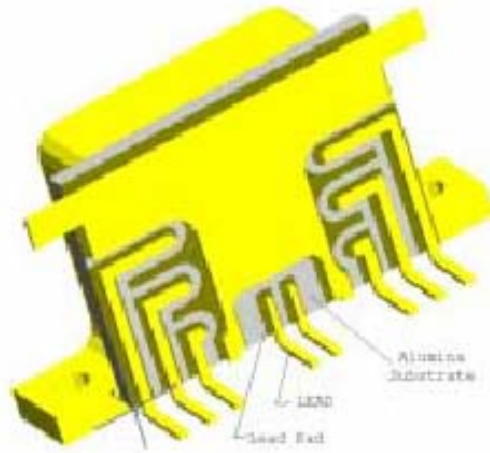
Figure 1b. NTK package without hybrid board, lid, or dice (bottom view with bent leads).

Figure 1c. NTK package (cut in half) with hybrid board, lid, Rx chip, and wire bond (top view without fiber or ferrule).
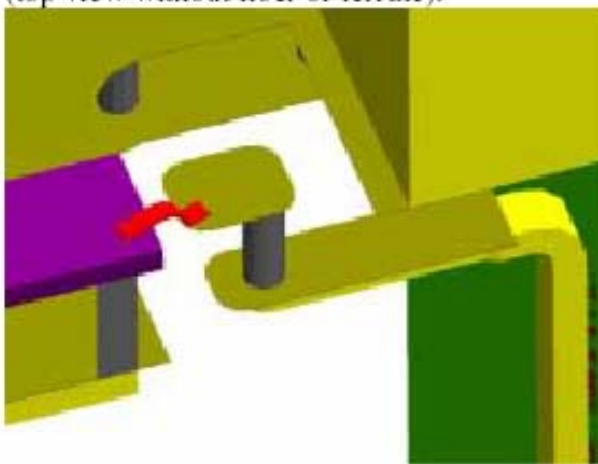
Figure 1d. NTK package (cut in half) with hybrid board, lead, lead pad, pad, vias, Rx chip, and wire bond (without substrate).

150
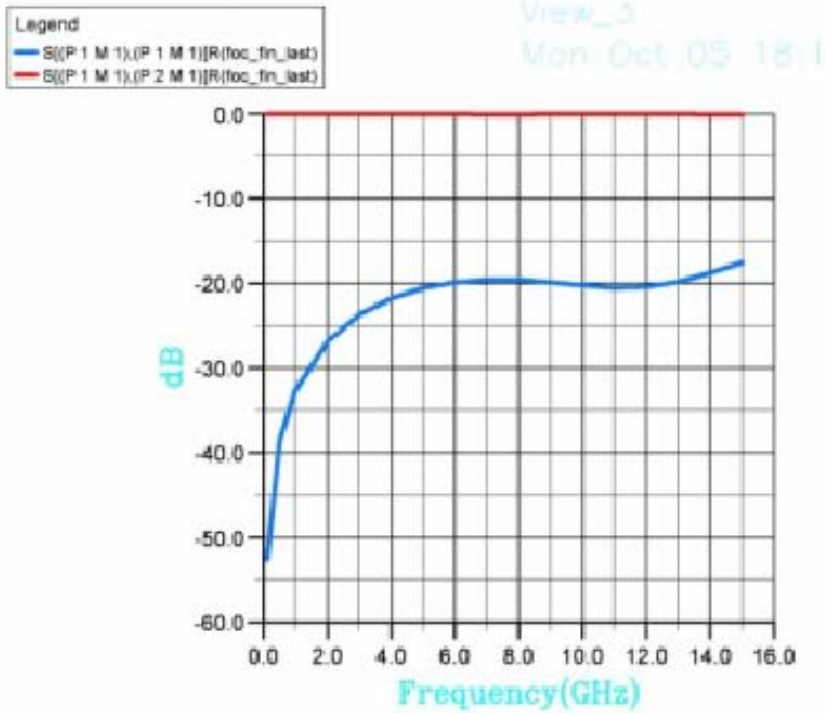
Figure 2. NTK's simulation results showing reflection loss (S11) and transmission loss (S21).
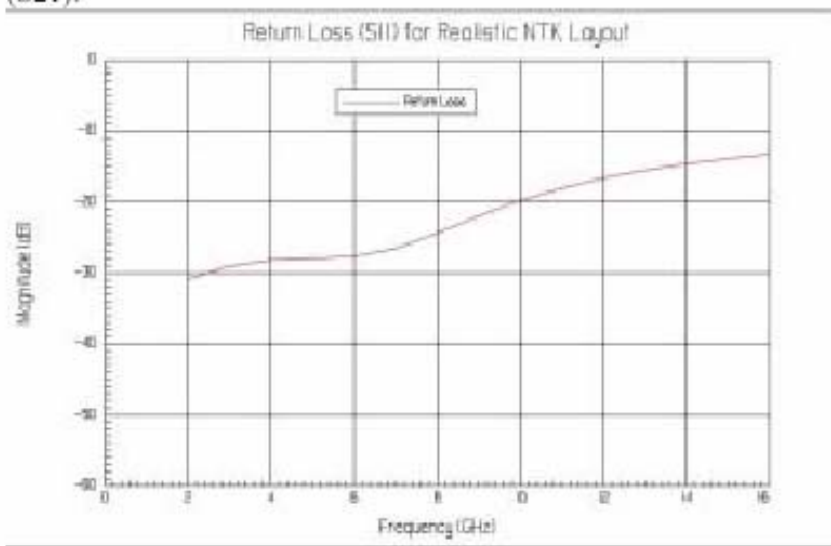

Figure 3. Results of a more realistic simulation of NTK package using appropriate bond ribbon. Reflection loss (S11) and transmission loss (S21) are shown.

Another way to view the electrical response of a package is with Time-Domain Reflectrometry (TDR). In TDR a signal is sent down an electrical path (either on a device or in a simulation) and the amplitude of the reflected and/or transmitted signal is proportional to impedance discontinuities on the line. The simulated TDR is shown in figure 4.
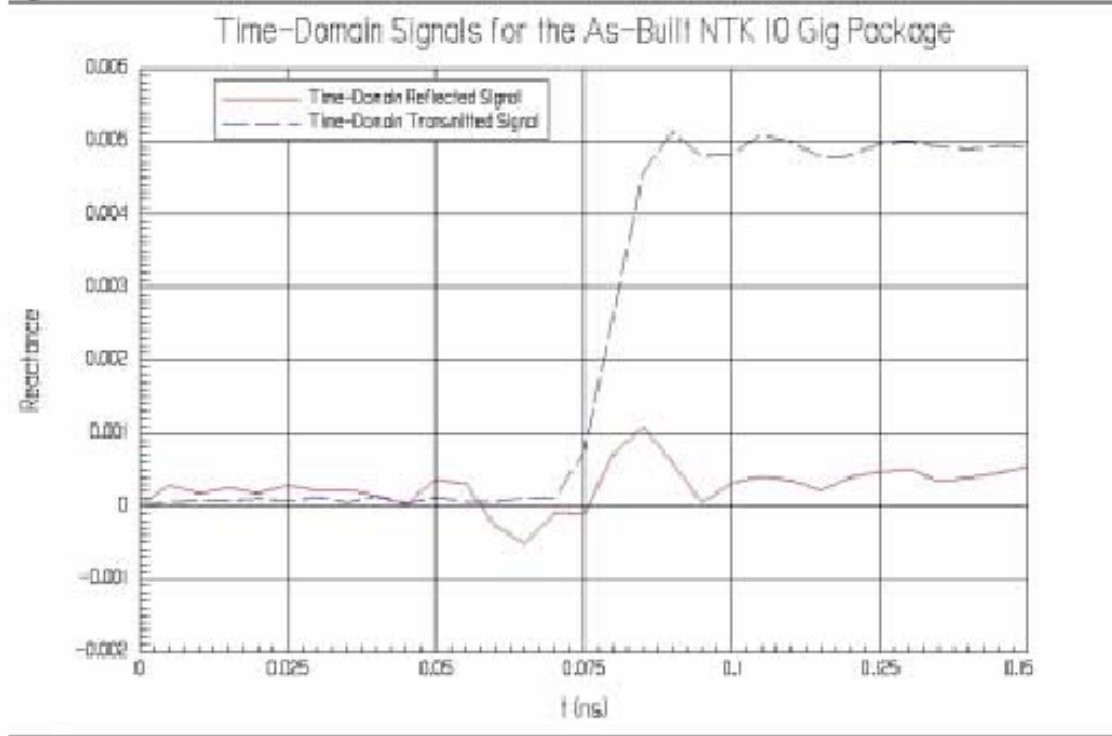

**Figure 4**. Simulated TDR for the realistic NTK package.

The electrical path was optimized for differential mode operation. The optimization dramatically improved the return loss (figs. 5 & 6). After optimization the return loss, S_{11}, < -18 dB for frequencies up to 26 GHz (improved from 11 GHz). The improved pad size and location along with a minimum bond ribbon are shown in figure 7. The TDR also reflects the improvement (figs. 8 & 9).
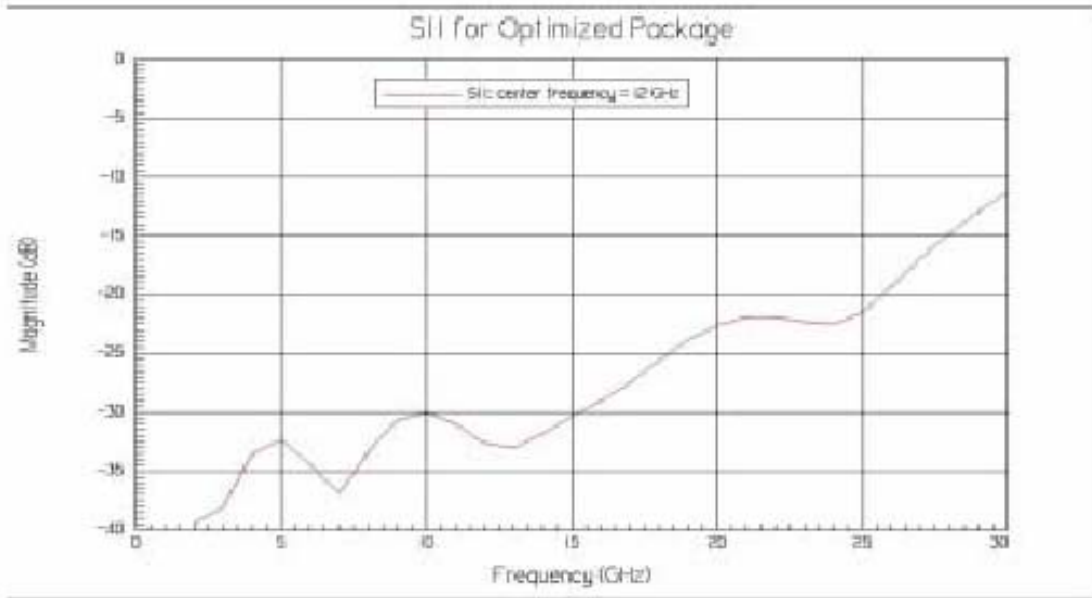
**Figure 5**. Reflection loss for the optimized NTK package.
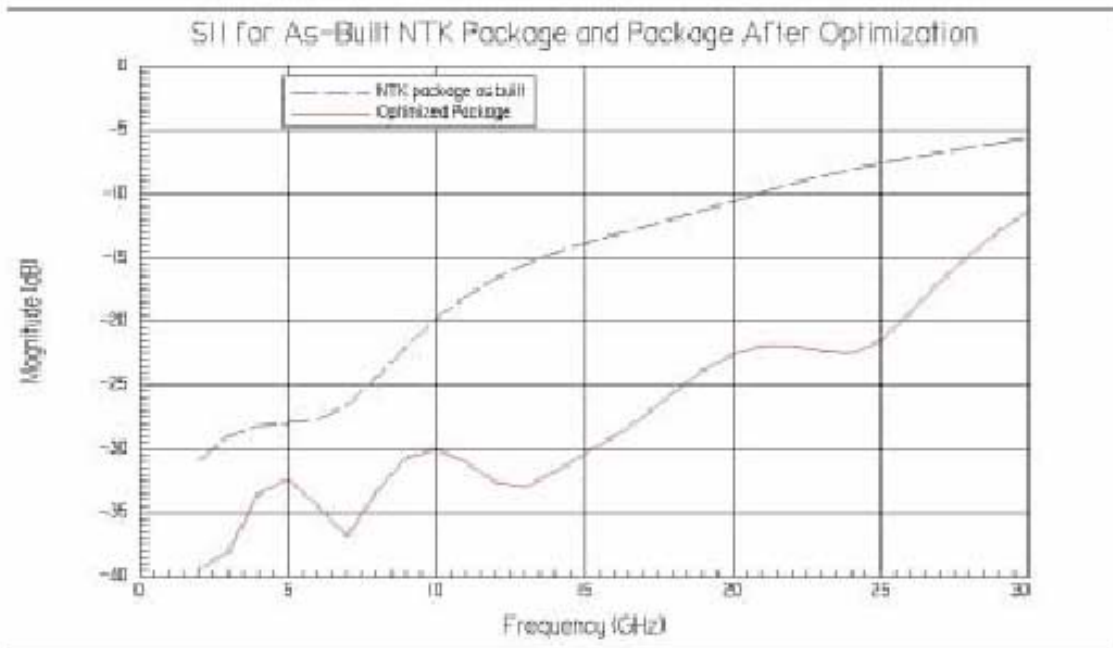
Figure 6. Reflection loss comparison of the as-built NTK package and the final, optimized package.
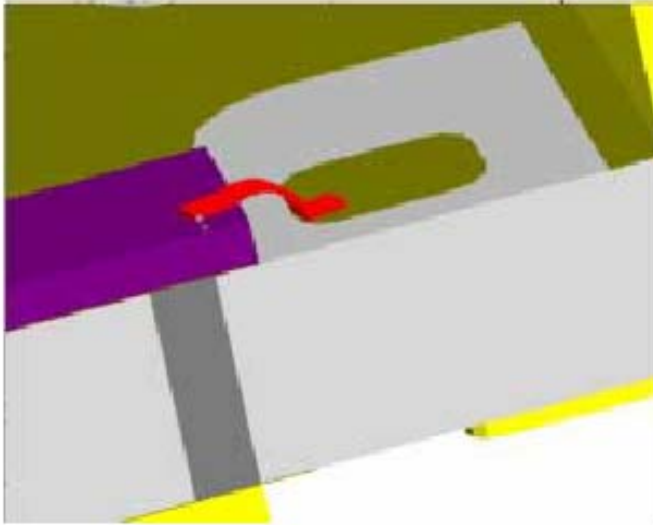
Figure 7. Part of the optimized package, including the improved pad size and location along with a minimum bond ribbon, is shown.
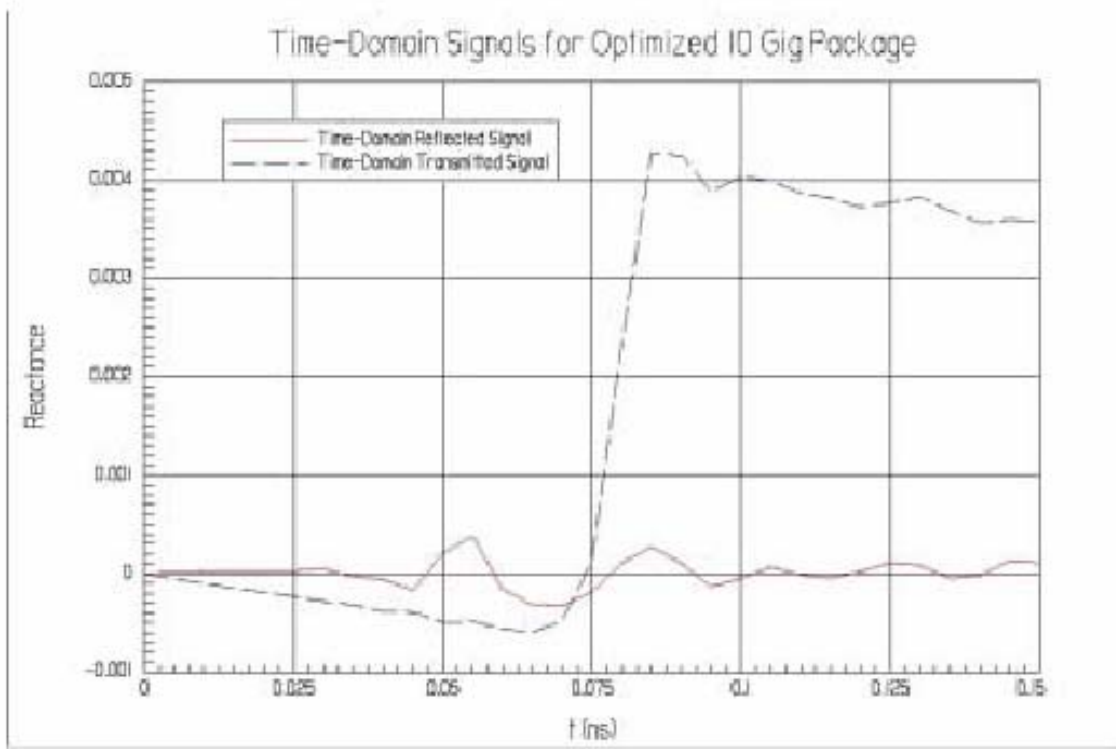

Figure 8. TDR for the optimized package.

154
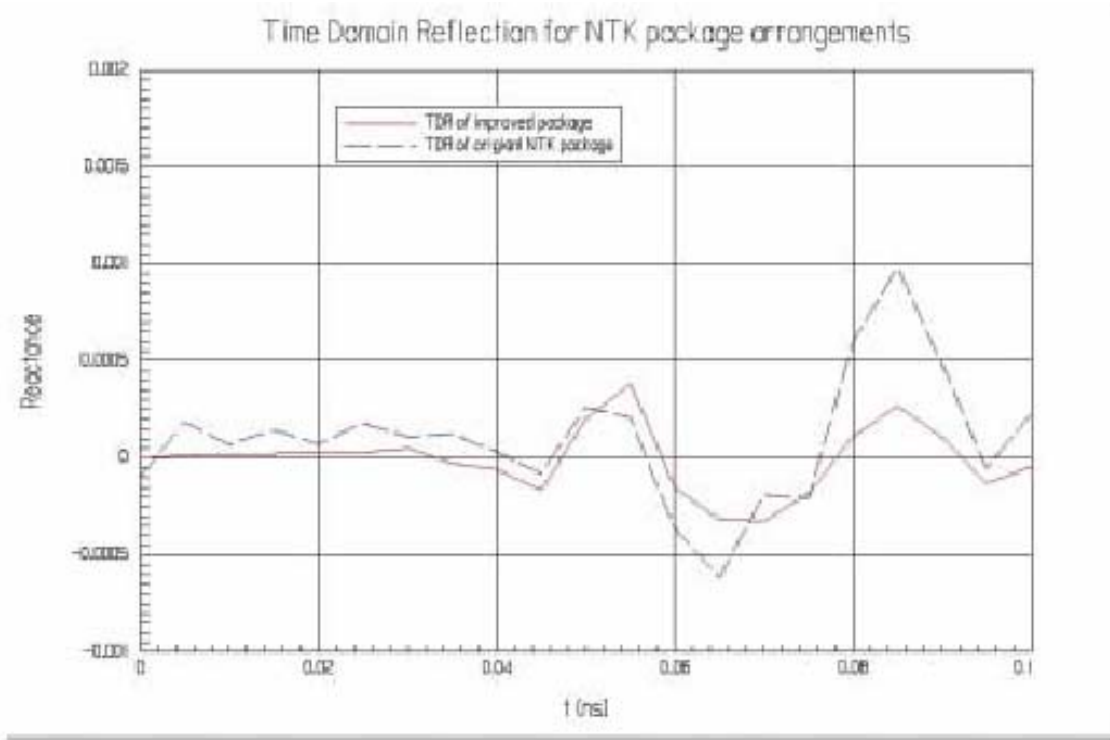
Figure 9. TDR comparison of the as-built NTK package and the final, optimized package.

The TDR simulations of the specified NTK package showed two places of inductance and one place of capacitance (fig. 10).
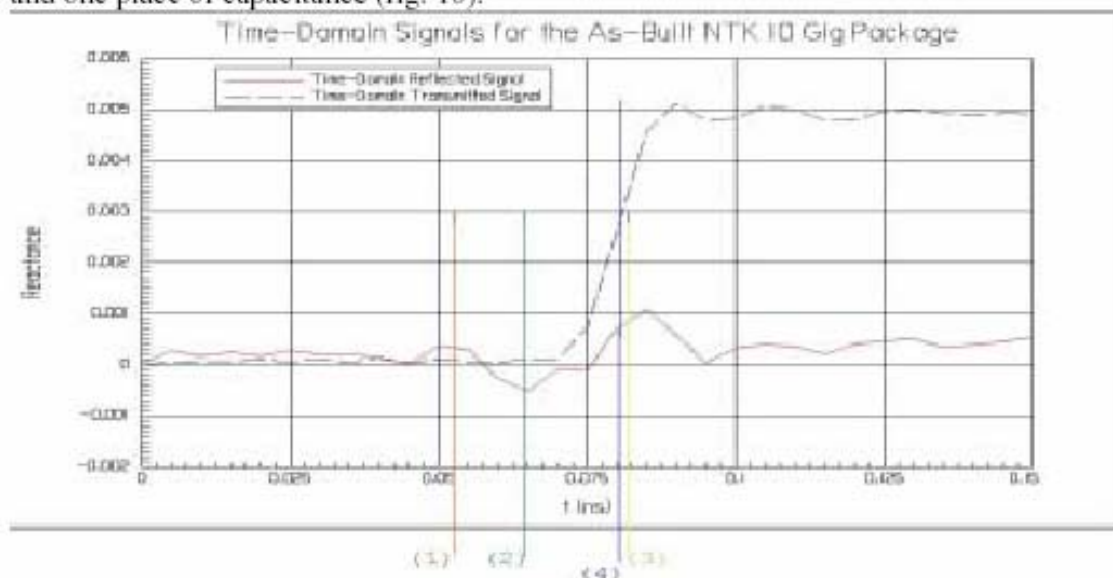
Figure 10. TDR with markers at the major features (for use with table 1).

Based on the geometry and materials it is possible to establish the locations of different parts along the electrical path as related to the theoretical time delay of a reflected input signal. The theoretical positions are then matched to the TDR simulation (see table 1). The first inductive part is the bend in the narrow lead (1). The inductance is relatively small and is a result of the transition from a flat trace to what appears to be a wire while turning 90 degrees. The capacitive part is the lead pad on the bottom of the Alumina (related to the pad on the top of the Alumina) (2). The capacitance is relatively small and is a result of the lead and pad appearing as the two plates of a capacitor. The last inductive part was the dominant feature in the NTK design and roughly corresponds to the bond ribbon (3). The inductance here is reduced to the order of the other two discontinuities in the optimized design. The time for the input to reach the output is designated by (4).

Table 1

	Time delay (ps)	Probable package feature	Predicted time delay to probable package feature (ps)
(1) Inductive (small)	52	Bend in lead	52
(2) Capacitive (small)	63	Lead pad/Pad parallel cap.	61 - 69
(3) Inductive (large)	83	Bond ribbon	77 - 84

Further improvements were attempted using a pad which had the same thickness as the chip, using two ribbons, and using a wider bond ribbon. None of these attempts made significant improvements.

The guidelines for optimizing the electrical path along with some tolerances are listed below. For clarification of the terms pad, bond ribbon, conducting top plate, lead, and lead pad, see figure 1.

Optimization:

1) The pad should be moved and/or extended to within approximately .004" of the conducting top plate (of the Alumina substrate). This has the most dramatic effect. Tolerances should be within +/-.001".

2) The pad should be as far away from symmetry plane as is reasonable. The pad could be made narrower or relocated by up to .005". Further work could look at moving the via and lead. Tolerance is tight on the edge near the symmetry plane: +/- .001". Also, the pad should be approximately centered over via if possible.

3) The bond ribbon should be as short as possible without hanging over the edge of the pad. Minimizing the length should use both bond placement and arch.

4)   The lead pad on bottom of Alumina substrate should be as narrow as possible. This reduces capacitance and therefore reflections due to impedance discontinuities. Width could be reduced from .016" to .012" with increasing tolerances for the narrower lead (brazing of bent lead to the lead pad). The lead pad should also be as far away from symmetry plane as is reasonable. This reduces peak field intensities.

The optimized package improves performance dramatically. S_{11} is now less than -18 dB for frequencies up to 26 GHz. Further improvements in performance might be possible by reconfiguring the vias.